PERFORMANCE AND STALLING BEHAVIOR OF AN AXIAL-FLOW COMPRESSOR SUBJECTED TO THREE CIRCUMFERENTIAL INLET DISTORTION LEVELS

by

William H. Gauden

Thesis submitted to the graduate faculty of the
Virginia Polytechnic Institute and State University
in partial fulfillment of the requirements for the degree of

MASTER OF SCIENCE

in

Mechanical Engineering

APPROVED:

W. F. O'Brien, Jr., Chairman

H. L. Moses

W. C. Thomas

October, 1977

Blacksburg, Virginia

II. ACKNOWLEDGEMENTS

The author wishes to thank the members of his advisory committee: Professors W. C. Thomas, H. L. Moses, and W. F. O'Brien, Jr., Chairman. The direction and guidance provided by Dr. O'Brien throughout the investigation was especially appreciated.

III. TABLE OF CONTENTS

TABLE OF CONTENTS (Continued)

IV. LIST OF FIGURES

LIST OF FIGURES (Continued)

LIST OF FIGURES (Continued)

LIST OF FIGURES (Continued)

V. LIST OF TABLES

VI. LIST OF SYMBOLS

A_1	discharge duct cross-sectional area
A_2	orifice cross-sectional area
A_i	inlet annulus area
C	absolute air velocity
C_v	orifice flow coefficient
d	orifice diameter
D	discharge duct diameter
F.F.	flow adjustment factor
g_c	gravitational constant
Δp	static pressure drop
P	total pressure (Section IX only)
P_S	static pressure
P_T	total pressure
PRS	stall pressure ratio
ΔP_o	total pressure rise
ΔPRS	reduction in stall pressure ratio
ΔPSM	reduction in stall pressure margin
Q_{inlet}	inlet flow rate
U	rotor blade velocity
V	relative air velocity
α	absolute air angle
β	relative air angle
Θ	circumferential extent of distortion

LIST OF SYMBOLS (Continued)

Θ_c	critical angle of extent
ρ	density

Subscripts

1	refers to rotor inlet
2	refers to rotor exit
avg	average
D	distorted
max	maximum
N	constant corrected rotor speed
screen	refers to minimum pressure behind screen
tip	rotor blade tip
U	undistorted
x	axial
ω	whirl

Superscripts

e	effective

VII. INTRODUCTION

Compressor stall or surge represents a serious operating limitation of modern jet engines. Newly developed aircraft engines must maintain optimum performance over a wide range of flight conditions without compromising engine stability. Inlet flow distortions alter stable operation by reducing the compressor stall margin. Thus, extensive testing to determine the effects of inlet distortion on compressor performance must be conducted during engine development.

Inlet distortion may be detected at the engine-inlet interface as variations in pressure and/or temperature. Pressure distortions may result from operation at high angles of attack or yaw, and wakes from nearby aircraft. Temperature distortions are caused by the ingestion of hot exhaust gases from aircraft carrier catapult systems, thrust reversers, and exhaust plumes of other aircraft. Careful inlet-engine design is required to minimize flow distortions due to inlet-boundary layer interactions.

The investigation presented in this report concerns compressor response to circumferential inlet total pressure distortion. Three basic parameters characterizing this distortion pattern are; 1) the circumferential extent, 2) the distortion level (magnitude of the total pressure loss in the distorted flow region), and 3) the time interval during which the distortion exists.

In the present study, the performance and stability of a low-speed single-stage compressor subjected to several different circumferential distortion patterns was investigated. Overall compressor

performance measurements were recorded for undistorted operation and for all distortion levels and extents. Parallel compressor model predictions of distortion-induced reductions in compressor stall margin are compared with experimental data. An analysis of the effects of inlet distortion on the stable rotating stall behavior of the compressor was conducted through the use of high response dynamic pressure probes. Rotor blade response to inlet distortion was measured in the form of average blade pressure profiles by using a scanning valve.

The experimental apparatus, testing procedures, and results of this investigation are presented in the following material.

VIII. REVIEW OF LITERATURE

During engine development, design efforts must be directed towards achieving optimum performance without compromising engine stability. The reduction in compressor stall margin due to inlet distortion has been documented by numerous experimental investigations. In recent years, extensive research has been conducted to further investigate the effects of inlet distortion on the performance and stalling behavior of axial-flow compressors.

In 1959, Pearson and McKenzie [1]* introduced parallel compressor theory as a method of analyzing the performance of a compressor subjected to distorted inflow. Parallel compressor theory employs the following basic assumptions as described by Braithwaite, Graber, and Mehalic [2];

1) the distorted compressor is assumed to consist of two or more independently operating sub-compressors,
2) all of the sub-compressors have individually uniform inlet conditions and they all operate on the undistorted compressor performance characteristic,
3) no circumferential cross-flow occurs between the isolated compressors,
4) the exit static pressures of all sub-compressors are assumed identical, and

*Numbers in brackets indicate references in the Bibliography.

5) the entire compressor is assumed to stall when the pressure rise across any sub-compressor equals that of the undistorted compressor stall pressure ratio.

A more detailed discussion of parallel compressor theory, including its application, is presented in a later section of this thesis.

A number of experimental investigations have been conducted to determine the effects of inlet distortion on compressor stall margin reduction. Parallel compressor model predictions of loss in stall pressure ratio have generally agreed with experimental data for extents of distortion greater than the critical area of spoiling. Calogeras, Mehalic, and Burstadt [3] described the critical area of spoiling, hereafter referred to as the critical angle, as being related to the minimum blade residence time required for the compressor to respond in a steady-state manner. Reid [4] studied the response of a six-stage axial-flow compressor to a range of circumferential extents of distortion. He discovered a rapid decrease in surge delivery pressure for spoiled sector angles ranging from zero to 90 degrees. However, for distortion extents greater than 90 degrees, the surge delivery pressure approached a constant minimum value. From these results, Reid concluded that the compressor responded to a critical angle having a value between 60 and 90 degrees.

A similar experiment was performed by Calogeras, Mehalic, and Burstadt [3] in 1971 on a General Electric J85-13 turbojet engine. The authors found the critical angle of the engine's eight stage compressor to be approximately 60 degrees. Three years later

Calogeras, Johnsen, and Burstadt [5] extended the above study by performing similar tests on two more J85-13 engines. Both compressors responded to a critical sector angle of 60 degrees. Upon comparison of results with the earlier study, the three compressors responded similarly to circumferentially distorted inlet flow.

Roberts, Plourde, and Smakula [6] found that parallel compressor theory predictions were in good agreement with experimental data for mild pressure distortions away from the peak pressure coefficient. For a more severe distortion level and at the peak pressure coefficient, experimental results differed substantially from theoretical predictions. The authors attributed these discrepancies to the incorrect assumption of parallel compressor operation on the undistorted characteristic under these conditions.

Graber and Braithwaite [7] used the parallel compressor model to predict the distortion-induced reduction in stall pressure ratio of a two-spool turbofan engine. Theoretical predictions for the loss in stall pressure ratio were in good agreement with experimental data. The successful application of parallel compressor theory to the turbofan engine was significant in that the model predictions proved to be a useful tool in understanding the stall behavior of a more complicated system. The model was applied to each compressor unit in the turbofan engine individually.

Plourde and Stenning [8] developed a mathematical technique capable of solving for the flow field within a compressor subjected to inlet distortion. Comparing the model solution to available

experimental data, it was concluded that for compressors with normal axial clearances between blade rows, circumferential flow within the compressor may be neglected in a first analysis of inlet distortion effects. This conclusion reinforces a basic assumption of parallel compressor theory.

Mikolajczak and Pfeffer [9] submit an explanation of the discrepancies which result from applying parallel compressor theory to experimental data for small extents of distortion through the use of a reduced frequency parameter. The frequency parameter is a function of rotor blade chord length, compressor radius, distortion extent, blade speed and air axial velocity. The authors conclude that for small extents of distortion the rotor responds to average circumferential flow conditions. Therefore, the compressor is less sensitive to narrow extents of distortion than predicted by parallel compressor theory.

Ehrich [10] contributed a two-dimensional mathematical solution for the attenuation of an inlet velocity distortion through an axial flow stage of turbomachinery. The solution indicated that the design criteria for distortion attenuation and minimum blade load fluctuations are contradictory and must be compromised.

Hartmann and Sanger [11] investigated the effect of 90 degree circumferential inlet pressure distortion on the performance of two single-stage fans having different design pressure ratios. The reduction in stall pressure ratio due to distorted inflow was determined for the rotor blade row as well as for the complete stage including

stators. At design speed both rotors experienced a loss in stall pressure ratio, with the more highly loaded rotor showing a slightly lower loss. However, comparing complete stages (rotor plus stator), the higher-loaded stage showed a greater loss in pressure ratio at stall than the lower-loaded stage. The authors attributed this variation in response between stages to differences in stator flow. This result indicates the need for careful selection of stator blade profiles in compressor design.

Peacock and Overli [12] subjected a lightly loaded compressor to square-wave and sine-wave (with respect to compressor circumference) inlet pressure distortions. Up to the point of instability the rotor blade pressure profiles for the sine-wave distortions were similar to those for square-wave distortions. Stall was initiated at the rotor blade trailing edge for the sine-wave distortions. The rotor blade unsteady response to the square-wave distortions was precipitated at the leading edge.

In Ref. 13, Dancy employed a scanning valve* described by Schultz [14] to study the performance and stalling behavior of an axial flow compressor subjected to circumferential inlet total pressure distortion. The scanning valve enabled chordwise and spanwise blade surface pressures to be examined. Dancy found that inlet distortion substantially decreased the overall performance of the single-stage compressor. The critical angle was determined to be approximately 60

*"Scanivalve ®", manufactured by the Scanivalve Corp., San Diego, California.

degrees for the compressor tested. At reduced volumetric flow rates, a stable rotating stall condition developed.

The present study is an extension of Dancy's contribution. Results of both investigations are compared where appropriate. The overall performance of the same test compressor was determined for two more severe levels of total pressure distortion. An in-depth analysis of the effects of inlet distortion on rotating stall behavior was made possible by using high response dynamic pressure probes. These probes, positioned at two circumferential locations behind the rotor enabled "stall cell" information to be obtained. The Scanivalve was used to measure midspan rotor blade average pressures for several flow conditions. Further discussion of all aspects of the study is provided in the following material.

IX. DISCUSSION OF PARALLEL COMPRESSOR THEORY

The basic assumptions of parallel compressor theory presented earlier are outlined in Fig. 1. Figure 2 shows the individual operating points for the undistorted (A) and distorted (B) sub-compressors on the undistorted performance characteristic. Point S represents the overall stall pressure ratio for the distorted compressor obtained by applying the parallel compressor model. For a circumferential total pressure distortion as shown in Fig. 3, parallel compressor theory employs the definition [15]

$$\Delta PRS_N \equiv \frac{PRS_U - PRS_D}{PRS_U} = \frac{\dfrac{P_2}{P_{screen}} - \dfrac{P_2}{P_{avg}}}{\dfrac{P_2}{P_{screen}}} \qquad (1)$$

where ΔPRS_N is the reduction in stall pressure ratio at constant corrected rotor speed,

PRS_U is the undistorted stall pressure ratio, and

PRS_D is the distorted stall pressure ratio for the same corrected rotor speed.

The compressor investigated had a relatively low total pressure rise at design. Therefore, Eq. (1) was modified to be expressed in terms of pressure "differences" rather than pressure ratios to yield [13]

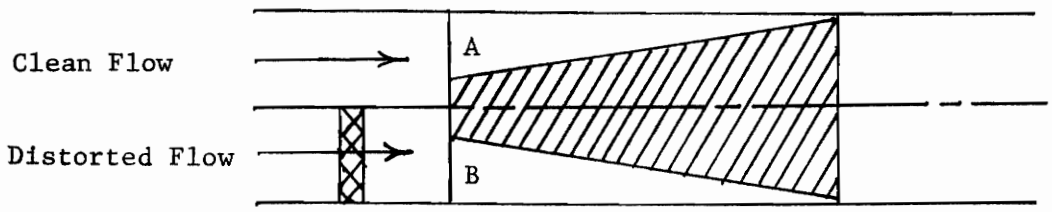

1) Sectors A and B are considered as independent parallel sub-compressors

2) Both sides follow same map as undistorted compressor

3) No cross-flow between parallel sub-compressors

4) Both exit to a common static pressure

5) Stall occurs when pressure rise across A or B equals stall pressure ratio of undistorted compressor

Figure 1. Basic Assumptions of Parallel Compressor Model (Adapted From Reference 2)

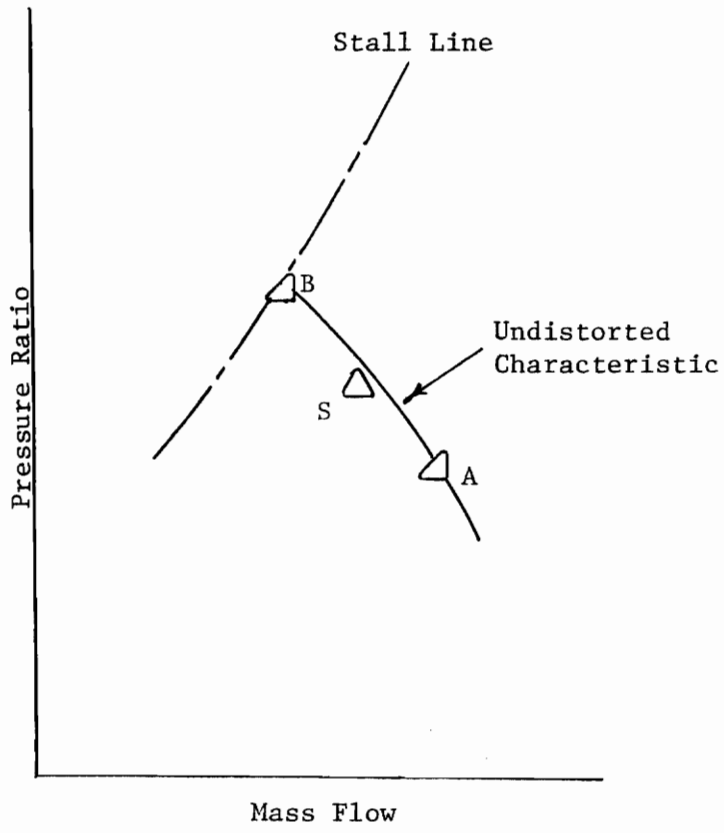

Figure 2. Application of Parallel Compressor Model

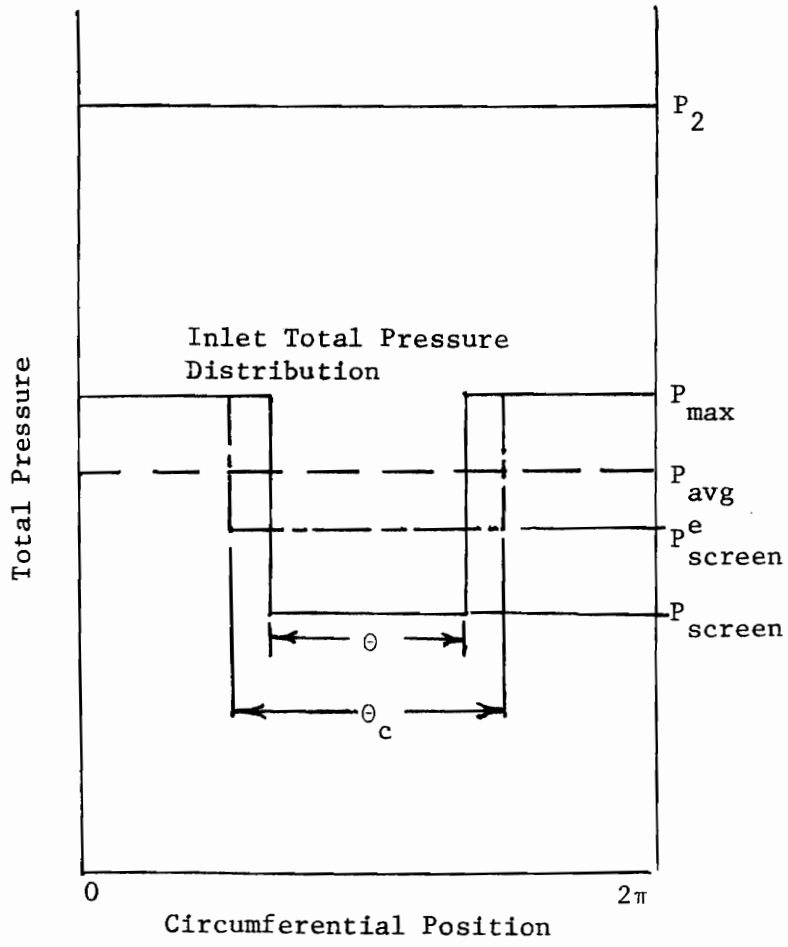

Figure 3. Total Pressure Distribution at Compressor Inlet and Outlet

$$\Delta PSM_N = \frac{(P_2 - P_{screen}) - (P_2 - P_{avg})}{P_2 - P_{screen}} = \frac{P_{avg} - P_{screen}}{P_2 - P_{screen}} \qquad (2)$$

where ΔPSM_N is the reduction in stall pressure margin at constant corrected rotor speed,

P_2 is the discharge plenum total pressure,

P_{screen} is the minimum pressure behind the distortion screen, and

P_{avg} represents the average total pressure entering the compressor.

Referring to Fig. 3, the average pressure, P_{avg}, may be expressed as

$$P_{avg} = \frac{(2\pi - \theta)\, P_{max} + \theta(P_{screen})}{2\pi} . \qquad (3)$$

In Eq. (3), P_{max} is the undistorted total pressure at the compressor inlet and θ refers to the circumferential extent of distortion. Substituting Eq. (3) into Eq. (2) gives the result

$$\Delta PSM_N = \frac{(1 - \frac{\theta}{2\pi})\, P_{max} + (\frac{\theta}{2\pi} - 1)P_{screen}}{P_2 - P_{screen}} . \qquad (4)$$

To apply the parallel compressor model, P_{max}, P_{screen}, and P_2 were measured at the stall point of the distorted compressor. The model predictions of loss in stall margin for the two distortion

levels tested are shown in Figs. 4 and 5 as a straight dotted line. The theoretical curve was obtained using average values of P_{max}, P_{screen}, and P_2. Experimental results are tabulated in Appendix A and plotted in Figs. 4 and 5.

Comparing experimental and theoretical results, reasonable agreement was obtained for distortion extents greater than some critical value. For extents of distortion less than the critical angle, the discrepancy between results grew rapidly. Mokelke [15] attributed this behavior to the unsteady response of the rotor blades to narrow extents of distortion. Under these conditions, the assumption of isolated sub-compressor operation on the undistorted characteristic is invalid. Reid [4] proposed a method of solution combining concepts of parallel compressor theory and "critical angle of spoiling." For distortion extents less than the critical angle, Reid defined an "effective" distortion having an extent equal to the critical angle by employing the following relation

$$\theta_c \ (P_{max}-P^e_{screen}) = \theta(P_{max}-P_{screen}) \qquad (5)$$

where θ_c is the critical sector angle,

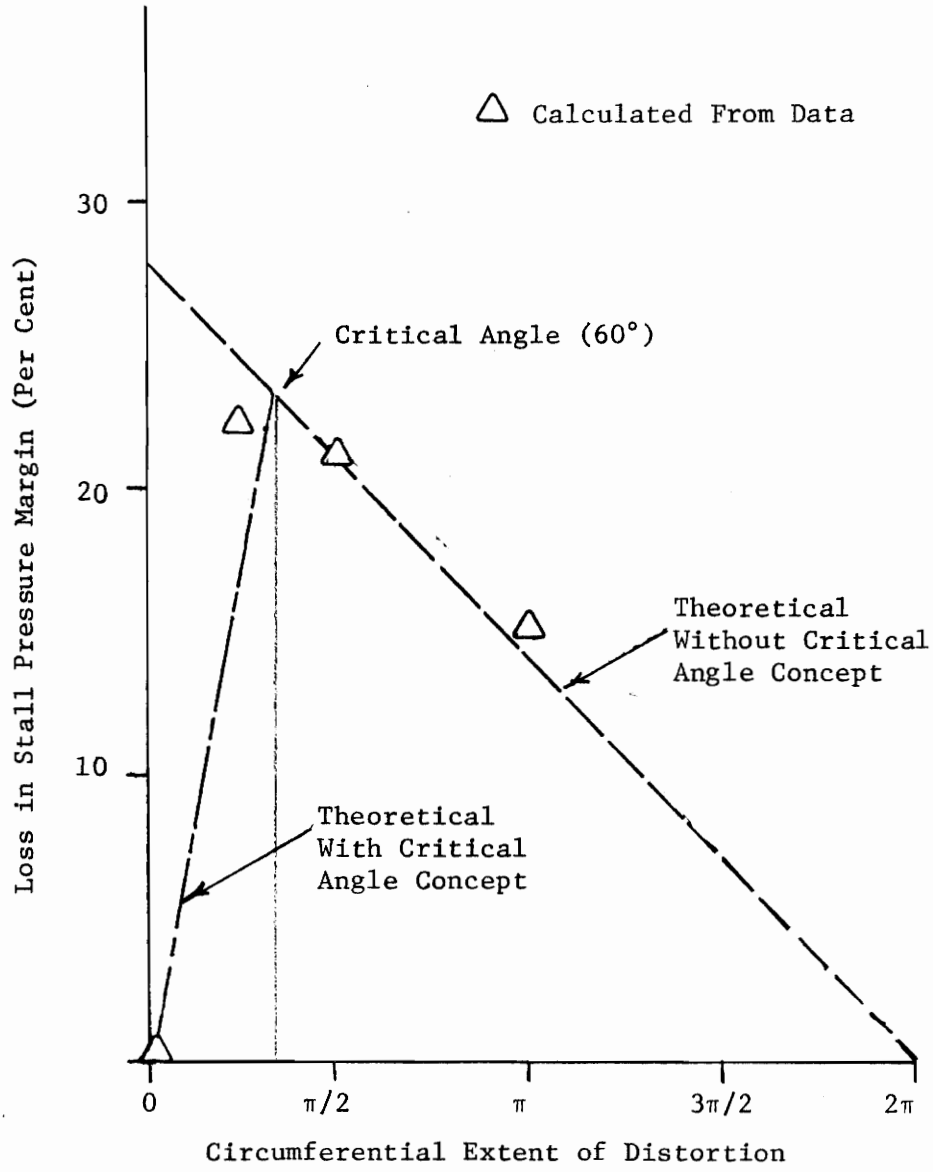

Figure 4. Experimental and Theoretical Loss in Stall Pressure Margin as a Function of Distortion Extent; Distortion Level 2

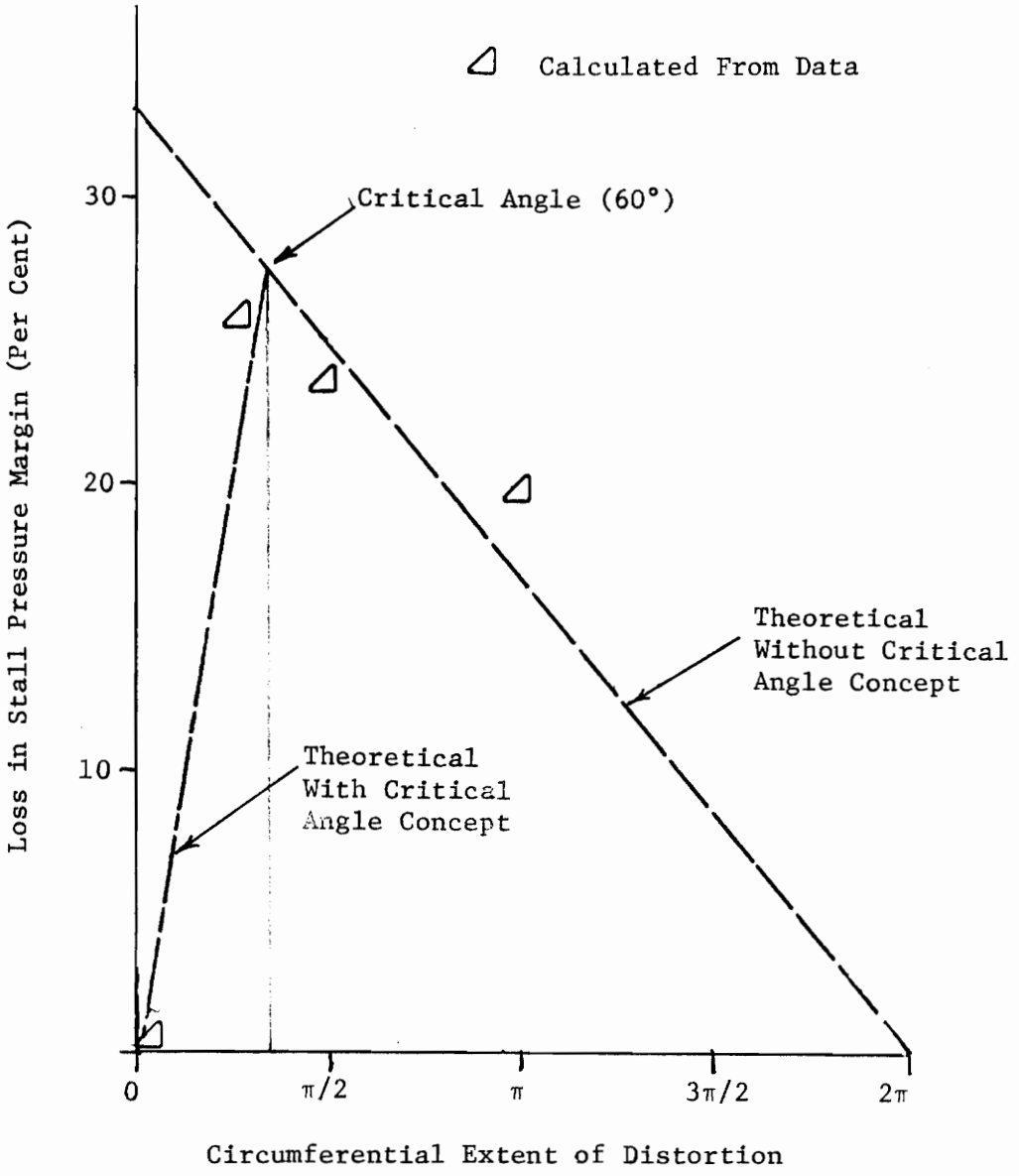

Figure 5. Experimental and Theoretical Loss in Stall Pressure Margin as a Function of Distortion Extent; Distortion Level 3

P^e_{screen} is the effective distortion level (see Fig. 3), and all other variables remain as defined previously.

Solving for P^e_{screen} yields,

$$P^e_{screen} = P_{max} - \frac{\Theta}{\Theta_c} (P_{max} - P_{screen}). \quad (6)$$

Replacing P_{screen} in Eq. (4) with P^e_{screen} results in the following expression;

$$\Delta PSM_N = \frac{(1 - \frac{\Theta}{2\pi}) P_{max} + (\frac{\Theta}{2\pi} - 1)[P_{max} - \frac{\Theta}{\Theta_c} (P_{max} - P_{screen})]}{P_2 - P_{screen}} \quad (7)$$

for Θ less than Θ_c.

The procedure used to determine the critical angle of the test compressor is discussed in a later section of this report. At this point, it is sufficient to indicate that 60 degrees was found to be the critical angle for both distortion levels. Using this value of Θ_c and average values of P_{max}, P_{screen}, and P_2 in Eq. (7) resulted in the corrected portion of the theoretical solution shown by the dashed-dotted curve in Figs. 4 and 5. Similar results were obtained by Dancy [13] for the compressor subjected to a less severe distortion level. Thus, Reid's concept of an "effective distortion" for distortion extents less than the critical angle provided theoretical predictions in good agreement with experimental data.

X. THE INVESTIGATION

Introduction

The purpose of this investigation was to extend the analysis of Dancy [13] by studying the performance and stalling behavior of the same test compressor subjected to more severe circumferential total pressure distortion levels. Using [13] as a reference, "classical" square-wave mesh screens were stacked to generate two distortion levels of greater magniture than that used by Dancy. To provide for ease in comparison between studies, distortion extents of 45, 90, and 180-degrees were tested as in the previous investigation. The scope of the study presented in this thesis encompassed an analysis of the effects of screen-induced total pressure distortion on

1) the overall compressor performance characteristic,
2) the stalling behavior of the compressor, particularly with respect to rotating stall cell behavior, and
3) rotor blade mean pressures for several flow conditions.

The above analysis was conducted with experimental data for undistorted flow and for three extents (45^{o}, 90^{o}, 180^{o}) of each of the three distortion levels (level used by Dancy plus the two more severe levels), defining ten inlet flow conditions. The air flow rate was manually controlled by means of a discharge valve which regulated the compressor back pressure. Several different valve settings were used during the investigation ranging from valve position 0 (maximum flow)

to the valve position at stall for a particular inlet condition. Stall was achieved by closing the valve to increase the back pressure. All tests were performed at a compressor rotational speed of 2400 RPM.

Experimental Apparatus

The experimental arrangement used throughout the investigation is shown in Fig. 6. The test apparatus included 1) a single-stage low-speed axial-flow compressor, 2) circumferential inlet distortion screens, 3) stationary instrumentation, 4) stall cell analysis equipment, and 5) an on-rotor pressure measurement system.

Axial Flow Compressor

The compressor used in this study was a General Electric Company model 5GDY34A1. The unit consisted of an axial-flow fan directly coupled to a 5.6 kilowatt (7.5 horsepower) cradled dynamometer mounted on a common bed plate. The dynamometer speed range extended from 500 to 3000 RPM. All tests were conducted at a compressor speed of 2400 RPM. The dynamometer scale and tachometer enabled the measurement of power supplied to the compressor.

The single-stage compressor consisted of a row of 37 adjustable inlet guide vanes positioned just upstream of the rotor. At mean radius the stator blade angle was 16 degrees. An eight degree angle of twist produced blade angles at the root and tip of 12 and 20 degrees, respectively. The blade span, 70.1 mm (2.76 in.), and the chord length, 44.5 mm (1.75 in.), produced an aspect ratio of 1.58.

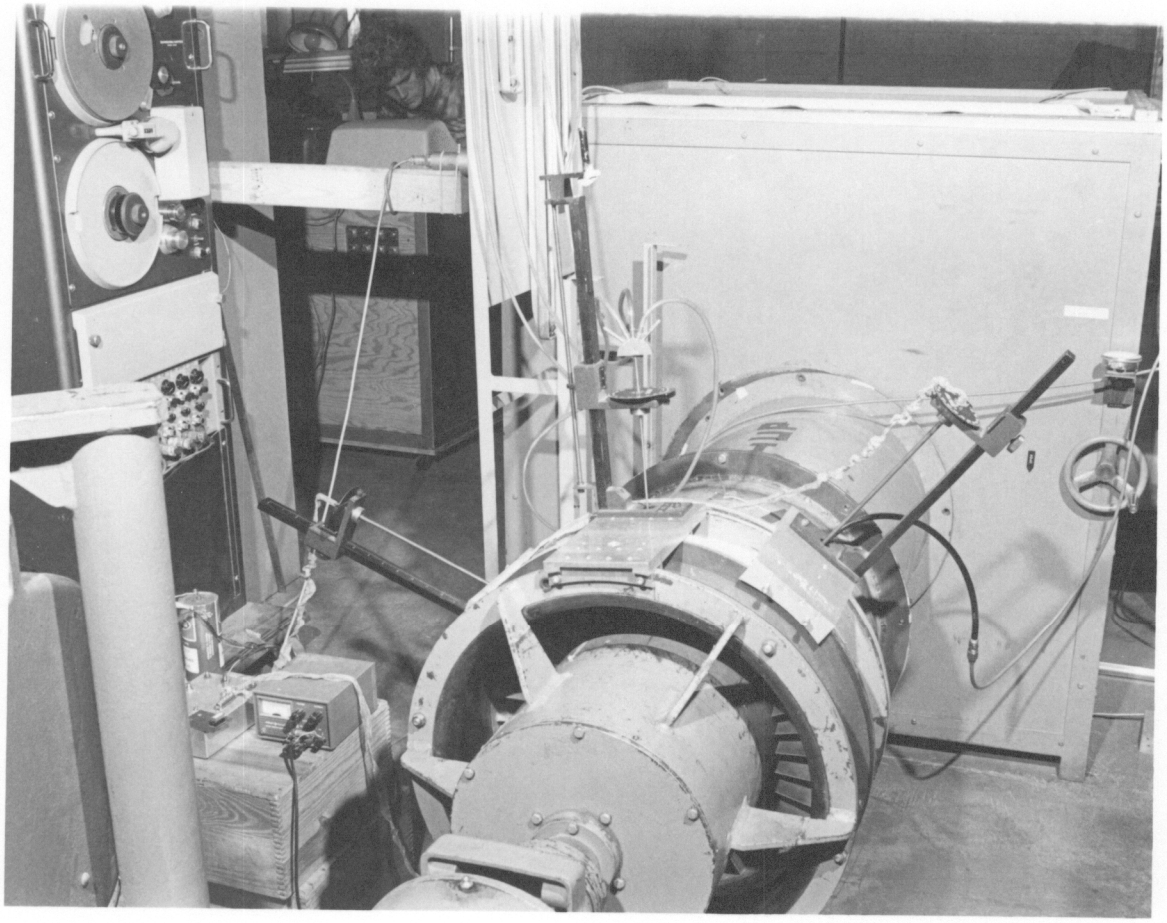

Figure 6. Photograph of Experimental Arrangement

The rotor section of the compressor consisted of 24 adjustable blades. The blade airfoil shapes were RAF #6 propeller sections having a blade angle at mean radius of 60 degrees. Root and tip blade angles were 58 and 62 degrees, respectively, due to a four degree angle of twist. The rotor blade span was 70.1 mm (2.76 in.). A chord length of 42.3 mm (1.67 in.) produced an aspect ratio of 1.66. Rotor blade solidity at mean radius was 0.84. The inner casing diameter was 314.3 mm (12.375 in.) producing a hub-tip ratio of 0.687. The outer casing diameter was 457.2 mm (18.0 in.), producing a tip clearance of 1.3 mm (0.05 in.). Typical air velocity diagrams at mean radius are shown in Fig. 7.

The compressor unit exhausted to a rigid cube-shaped plenum (1.2 m x 1.2 m x 1.2 m). A discharge duct, 50.17 cm (19.75 in.) in diameter, was connected to the plenum. Flow rate was controlled by a discharge valve which regulated air passage from the plenum into the discharge duct, allowing manual adjustment of the back pressure, and hence the flow rate. Stall was achieved by gradually increasing the back pressure. The compressor, plenum, and discharge duct arrangement is shown in Fig. 8.

A flat plate orifice was installed at the end of the discharge duct to measure volumetric flow rate. The orifice diameter was 43.18 cm (17 in.) producing a orifice-duct diameter ratio, $\frac{d}{D}$, of 0.86.

Circumferential Inlet Distortion Screens

Nine circumferential distortion screens were employed in this

U: rotor blade velocity

C_x: air axial velocity

C_ω: air tangential velocity

C: absolute air velocity

V: relative air velocity

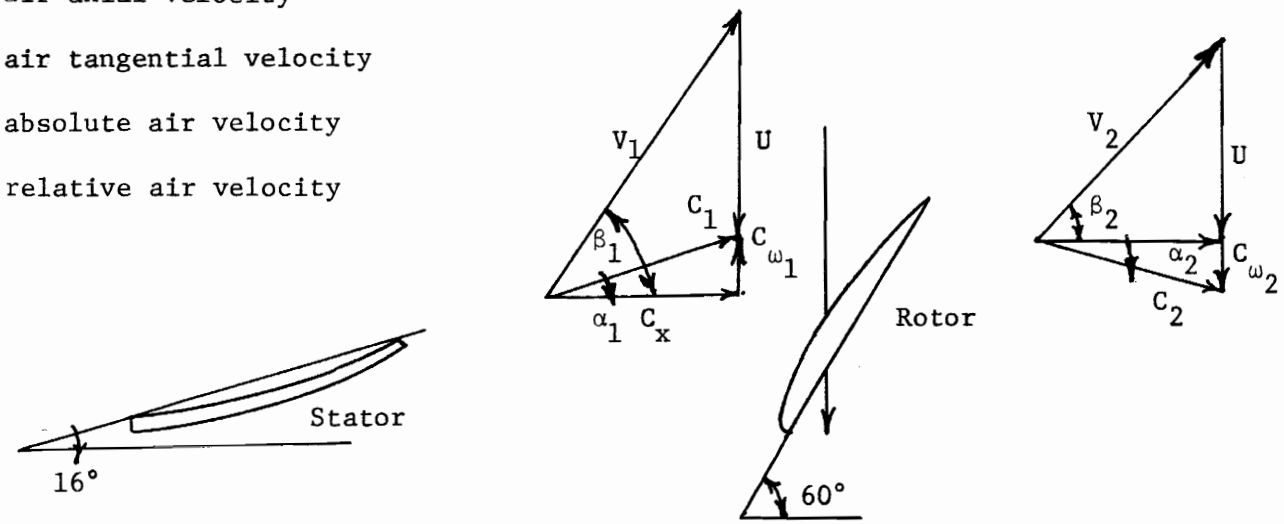

Figure 7. Typical Air Velocity Diagram at Mean Radius

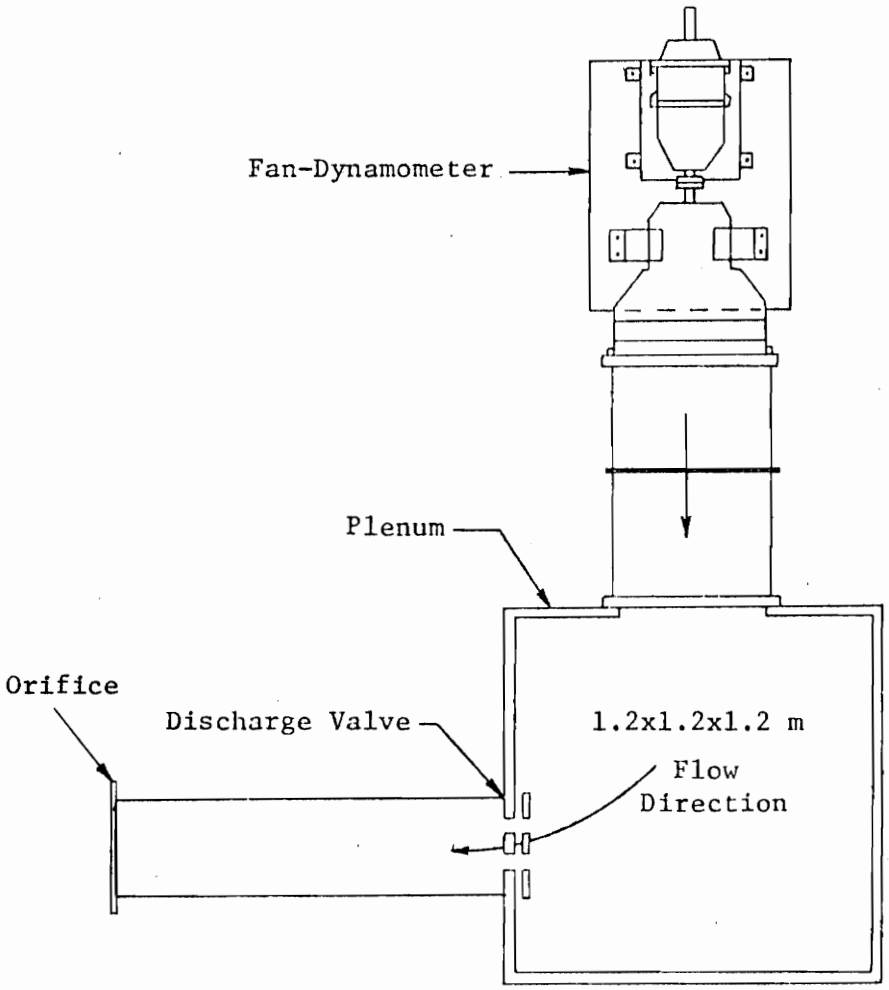

Figure 8. Compressor, Plenum, and Discharge Duct Arrangement (Adapted From Reference 13)

investigation. These nine screens generated three different distortion levels with three extents for each level being tested. The screen combinations used for the three distortion levels, presented in order of increasing total pressure loss were

1) two layers of #4 mesh steel gauze sandwiched around a #18 mesh support screen,
2) four layers of #18 mesh support screen attached to a #4 mesh support grid, and
3) six layers of #18 mesh screen sandwiched around a #4 mesh support grid.

The distortion levels provided by the screens described in 1), 2), and 3) are referred to as level 1, level 2, and level 3, respectively, in the remainder of this report. Total pressure losses behind levels 1, 2, and 3 were as high as 3.0 cm (1.2 in. H_2O), 5.3 cm (2.1 in. H_2O), and 6.4 cm (2.5 in. H_2O) at maximum flow rate. It should be mentioned here that level 1 was used by Dancy [13] in the earlier study. Circumferential extents of 45, 90, and 180-degrees were tested for each level. During compressor operation, the screens were held in place against the upstream edges of the inlet guide vanes by suction created at the inlet. Figure 9 presents a photograph of a 90-degree distortion screen placed against the inlet guide vanes.

Stationary Instrumentation and Procedure

The objective of this portion of the investigation was to determine

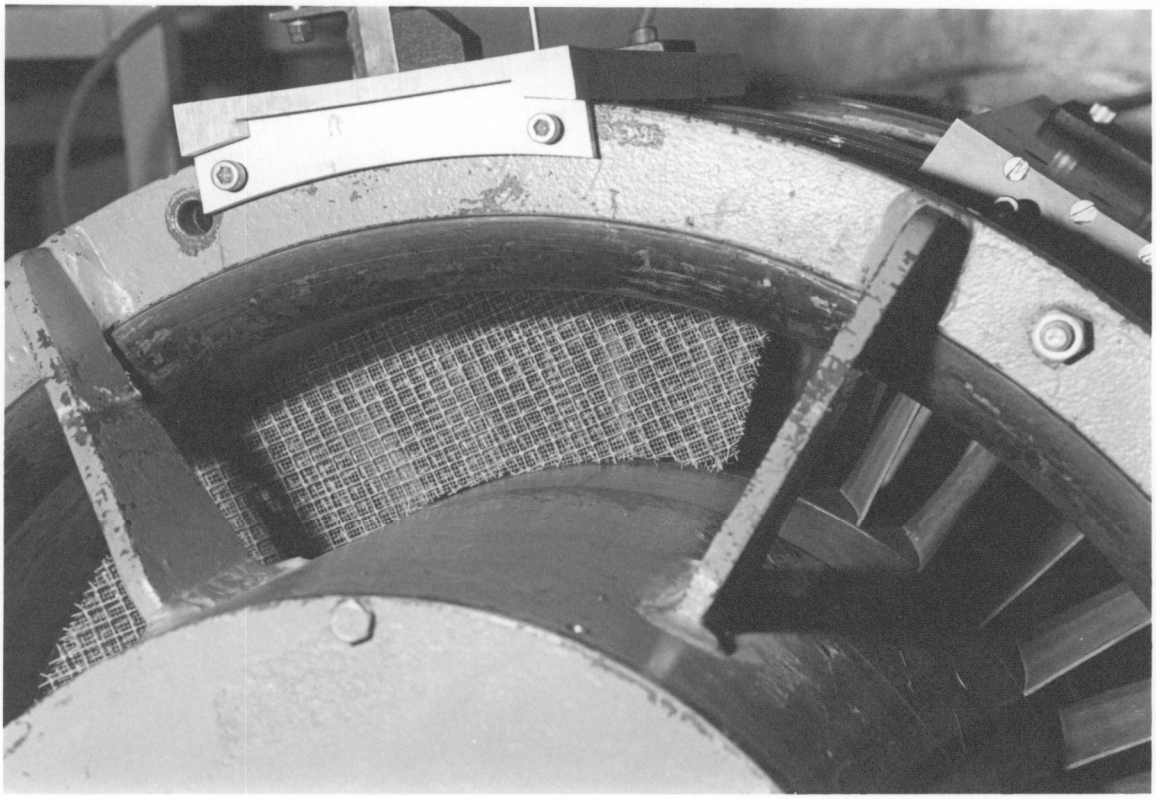

Figure 9. Photograph of 90-Degree Distortion Screen Placed Against Inlet Guide Vanes

the compressor performance characteristic for undistorted and distorted operation. Plenum pressure and volumetric flow rate measurements were required. The plenum pressure was measured through a tap in the plenum wall, using a slant-tube water manometer. This pressure represented the static (or total) pressure rise across the machine including flow losses occuring in the duct from the rotor to the plenum. An orifice installed at the end of the plenum discharge duct (see Fig. 8) was used to measure flow rate. During distorted operation, circumferential static and total pressure profiles were measured in front of and behind the rotor. These profiles were obtained by rotating the distortion screen with respect to a stationary United Sensor DC 125 directional probe. The directional probe, capable of measuring flow angles, was also used to calibrate the orifice. An adjustable mounting enabled the operator to position the probe in any radial or circumferential position between two adjacent guide vanes. The orifice calibration procedure and results of all measurements described above are presented later in this report.

Stall Cell Analysis Instrumentation and Procedure

An analysis of the effects of inlet distortion on the rotating stall behavior of the compressor was made possible through the use of two high response dynamic pressure transducers. The transducers (probes) were Kulite Semiconductor Products, Inc. Model XCQH-152-15D, having rated and maximum pressures of 103.8 KPa (15 psi) and 207.6 KPa (30 psi), respectively. The pressure reference tube was extended to

ambient conditions outside the casing throughout the investigation so as to obtain a constant reference for pressure measurements. The probes were positioned 5.08 cm (2 in.) downstream from the rotor at two circumferential locations spaced 105 degrees apart. An adjustable mounting enabled the probes to be traversed radially to the desired span position.

Transducer excitation of 9 volts D.C. was supplied to each pressure probe by two Hewlett-Packard model 6218A power supplies. The pressure signal was transmitted to a pre-amplifier which amplified the signal level approximately 800 times. A Honeywell Accudata-123 D.C. amplifier further amplified the signal and filtered frequencies above 100 Hz that appeared in the pressure signal. The system was calibrated through the use of calibrating resistors to produce an output of 1 volt corresponding to 2.54 cm (1 in.) of water pressure. The stall cell measurements were recorded on oscilloscope photographs. Before each experiment all of the analysis equipment was calibrated. Figure 10 presents a photograph taken facing upstream from behind the rotor to show the positions of the two dynamic pressure probes. The Scanivalve is also shown in the photograph.

On-Rotor Instrumentation and Procedure

Rotor blade mean pressures were measured using the pressure scanner (Fig. 10) manufactured by Scanivalve Corporation, Model #36 TR. The Scanivalve had 36 ports available for pressure measurement. However, for this investigation only ten ports were used. Six of the

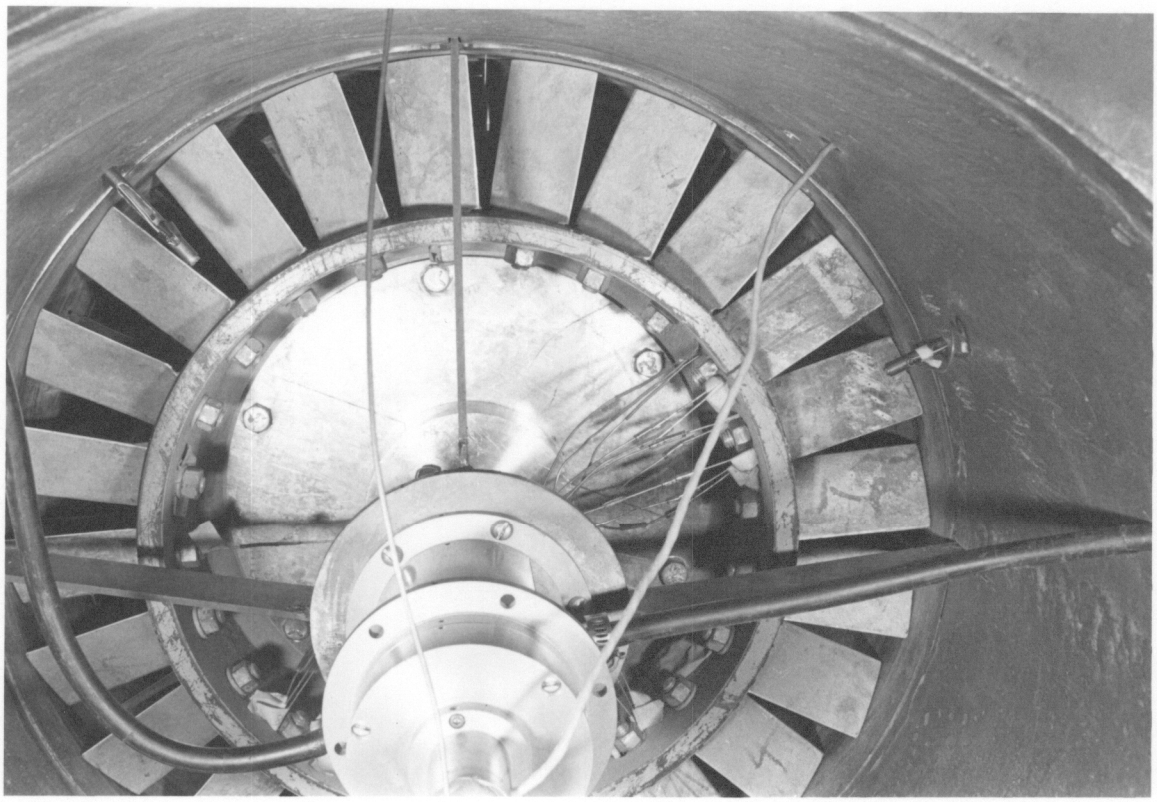

Figure 10. Photograph of Dynamic Pressure Probes and Scanivalve

rotor blades were fitted with static pressure taps. Three blades had pressure side taps at 25, 50, and 75 per cent span and the remaining three blades had suction side taps at the same positions. Each blade had 5 taps at 10, 25, 45, 65, and 85 per cent chord. In this study, data were recorded from the 10 suction and pressure side taps at 50 per cent span. The stagnation pressure at midspan was measured by a probe positioned at the rotor blade leading edge.

Metal tubes inserted in milled slots in the blades conveyed the pressure signal from the rotor blade to the Scanivalve. Through the use of an air-stepping motor which stepped once each time the flow direction was reversed, the Scanivalve scanned the ports one at a time. The pressure from each port was measured by a Druck Ltd. type PDCR 22 pressure transducer. Transducer excitation of 12 volts D.C. was supplied by a Hewlett-Packard power supply. The Honeywell D.C. amplifier was employed to amplify the output to .1 volt corresponding to 2.54 cm (1 in.) of water. The amplifier also eliminated frequencies above 100 Hz that appeared in the pressure signal. The amplified transducer output was indicated on a digital voltmeter. A low-pass filter (1000 μf capacitor and 1000 ohm resistor) was introduced in the system between the amplifier and the digital voltmeter. The filter had a cutoff frequency of .16 Hz and enabled the average blade pressures to be read as a stable signal. Before each test the Scanivalve system was calibrated. The results of the stall cell analysis and the on-rotor pressure measurements are presented in a subsequent section of this report.

Stationary Results

The purpose of this portion of the investigation was to determine the effects of circumferential inlet total pressure distortion on the overall performance of the compressor. This was accomplished by obtaining the performance characteristics for all ten inlet flow conditions. As stated previously, the flow rate was controlled throughout the investigation by regulating the back pressure via a discharge valve. Several valve settings were used to obtain the required data, ranging from valve position 0 (maximum flow) to the valve position at stall for a particular inlet condition. An orifice installed at the end of the plenum discharge duct was used to measure the flow rate.

A preliminary test was conducted to determine the relative magnitudes of distortion levels 1, 2, and 3. This involved measuring the circumferential inlet static and total pressure profiles for the 45, 90, and 180-degree extents of levels 2 and 3. The earlier study performed by Dancy [13] provided similar information for level 1. Static and total pressures were measured at the mean radius using the United Sensor directional probe placed just behind the inlet guide vanes. These pressure profiles were recorded for reference valve positions 0, 3, 5.5, 6.5, 7, and 8. Figure 11 represents the non-dimensionalized pressure distributions in front of and behind the rotor for the 180-degree extent of level 2. Similar data for level 3 are shown in Fig. 12. The results presented in these figures were obtained at maximum flow rate (valve position 0). Table 1 lists the complete average circumferential inlet static pressure readings for the three

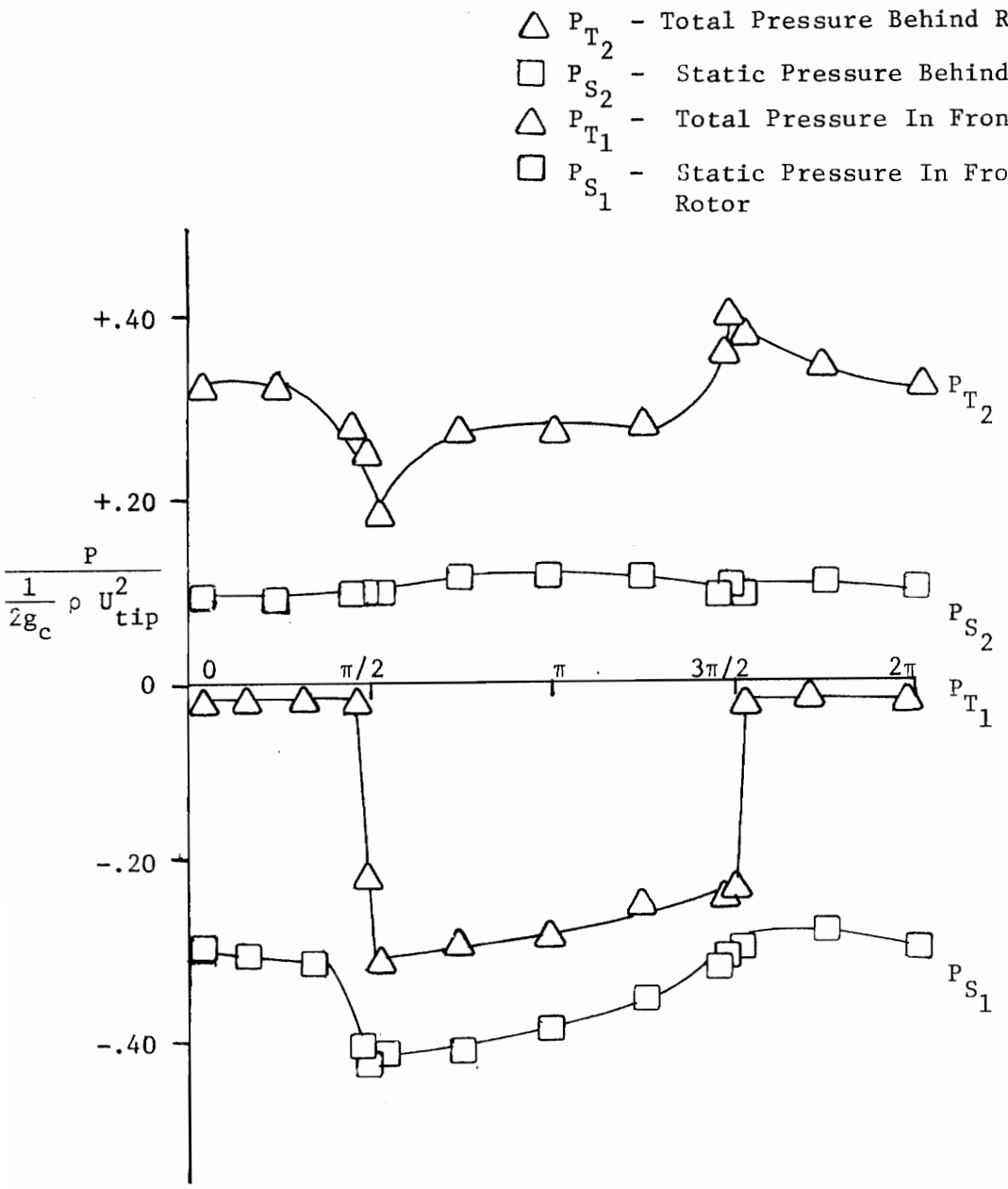

Figure 11. Inlet Static and Total Pressure Profiles In Front of and Behind Rotor for 180-Degree Extent of Distortion Level 2; Valve Position 0

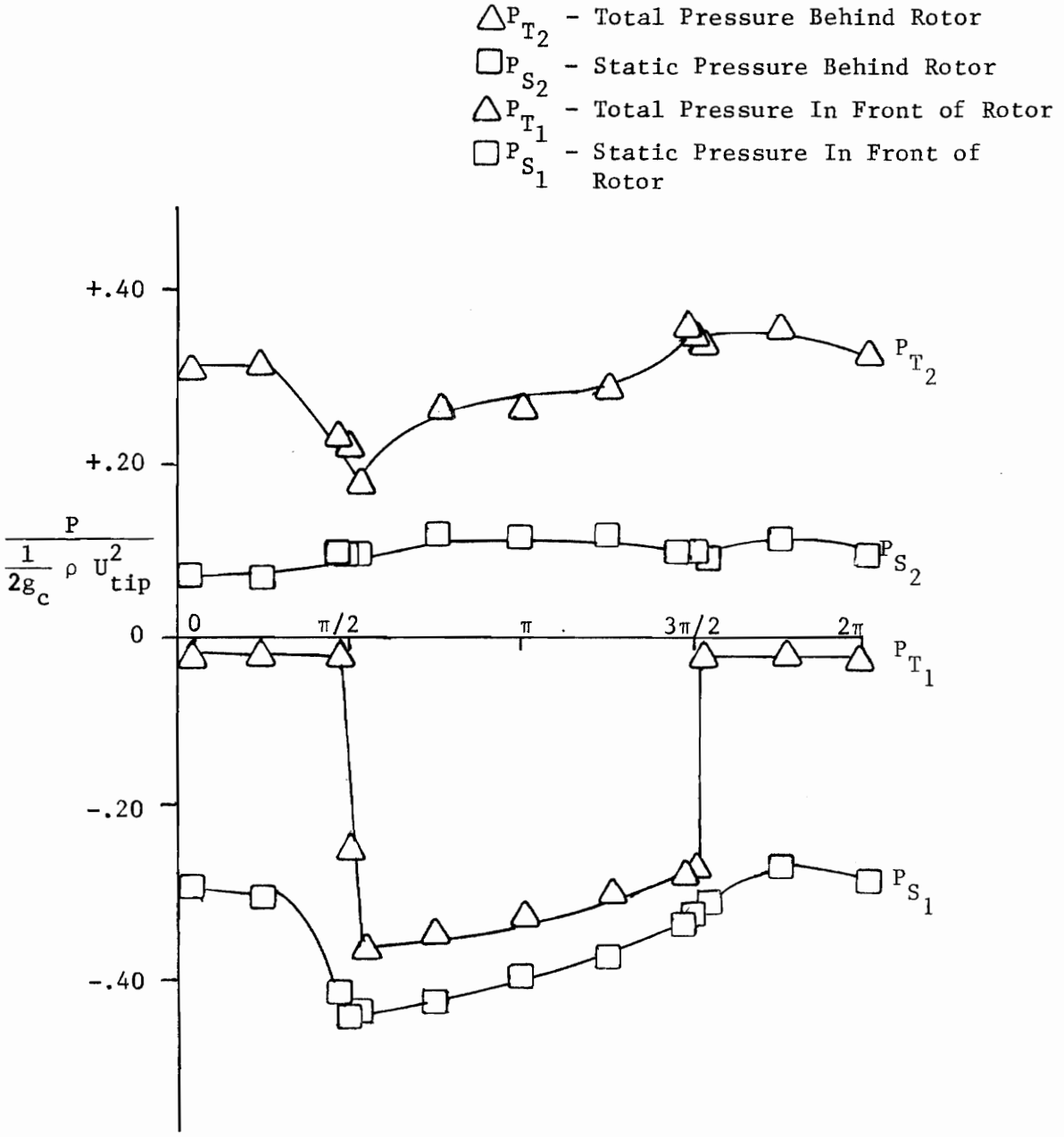

Figure 12. Inlet Static and Total Pressure Profiles In Front of and Behind Rotor for 180-Degree Extent of Distortion Level 3; Valve Position 0

Table 1. Average Circumferential Inlet Static Pressures
cm H_2O (in. H_2O)

Valve Position	Undistorted Inlet	Level 2 Extent 45°	Level 3 Extent 45°	Level 2 Extent 90°	Level 3 Extent 90°	Level 2 Extent 180°	Level 3 Extent 180°
0	-4.98(-1.96)	-5.52(-2.17)	-5.69(-2.24)	-5.54(-2.18)	-5.67(-2.23)	-6.06(-2.39)	-6.32(-2.49)
3	-4.29(-1.69)	-4.76(-1.87)	-4.92(-1.94)	-4.76(-1.87)	-4.91(-1.93)	-5.15(-2.03)	-5.46(-2.15)
5.5	-2.91(-1.15)	-3.50(-1.38)	-3.67(-1.44)	-3.32(-1.31)	-3.58(-1.41)	-3.74(-1.47)	-4.08(-1.61)
6.5	-2.20(- .87)	-2.56(-1.01)	-2.93(-1.15)	-2.82(-1.11)	-2.93(-1.15)	-3.15(-1.24)	-3.34(-1.31)
7	-1.98(- .78)	-2.47(- .97)	-2.69(-1.06)	-2.65(-1.04)	-2.75(-1.08)	-3.01(-1.19)	-3.24(-1.28)
8	-2.24(- .88)	-2.50(- .98)	-2.65(-1.04)	-2.52(- .99)	-2.59(1.02)	-2.77(-1.09)	-2.98(-1.17)

Table 2. Average Circumferential Inlet Total Pressures
cm H_2O (in. H_2O)

Valve Position	Undistorted Inlet	Level 2 Extent 45°	Level 3 Extent 45°	Level 2 Extent 90°	Level 3 Extent 90°	Level 2 Extent 180°	Level 3 Extent 180°
0	-0.13(- .05)	-1.73(- .68)	-2.01(- .79)	-1.70(- .67)	-1.85(- .73)	-2.36(- .93)	-3.00(-1.18)
3	-0.13(- .05)	-1.52(- .60)	-1.75(- .69)	-1.47(- .58)	-1.65(- .65)	-2.06(- .81)	-2.59(-1.02)
5.5	-0.13(- .05)	-1.22(- .48)	-1.42(- .56)	-1.17(- .46)	-1.24(- .49)	-1.52(- .60)	-1.96(- .77)
6.5	-0.13(- .05)	- .99(- .39)	-1.19(- .47)	- .99(- .39)	-1.04(- .41)	-1.32(- .52)	-1.63(- .64)
7	-0.13(- .05)	- .91(- .36)	-1.12(- .44)	- .97(- .38)	-1.02(- .40)	-1.30(- .51)	-1.57(- .62)
8	-0.51(- .20)	-1.07(- .42)	-1.19(- .47)	-1.04(- .41)	-1.07(- .42)	-1.27(- .50)	-1.55(- .61)

extents of distortion levels 2 and 3 at several valve settings. Table 2 provides the same information for average circumferential inlet total pressures.

The total pressure loss in the distorted flow region (see Figs. 10 and 11) caused a reduction in the air velocity. The absolute air velocity was calculated from the static and total pressures by

$$P_T - P_S = \frac{1}{2g_c} \rho C^2 \tag{8}$$

where P_T is the total pressure,

P_S is the static pressure,

C is the absolute air velocity, and

ρ is the air density.

The axial velocity was then obtained from the relation

$$C_x = C \cos \alpha_1 \tag{9}$$

where α_1 is the flow angle produced by the stators, and

C_x is the axial velocity.

Figures 13, 14, and 15 present the axial velocity in front of the rotor as a function of circumferential position for all distortion levels and extents. The circumferential inlet velocity profiles for the 180-degree extents of distortion levels 1, 2, and 3 are shown in Fig. 13. Similar results for the 90 and 45-degree extents of the three distortion levels are presented as Figs. 14 and 15, respectively.

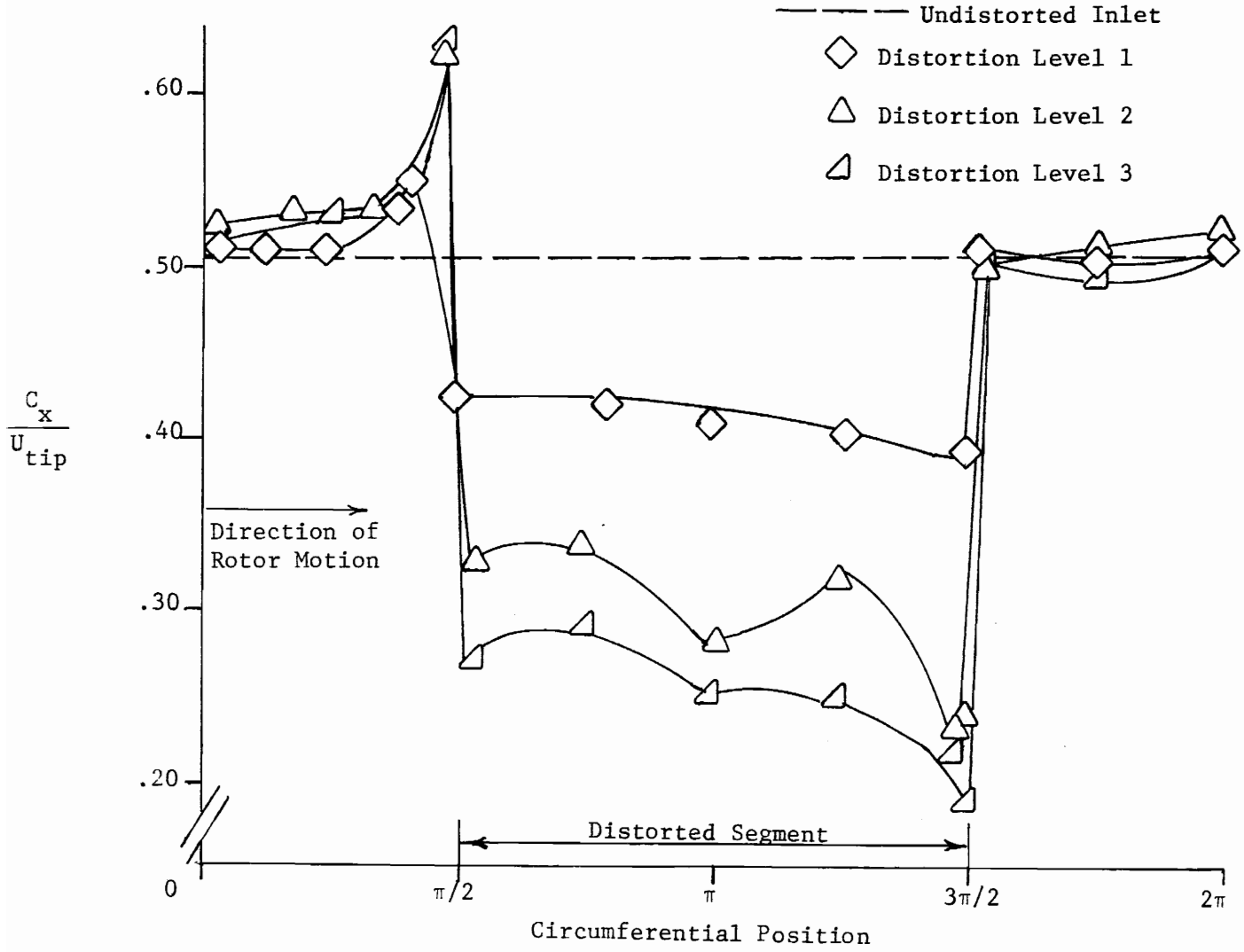

Figure 13. Circumferential Inlet Velocity Profiles for 180-Degree Extent of Distortion Levels 1, 2, and 3; Valve Position 0

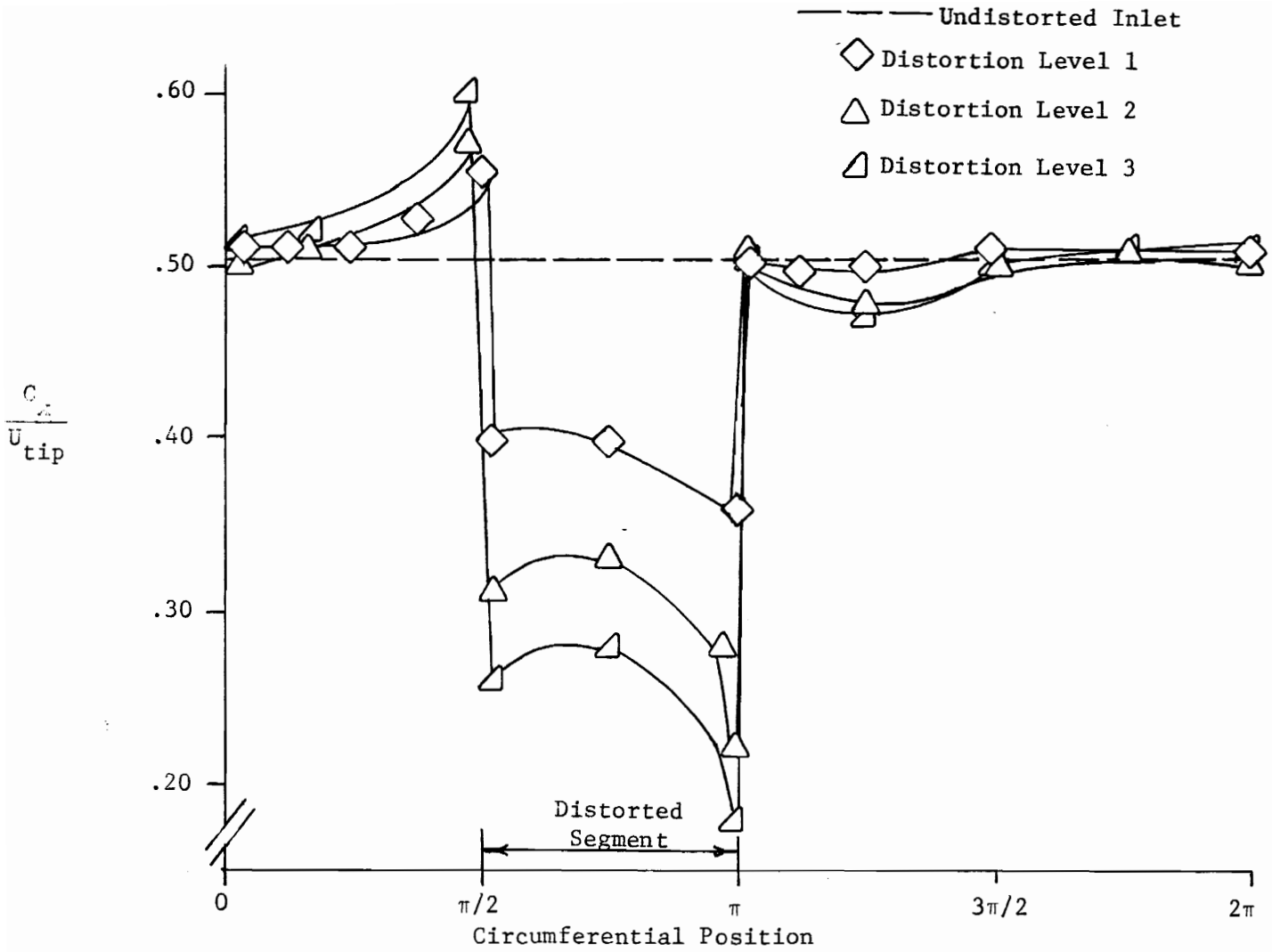

Figure 14. Circumferential Inlet Velocity Profiles for 90-Degree Extent of Distortion Levels 1, 2, and 3; Valve Position 0

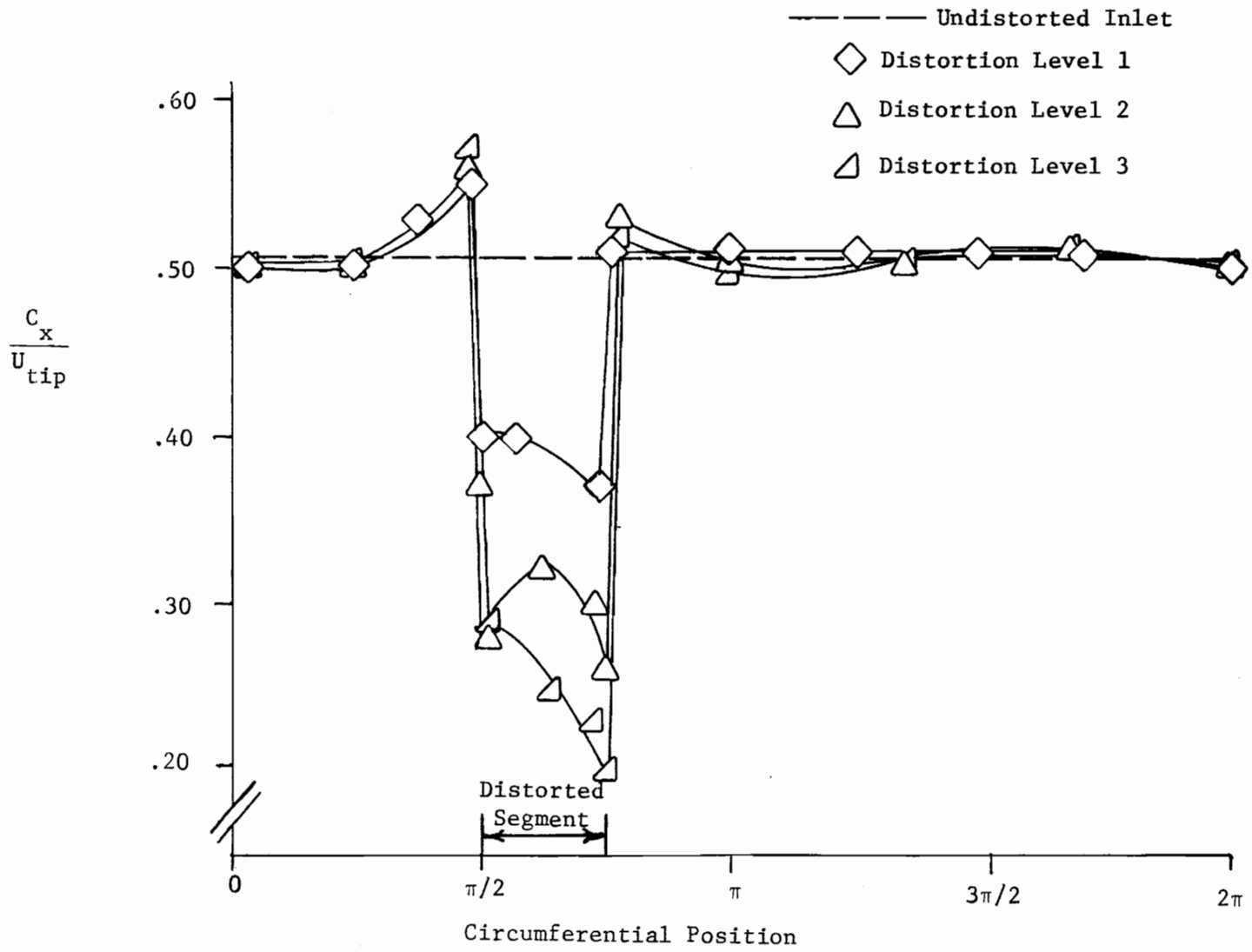

Figure 15. Circumferential Inlet Velocity Profiles for 45-Degree Extent of Distortion Levels 1, 2, and 3; Valve Position 0

All three figures represent results obtained for maximum flow rate. The axial velocity for undistorted operation is shown for comparison. The curves representing level 1 were taken from Dancy [13]. In these figures the axial velocity was non-dimensionalized by the rotor blade tip speed. The shape of the circumferential inlet velocity profiles remained approximately the same as the flow rate was decreased. Figures 16 through 19 present the axial velocity profile for the 180-degree extent of level 2 as the valve was gradually closed to induce stall.

In the distorted flow region, the reduction in axial velocity led to an increase in the air incidence angles. Incidence angles were calculated from the flow angle data measured by the directional probe. Average incidence angle values for several flow conditions (valve positions 0, 3, 5.5, 6.5, 7, and 8) are presented in Table 3. The circumferential variations in incidence angle for the 180-degree extents of levels 2 and 3 are shown in Fig. 20. This effect of inlet total pressure distortion contributes to compressor stall.

The average angle of attack was found to be 12.3 degrees at the onset of stall for undistorted operation. The normalized rotor inlet dynamic pressure profiles for the 180-degree extents of levels 2 and 3 are presented in Fig. 21, with several local angles of attack indicated. The curve representing level 1 in this figure was taken from Dancy [13]. The three curves depict the dynamic pressure profile for one complete rotor revolution during which the compressor is operating near the stable stall condition. Comparison of the three pressure profiles revealed discrepancies between distortion level 1 and levels

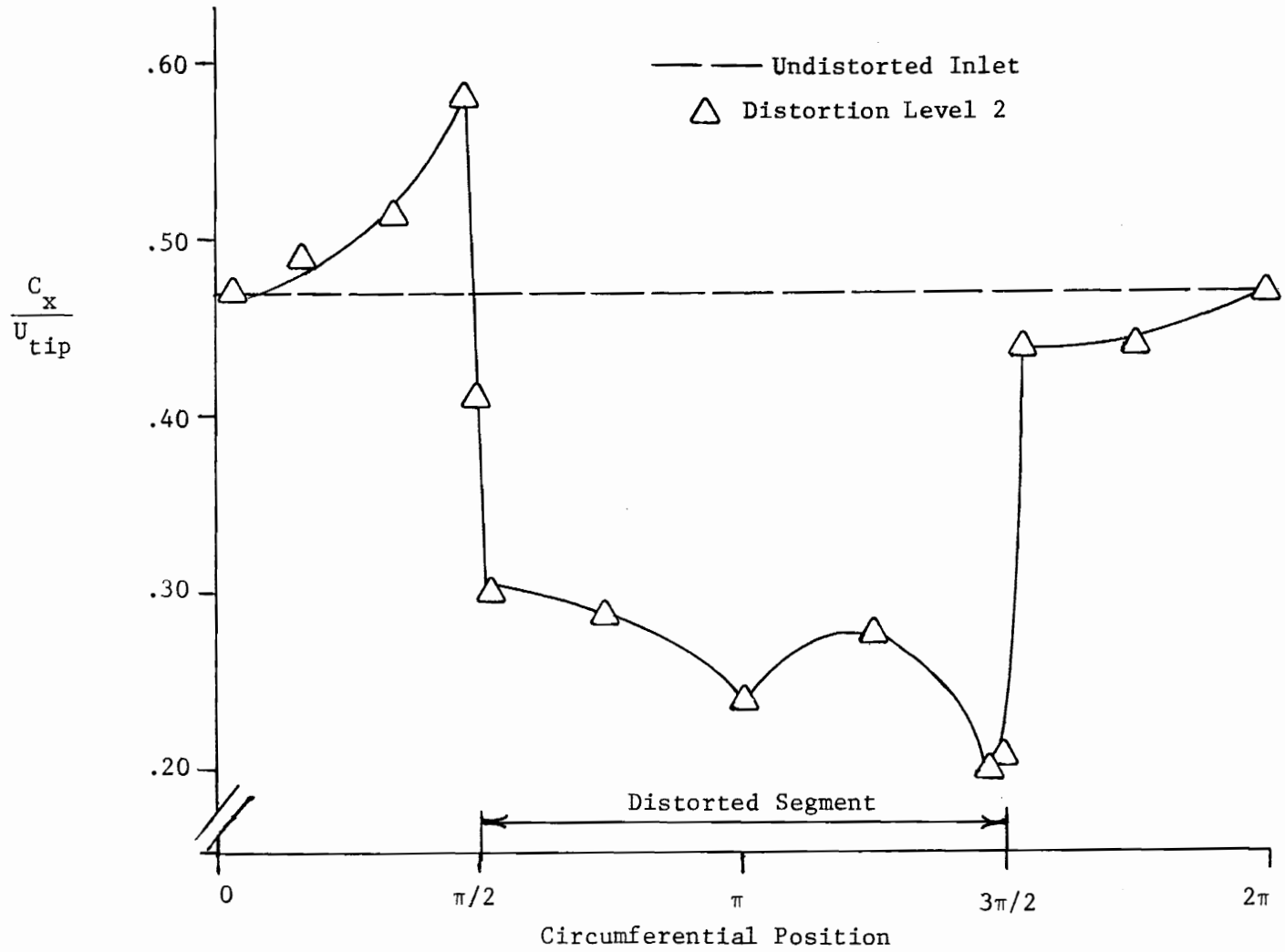

Figure 16. Circumferential Inlet Velocity Profile for 180-Degree Extent of Distortion Level 2; Valve Position 3

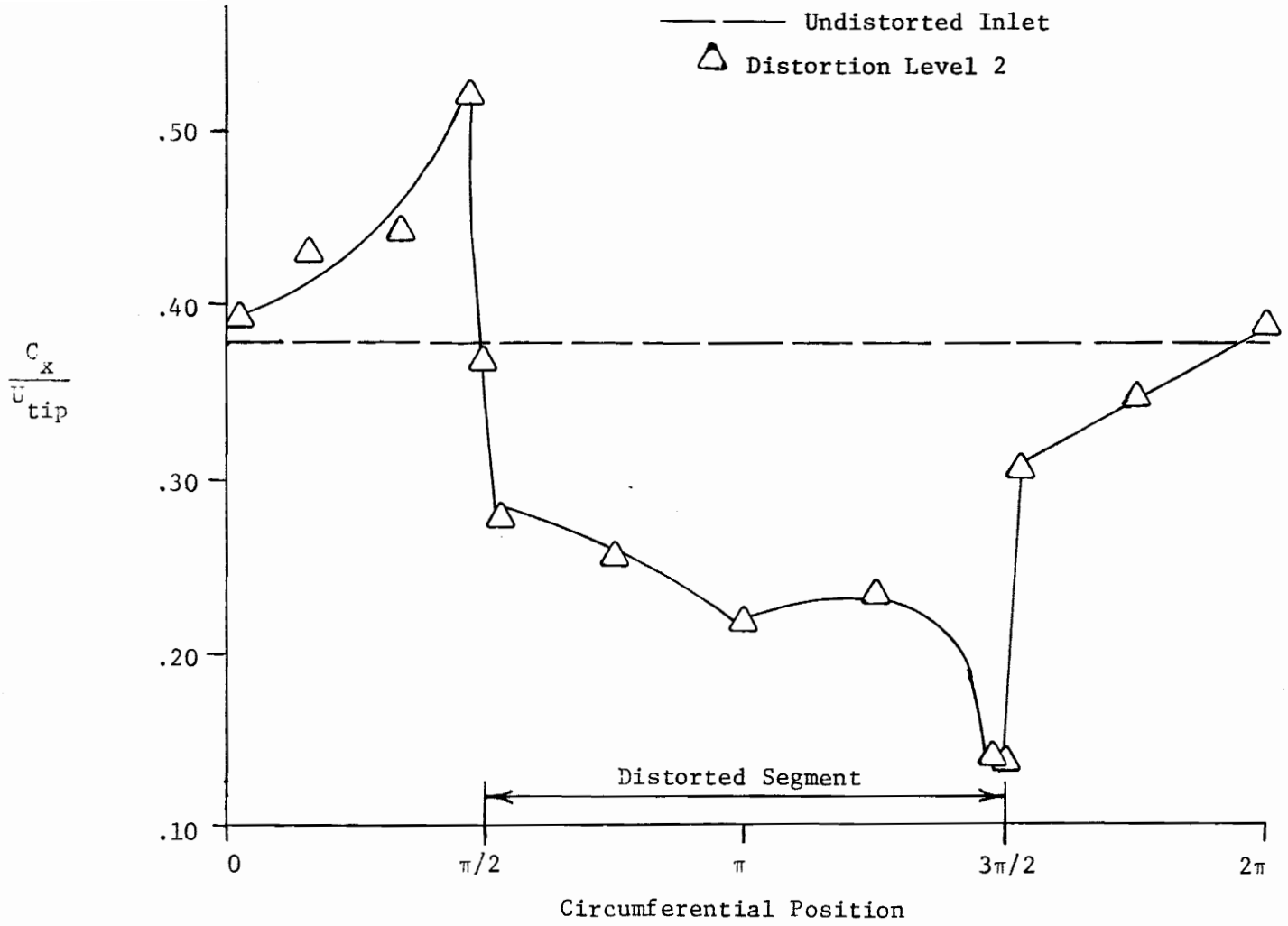

Figure 17. Circumferential Inlet Velocity Profile for 180-Degree Extent of Distortion Level 2; Valve Position 5.5

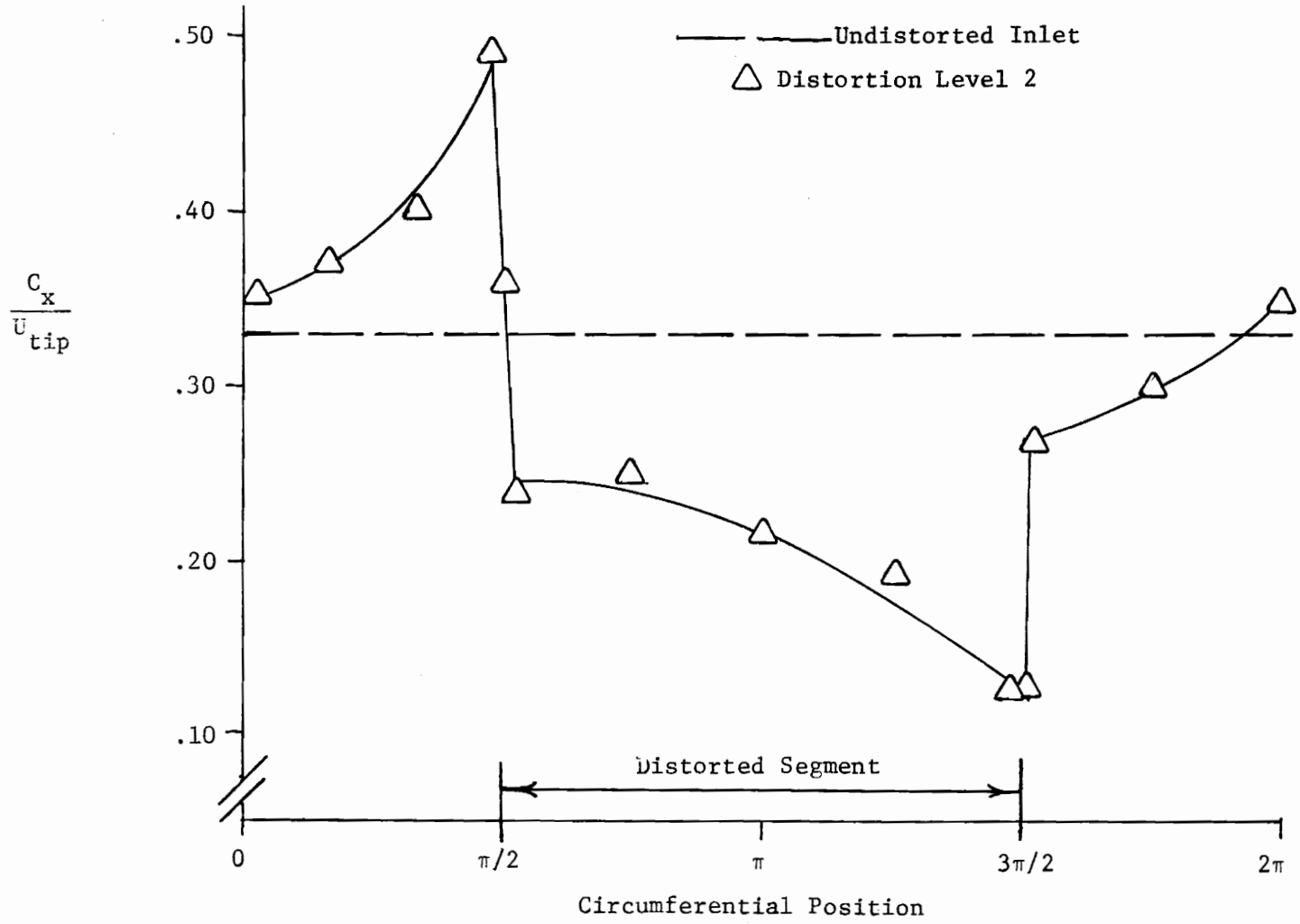

Figure 18. Circumferential Inlet Velocity Profile for 180-Degree Extent of Distortion Level 2; Valve Position 6.5

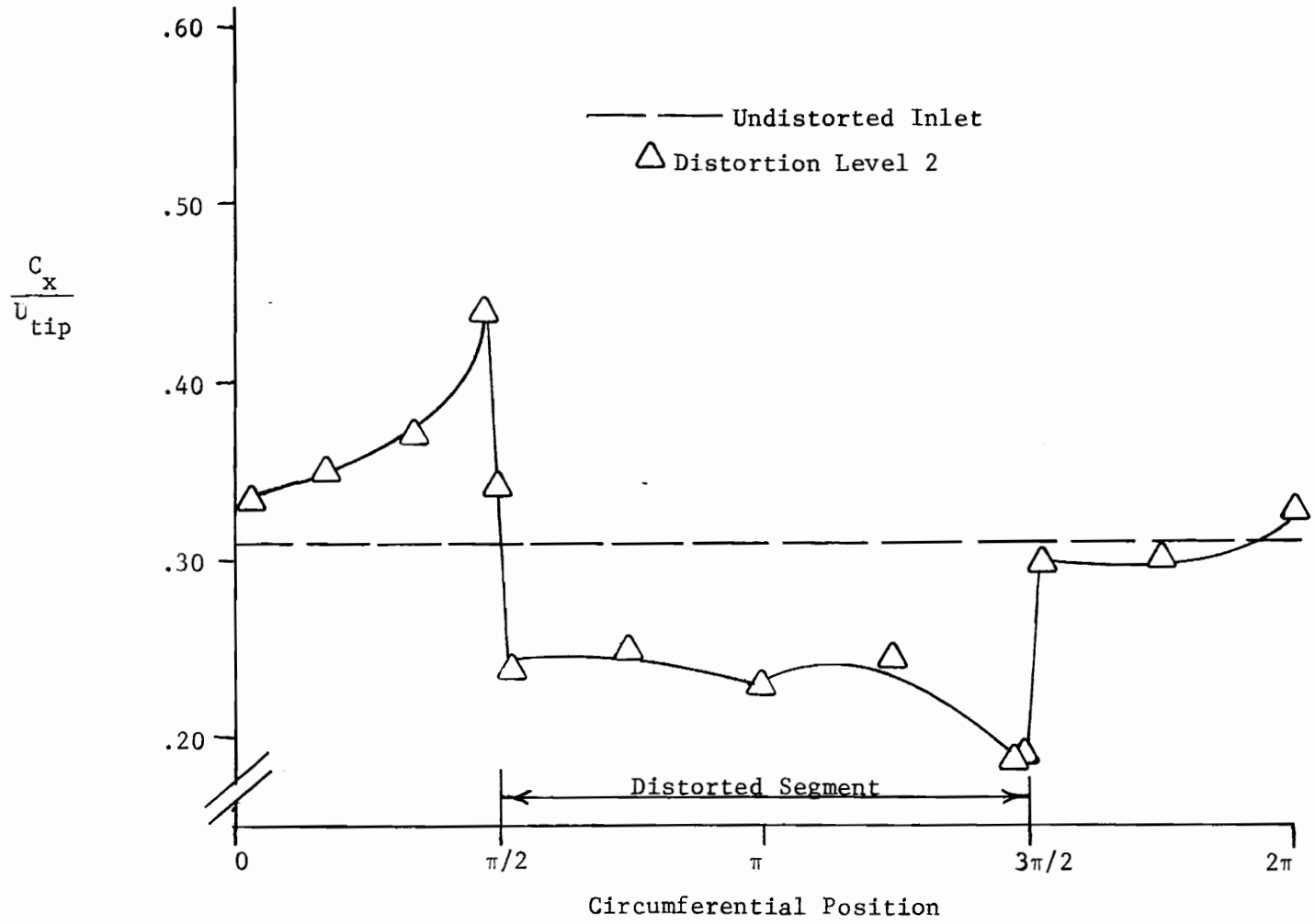

Figure 19. Circumferential Inlet Velocity Profile for 180-Degree Extent of Distortion Level 2; Valve Position 7

Table 3. Average Incidence Angles
(degrees)

Valve Position	Undistorted Inlet	Level 2 Extent 45°	Level 3 Extent 45°	Level 2 Extent 90°	Level 3 Extent 90°	Level 2 Extent 180°	Level 3 Extent 180°
0	5.6	8.6	9.2	8.3	9.1	9.5	11.1
3	7.0	10.0	10.5	9.8	10.4	11.0	12.3
5.5	10.4	12.5	13.0	12.4	12.9	13.5	14.3
6.5	12.4	14.3	14.6	14.2	14.6	14.7	15.8
7	13.6	15.1	15.3	14.2	14.3	14.4	14.9
8	13.0	14.6	14.5	14.4	14.3	14.4	14.8

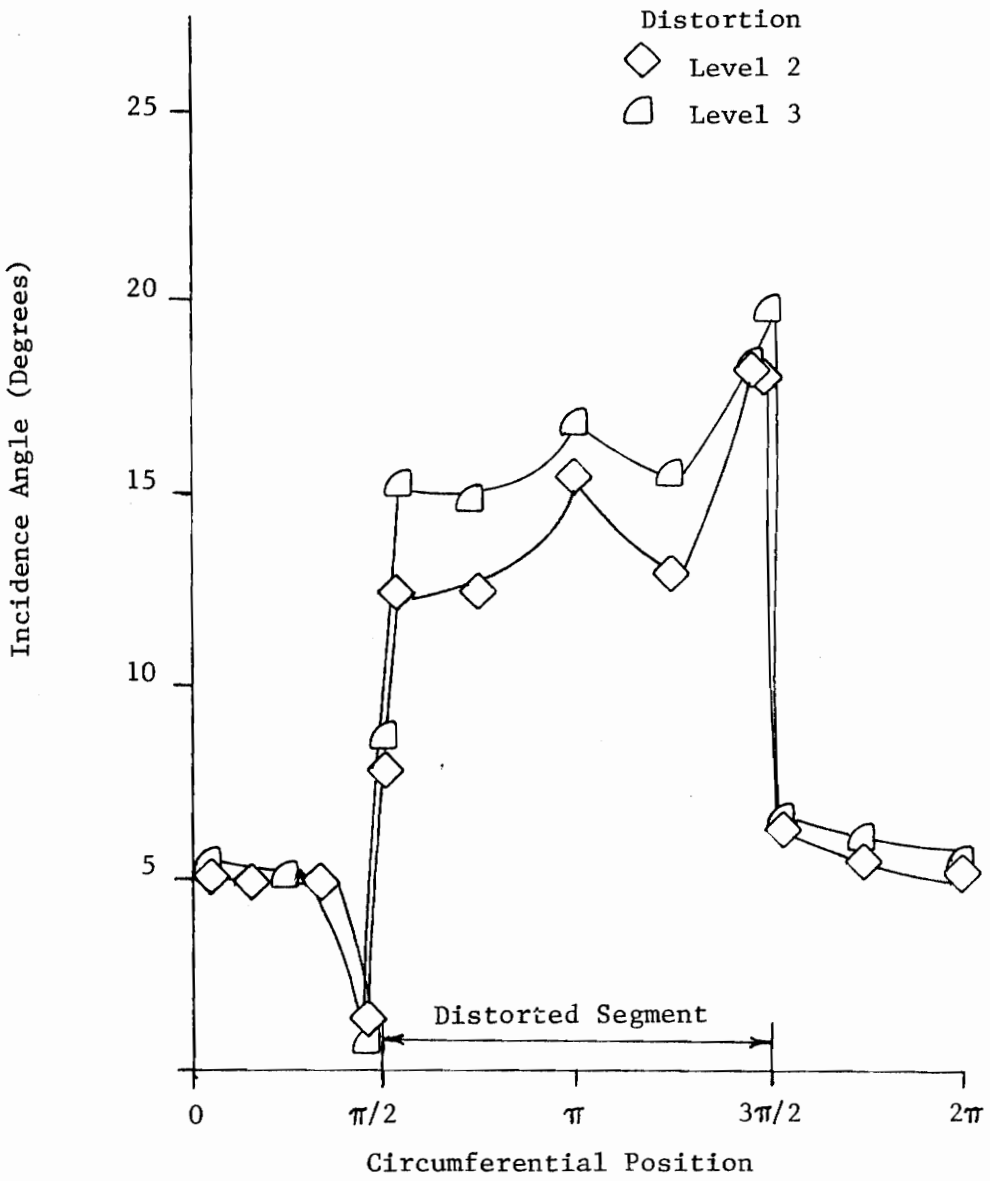

Figure 20. Incidence Angle as a Function of Circumferential Position for 180-Degree Extent of Distortion Levels 2 and 3; Valve Position 0

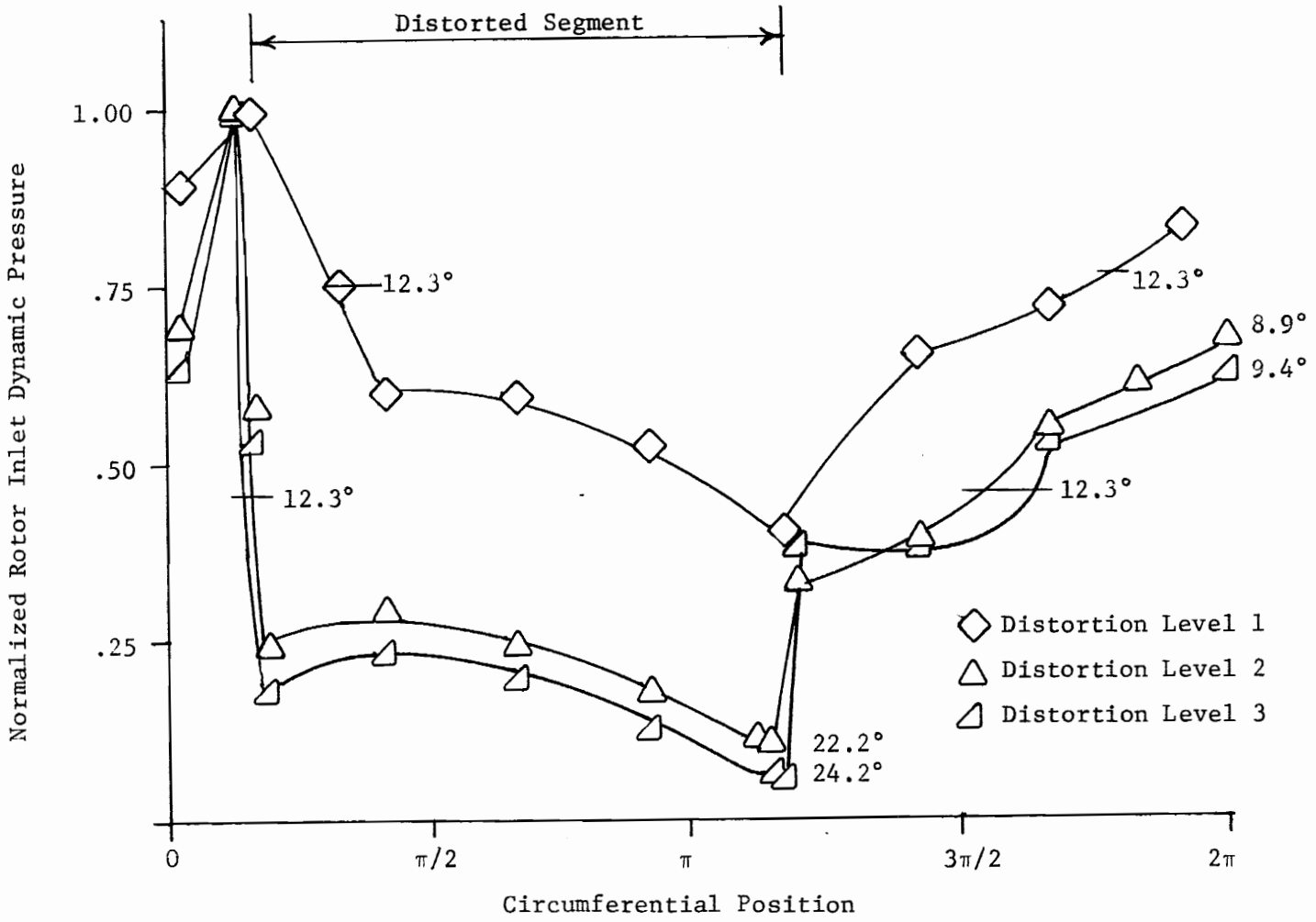

Figure 21. Rotor Inlet Dynamic Pressure Profiles for the 180-Degree Extent of Distortion Levels 1, 2, and 3; Valve Position 6.5

2 and 3 in angle of attack values at the same dynamic pressure. For valve position 6.5 (used for all three curves), stable operation was observed for the compressor subjected to distortion level 1. However, at the same valve position, the compressor operated very near stall when subjected to distortion levels 2 and 3. This contrast in flow stability at the same valve position for the three distortion levels probably accounted for the differences in angle of attack values.

It should be recalled that all of the above data were taken with the United Sensor directional probe at mean radius.

The above results provided a description of the flow distribution at the compressor inlet for each distortion level and extent. Next, the performance characteristics for all ten inlet conditions were obtained. This required the measurement of total pressure rise across the machine and the flow rate. The total pressure rise was taken as the difference between the plenum pressure and inlet total pressure which was assumed to be the ambient pressure. An orifice was used to measure the flow rate.

The orifice was calibrated with respect to the flow rate measured at the compressor inlet. For the flow rate calibration, the directional probe was positioned at 70 per cent span immediately behind the inlet guide vanes (undistorted inlet). Two "flow adjustment factors" to account for boundary layers near the inner and outer wall were required to obtain the "effective" annulus area. Boundary layer adjustment factors were determined for valve positions 0, 1, 2, 3, 4, 5, 5.5, 6, 6.5, and 7 corresponding to flow rates ranging from the

maximum value to that at the onset of stall. The measurement of radial velocity profiles enabled these factors to be obtained by dividing the average axial velocity by the velocity measured at 70 per cent span. For all valve settings used in this portion of the calibration process, the axial velocity at 70 per cent span represented the maximum axial velocity of each radial velocity profile. For this compressor, this is true for the range of unstalled flows. Therefore, the boundary layer adjustment factors essentially corrected the maximum velocity measured in each case to the average axial velocity. Figure 22 shows a typical radial velocity profile with the average axial velocity indicated by a dotted line. The flow adjustment factor to account for wakes behind the guide vanes was assumed to be 0.96 (from Dancy [13] for all valve settings. The boundary layer and wake adjustment factors were combined for each valve setting tested to provide the flow adjustment factors in Table 4.

Using the adjustment factors of Table 4, the inlet flow rate was calculated by

$$Q_{inlet} = C_{x_{meas}} \times F.F. \times A_i \qquad (10)$$

where Q_{inlet} is the flow rate measured by the directional probe at the compressor inlet.

$C_{x_{meas}}$ is the axial velocity measured at 70 per cent span,

F.F. is the flow adjustment factor, and

A_i is the inlet annulus area.

Equating the inlet flow rate to the expression for the flow rate

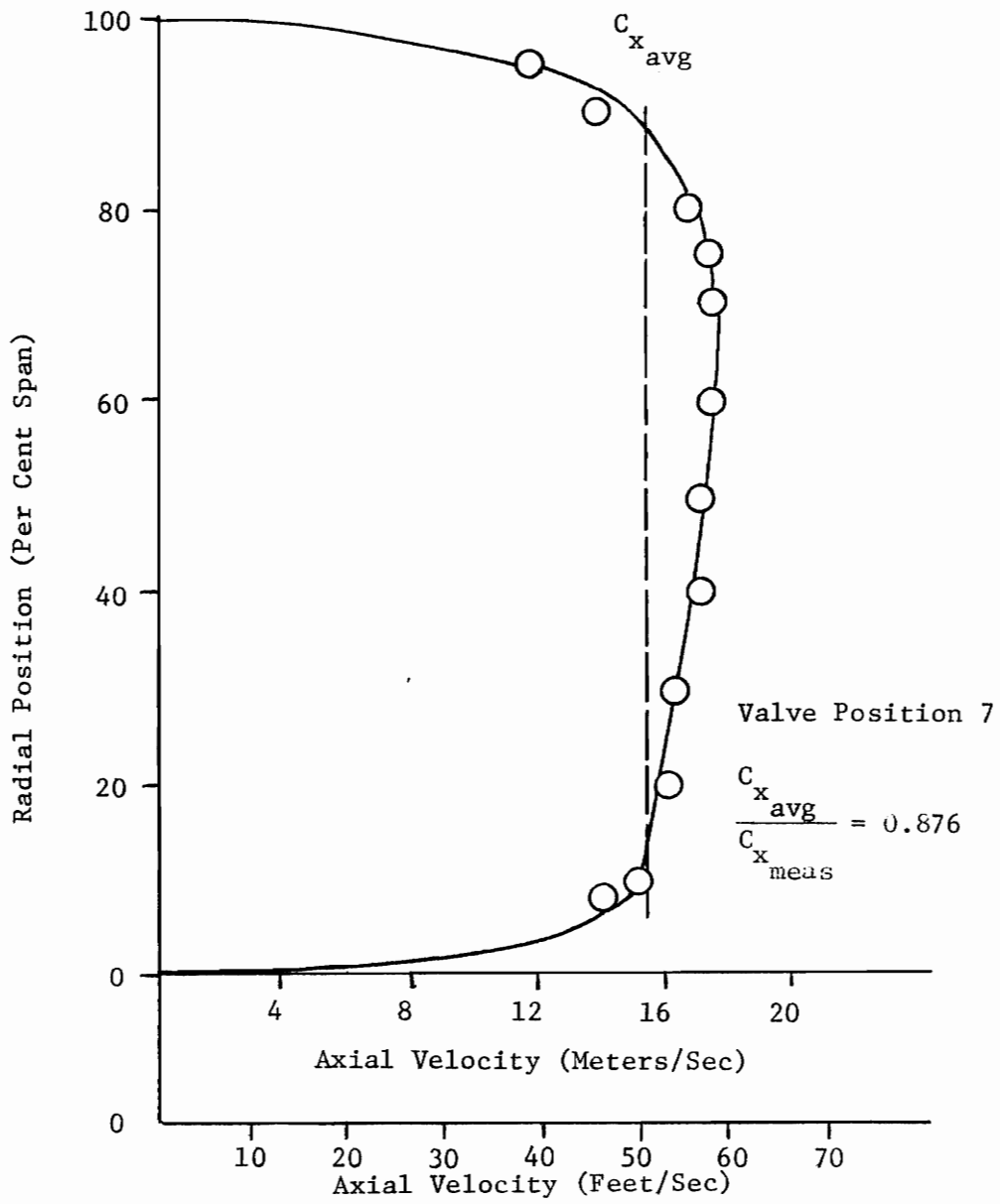

Figure 22. Radial Velocity Profile Behind Inlet Guide Vanes

Table 4. Flow Adjustment Factors for Several Valve Positions

Valve Position	Flow Adjustment Factor
0	0.900
1	0.900
2	0.878
3	0.878
4	0.878
5	0.878
5.5	0.862
6	0.862
6.5	0.840
7	0.840

measured by the orifice [16] gave

$$Q_{inlet} = \frac{C_v}{\sqrt{1 - (\frac{A_2}{A_1})^2}} A_2 \sqrt{\frac{2g_c}{\rho}} \sqrt{\Delta p} \qquad (11)$$

where C_v is the orifice flow coefficient,

A_1 is the cross-sectional area of the discharge duct,

A_2 is the cross-sectional area of the orifice, and

Δp represents the static pressure drop across the orifice.

The above equation was rearranged to solve for the orifice flow coefficient,

$$C_v = \frac{Q_{inlet} \sqrt{1 - (\frac{A_2}{A_1})^2}}{A_2 \sqrt{\frac{2g_c}{\rho}} \sqrt{\Delta p}} . \qquad (12)$$

The procedure described above was followed to calibrate the orifice at a number of valve settings corresponding to the flow rates ranging from the maximum value to that at the onset of stall.

Extending the orifice calibration curve to the flow rate at stable rotating stall required a slightly different technique than used previously. During stable rotating stall, the stall cell was found to extend forward, encompassing the original probe position behind the inlet guide vanes. At this point, the cell extended from about 70 per cent span to the annulus outer wall (stall cell details are presented in the next section). The presence of the stall cell

prevented measurements of the inlet radial velocity profile and hence, the average axial velocity. Therefore, for this case, the true flow rate was measured by placing the directional probe directly behind the rotor. At this position, the radial velocity profile was measured and the result is shown in Fig. 23. The average axial velocity is represented by the dotted line. Multiplying the average axial velocity by the annulus area permitted the true flow rate to be determined. From this point on, Eqs. 11 and 12 of the calibration procedure described previously were used to obtain the orifice flow coefficient with stable rotating stall. The orifice calibration curve for the entire range of flow rates investigated is shown in Fig. 24. The flow coefficient is presented as a function the orifice static pressure drop.

To determine the flow rate for the compressor performance characteristics, the pressure drop across the orifice was measured. The orifice calibration curve (Fig. 24) was used to find the flow coefficient for a particular pressure drop, enabling the flow rate to be calculated from the equation (shown previously as the right hand side of Eq. 11)

$$Q = \frac{C_v}{\sqrt{1 - \left(\frac{A_2}{A_1}\right)^2}} \sqrt{\frac{2g_c}{\rho}} \sqrt{\Delta p} \quad . \tag{13}$$

For the compressor performance characteristics, the flow rate was varied from valve position 0 to the valve position at stall for a particular inlet condition. The dynamic pressure probes were used to

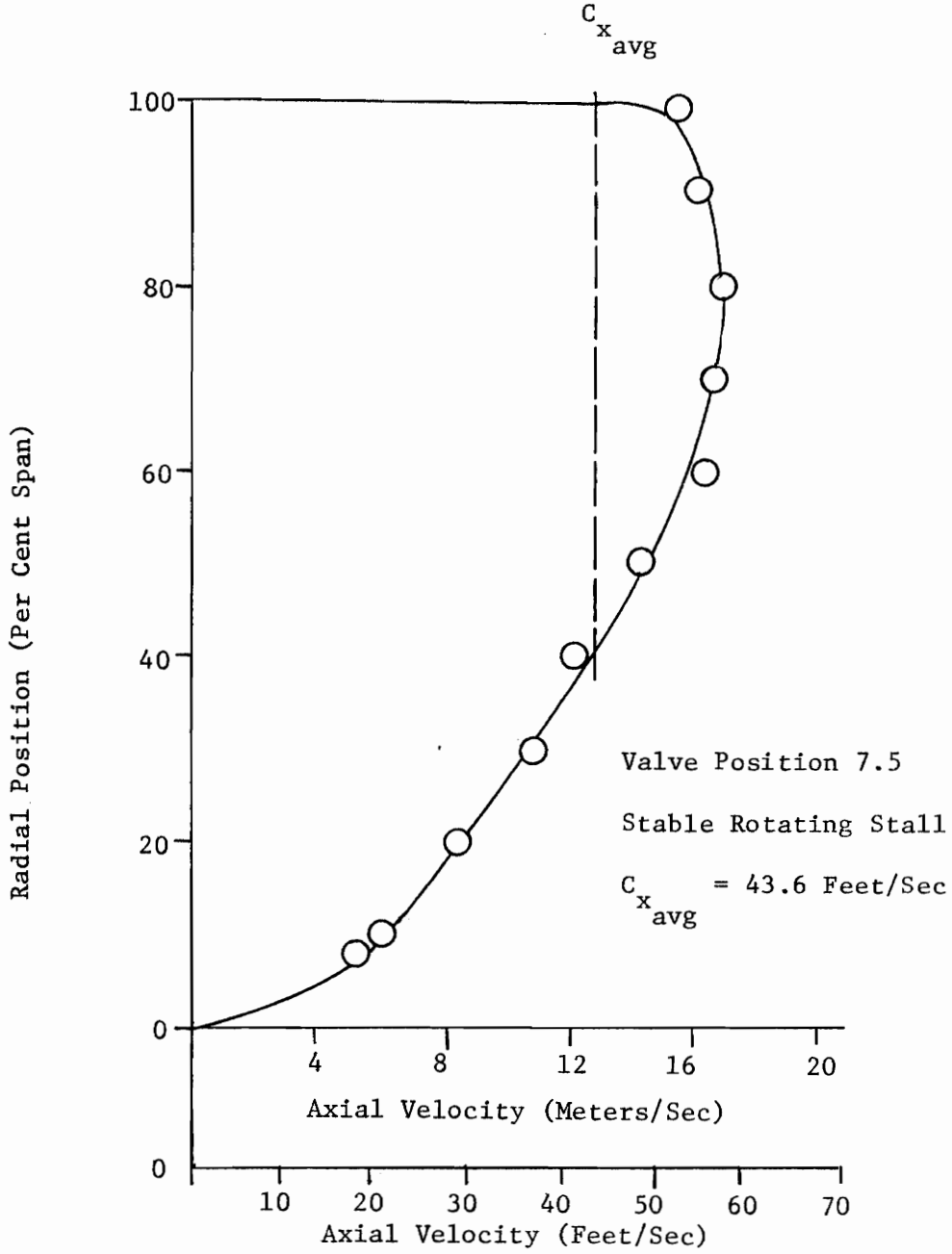

Figure 23. Radial Velocity Profile Behind Rotor

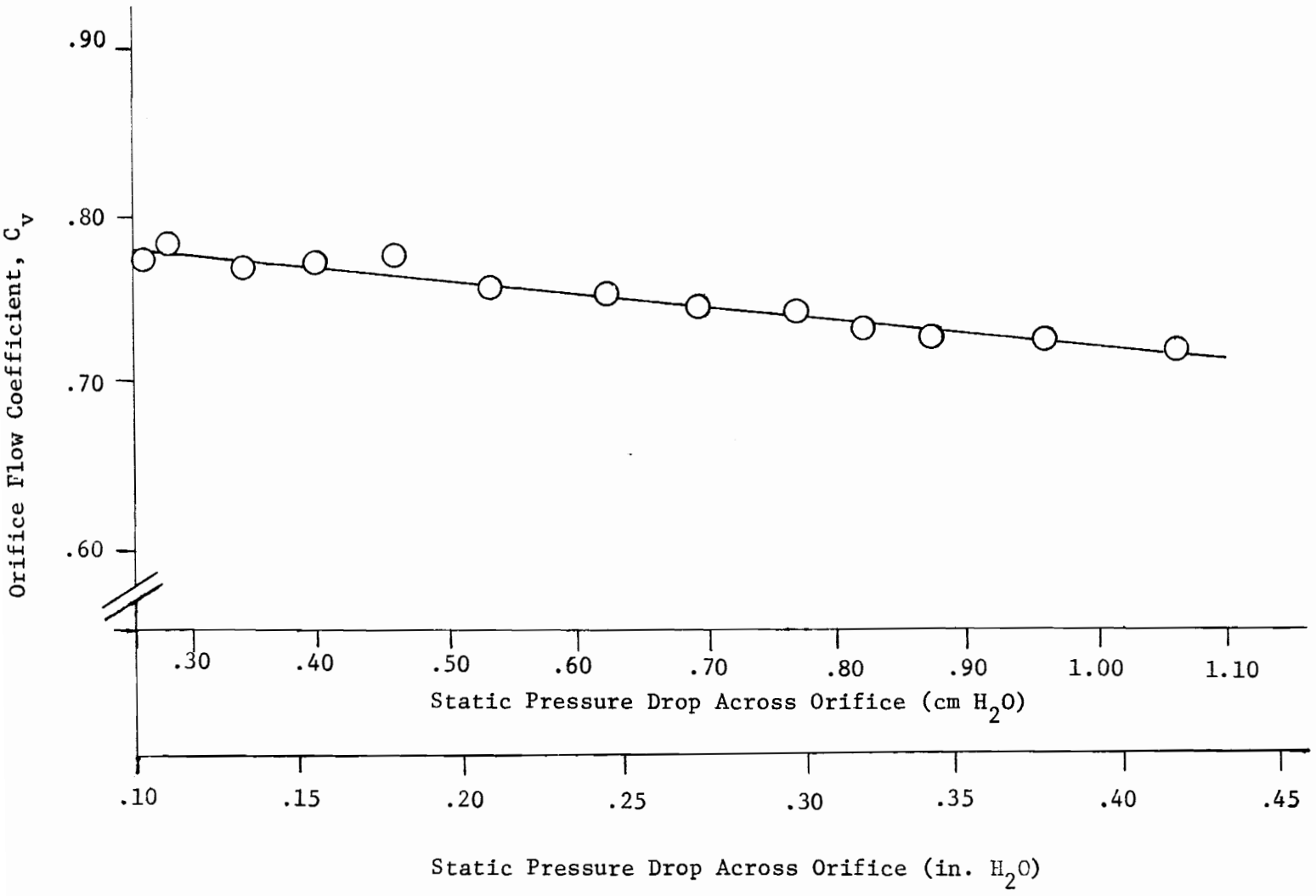

Figure 24. Orifice Calibration Curve

indicate the development of stable rotating stall. Table 5 lists the volumetric flow rates measured by the orifice in determining the performance maps. The performance characteristics for all ten inlet flow conditions are shown in Figs. 25, 26, and 27. In these figures, the flow rate has been expressed in terms of the flow coefficient C_x/U_{tip}. Figure 25 presents the characteristics for the 180-degree extents of distortion levels 1, 2, and 3. The performance characteristics for the 90 and 45-degree extents of the three distortion levels are shown in Figs. 26 and 27, respectively. The undistorted performance characteristic is included in the above figures for comparison.

Stall Cell Analysis Results

The dynamic pressure transducers were used to indicate the inception of rotating stall for the performance characteristics presented in the preceeding section. The compressor was found to enter rotating stall when the mass flow rate was lowered sufficiently. The distortion screens reduced the mass flow rate through the compressor due to their low porosity and precipitated stall at an earlier (more open) valve setting than for undistorted operation. In Appendix B, the ten different inlet flow conditions are listed with the valve position at which stable rotating stall occured for each condition.

The critical angle of spoiling for the compressor subjected to distortion levels 2 and 3 was also determined through the use of the dynamic pressure probes. Based on the undistorted compressor entering stall at valve position 7.25, the critical angle was

Table 5. Volumetric Flow Rates for Compressor Performance Characteristics (m^3/min)

Valve Position	Undistorted Inlet	45-Degree Extent			90-Degree Extent			180-Degree Extent		
		Level 1	Level 2	Level 3	Level 1	Level 2	Level 3	Level 1	Level 2	Level 3
0	132.6	131.4	131.4	130.2	130.2	127.8	125.1	126.3	120.7	114.8
1	130.2	128.4	128.4	127.8	127.8	123.7	122.2	123.7	117.7	111.2
2	127.8	125.1	126.3	123.7	123.1	120.7	119.2	120.7	115.4	106.2
3	123.7	121.6	122.2	120.1	119.2	116.2	114.8	116.2	107.9	102.0
4	117.7	116.2	114.8	113.0	113.0	109.7	106.2	107.9	102.0	96.1
5	106.2	105.3	104.1	102.0	102.0	100.2	98.2	100.2	94.0	89.3
6	94.0	94.0	92.8	94.0	91.6	89.3	89.3	89.3	84.2	81.5
*	(6.5) 86.9	(6.5) 85.4	(6.5) 86.9	(6.5) 86.9	(6.5) 84.2	(6.5) 84.2	(6.5) 81.5	(6.5) 84.2	(6.5) 78.9	(6.1) 78.9
	(7.0) 81.6	(6.75) 81.6	(7.0) 80.1	(6.75) 84.2	(7.0) 78.9	(6.6) 78.9	(6.75) 75.9	(6.6) 78.9	(6.6) 75.9	(6.35) 75.9
	(7.5) 73.0	(7.0) 78.8	(7.2) 75.9	(7.0) 78.9	(7.25) 72.9	(7.0) 75.9	(7.0) 72.9	(6.9) 75.9	(6.8) 72.9	(6.6) 72.9
		(7.25) 72.9	(7.25) 72.9	(7.25) 72.9	(7.25)	(7.1) 72.9		(7.1) 72.9		

*Due to stable stall occuring at different valve settings for the ten inlet flow conditions, the valve position is indicated in parentheses to the upper right of the flow rate for the remainder of the table.

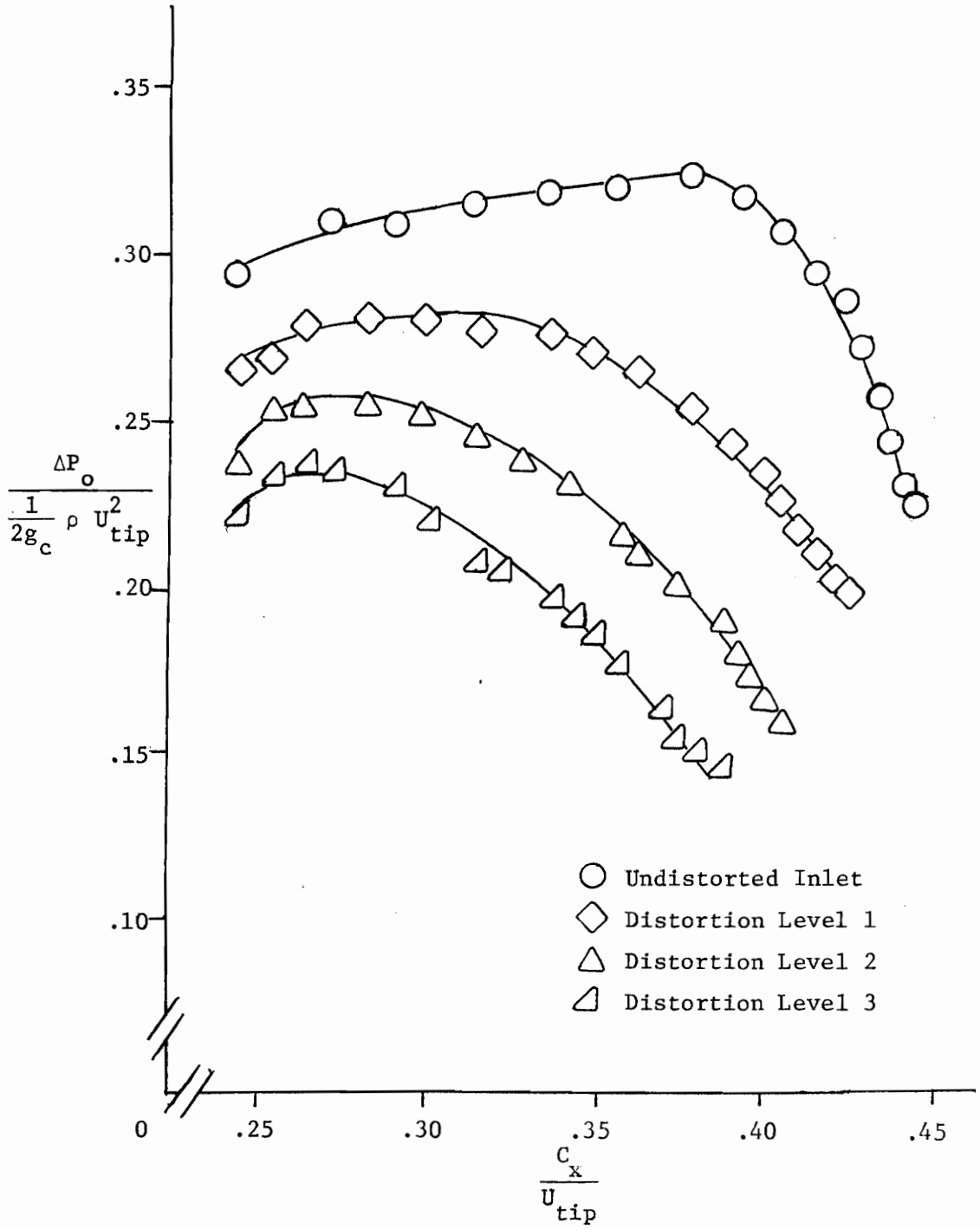

Figure 25. Compressor Performance Characteristics for Undistorted Inlet and 180-Degree Extent of Distortion Levels 1, 2, and 3

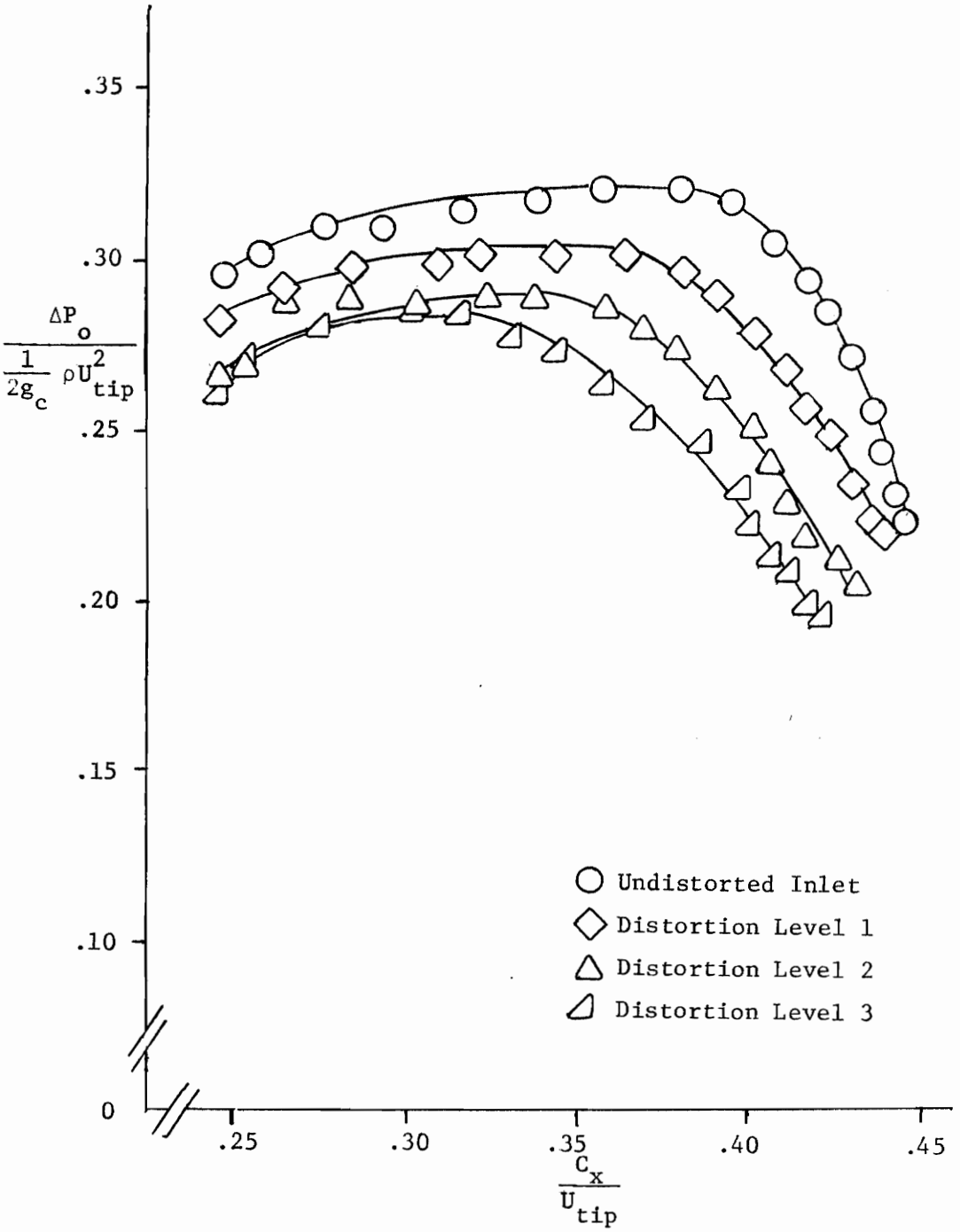

Figure 26. Compressor Performance Characteristics for Undistorted Inlet and 90-Degree Extent of Distortion Levels 1, 2, and 3

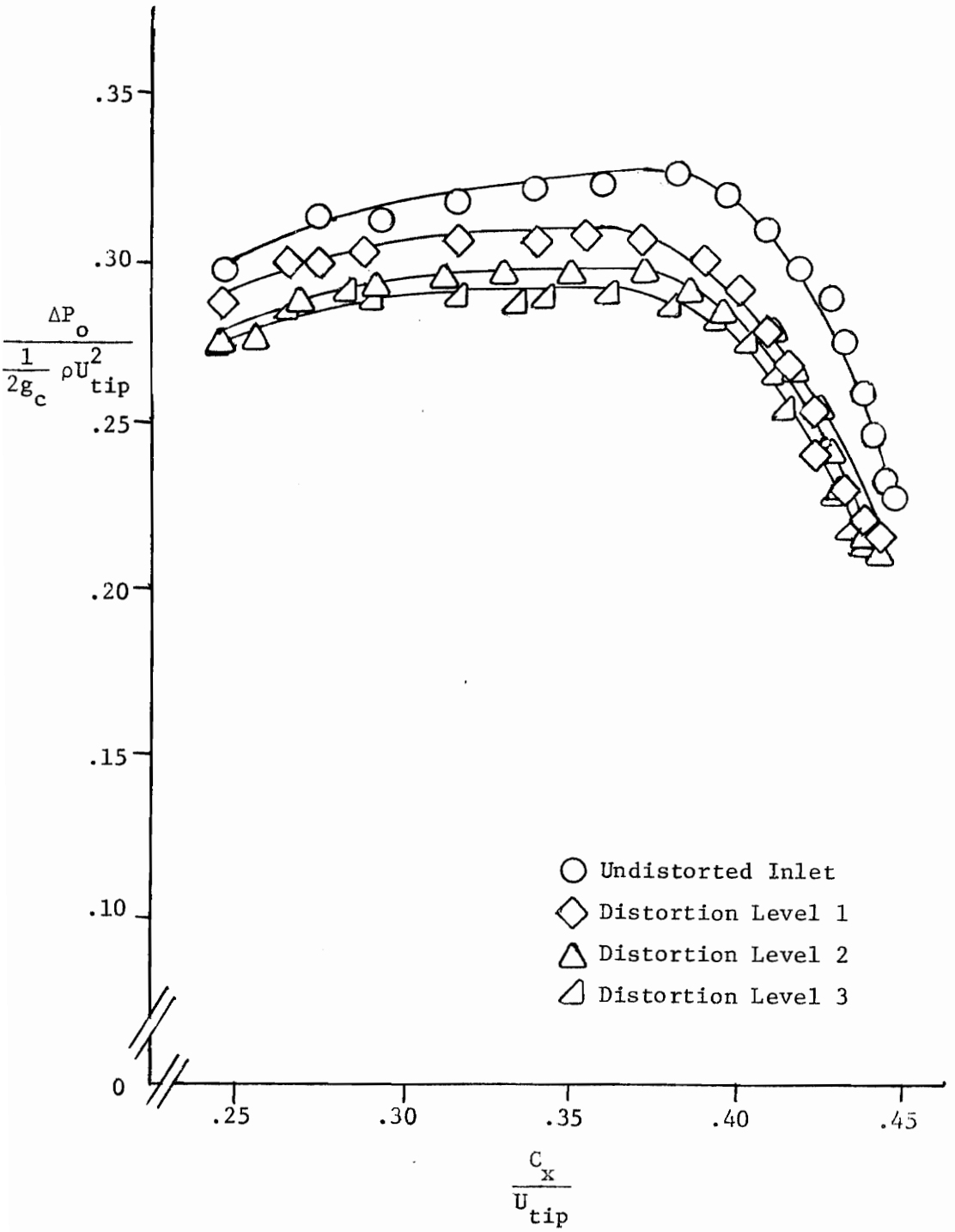

Figure 27. Compressor Performance Characteristics for Undistorted Inlet and 45-Degree Extent of Distortion Levels 1, 2, and 3

determined as that circumferential extent of distortion which resulted in the compressor stalling at an earlier valve setting. For 45 and 50-degree extents of the two distortion levels, the compressor entered stall for brief periods at valve position 7.0, but stable stall was not achieved until the valve was further closed to setting 7.25. However, for the 60-degree extents of distortion at levels 2 and 3, the compressor entered stable rotating stall at valve position 7.0. Thus, it was concluded that the compressor responded to a critical angle of 60 degrees when subjected to distortion levels 2 and 3. It should be noted that Dancy [13] found the critical angle of the compressor to be 60 degrees when subjected to distortion level 1. This critical angle value was used in Eq. 7 to complete the parallel compressor model predictions of loss in stall margin (see Figs. 4 and 5). Equation 7 was developed from Reid's method, employing an "effective" distortion to obtain reasonable agreement between theory and experiment for distortion extents less than the critical angle.

In addition to being used to indicate the onset of stable rotating stall, the dynamic pressure transducers were employed to observe and record stall cell data. The magnitudes of the relative pressure fluctuations in the stall cell and the radial and circumferential extents of the cell were measured and recorded on oscilloscope photographs for all ten inlet flow conditions.

A typical stall cell is shown in Fig. 28 (a). The oscilloscope photograph presented in this figure was obtained for undistorted flow with the probes positioned behind the rotor blade tip. The relative

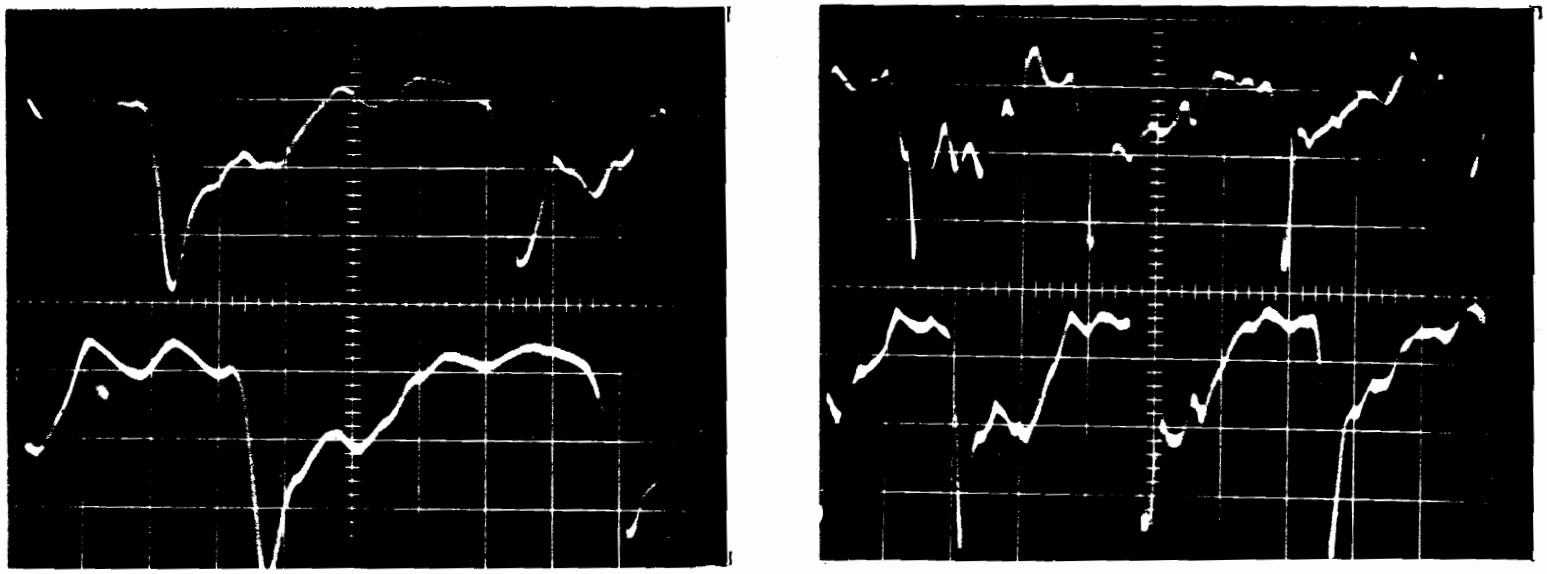

(a) (b)

Probe 1 at Tip
Probe 2 at Tip

Valve Position 7.25

Probe 1 at Tip
Probe 2 at Tip

Vertical Scale: 2.54 cm H_2O/Div. (1 in. H_2O/Div.)

Horizontal Scale: (a) 10 ms/Div.
(b) 20 ms/Div.

Figure 28. Typical Stall Cell Pressure Fluctuations With Undistorted Inlet

positions of the two pressure probes are illustrated in Fig. 29. The upper and lower signals on the photograph represent the outputs of probes 1 and 2, respectively. All stall cell data was measured and recorded with the probe 1 signal above the probe 2 signal on the oscilloscope photographs.

In Ref. 13, Dancy reported that the rotating stall cell revolved around the compressor in the same direction as the rotor blade but at half the rotor blade speed. This observation was verified in the present investigation by inspection of the stall cell in Fig. 28 (a) and similar data. From this figure, it was determined that the time interval required for the cell to complete one revolution was about twice that required for one rotor revolution. It was also found that the time required for the stall cell to pass from probe 1 to probe 2 was twice the time required by the rotor blades to travel the same distance. Thus, it was concluded that the rotating stall cell revolved around the compressor in the direction of the rotor motion, but at about one-half the rotor speed.

Figure 28 (b) shows rotating stall cells under similar conditions as in Fig. 28 (a), but with an extended time base. From this figure, the circumferential extent of the stall cell at the rotor blade tip was estimated to vary from 60 to 80 degrees. The extent of the cell was measured as the width of the most severe pressure fluctuation encountered during one rotor revolution. As shown in Fig. 28 (b), the total pressure gradually recovered from the initial severe loss until the maximum level was attained. It was

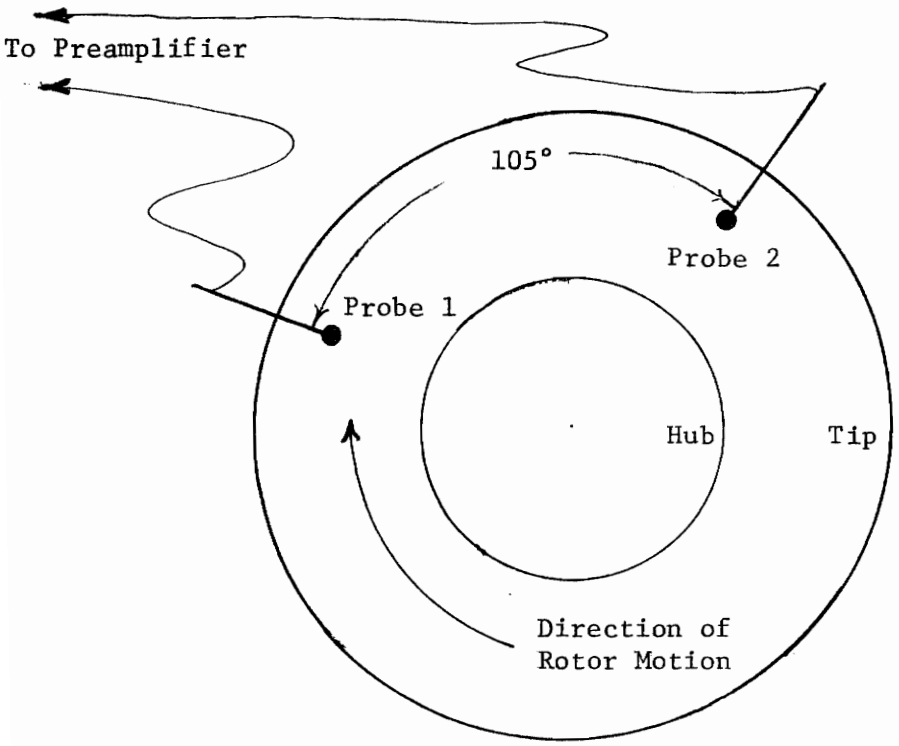

Figure 29. Relative Positions of Probes 1 and 2
(Shown Facing Downstream)

observed that further closing of the discharge valve resulted in an expansion of the circumferential extent of the stall cell. For the expanded stall cell, the recovery to maximum pressure was abrupt rather than gradual in nature. Hence, a more severe rotating stall condition was encountered under these conditions. Since the purpose of this investigation was to study the effects of inlet distortion on the inception of rotating stall, stable stall as defined in this thesis refers to the stall condition illustrated by Figs. 28 (a) and (b).

For undistorted flow, the radial extent of the stall cell encompassed the rotor blade tip region down to about midspan. This was determined from Figs. 30 (a) through (f). This sequence of oscilloscope photographs provided an indication of the relative magnitudes of the pressure fluctuations at several span positions. For these photographs, probe 2 (lower signal) was positioned at the blade tip while probe 1 was traversed radially from the tip to midspan, with measurements recorded at increments of 10 per cent span. Figure 31 (a) presents a comparison between the magnitudes of the stall cell pressure fluctuations at 50 per cent span and at the tip. The relative pressure loss in the stall cell at midspan was not as severe as at the tip region. From the same figure, the stall cell circumferential extent was estimated to be between 60 and 80 degrees at 50 per cent span. For Fig. 31 (b), probes 1 and 2 were positioned at the hub and tip, respectively. A low velocity region was found to exist at the hub with no indication of rotating stall in this locality. At the tip, severe pressure fluctuations in the rotating stall cell were observed.

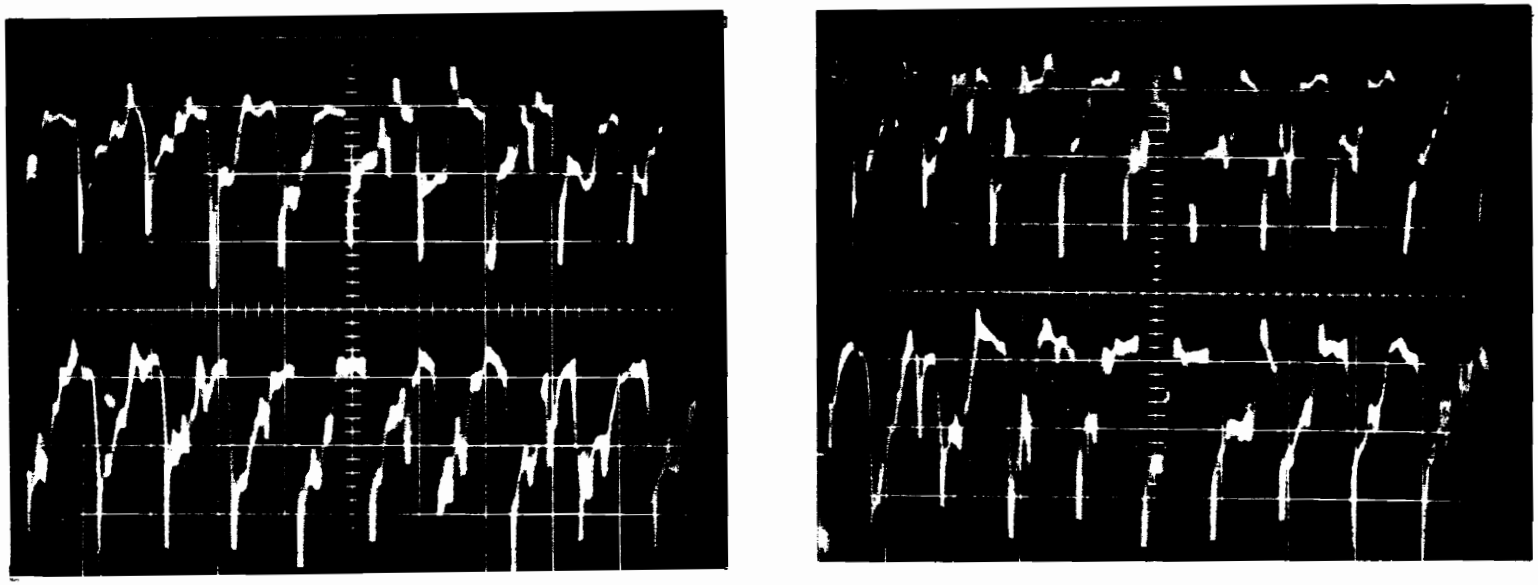

(a) (b)

Probe 1 at Tip
Probe 2 at Tip

Valve Position 7.25

Probe 1 at 90 Per Cent Span
Probe 2 at Tip

Vertical Scale: 2.54 cm H_2O/Div. (1 in. H_2O/Div.)

Horizontal Scale: (a) 50 ms/Div.
(b) 50 ms/Div.

Figure 30. Typical Stall Cell Pressure Fluctuations With Undistorted Inlet

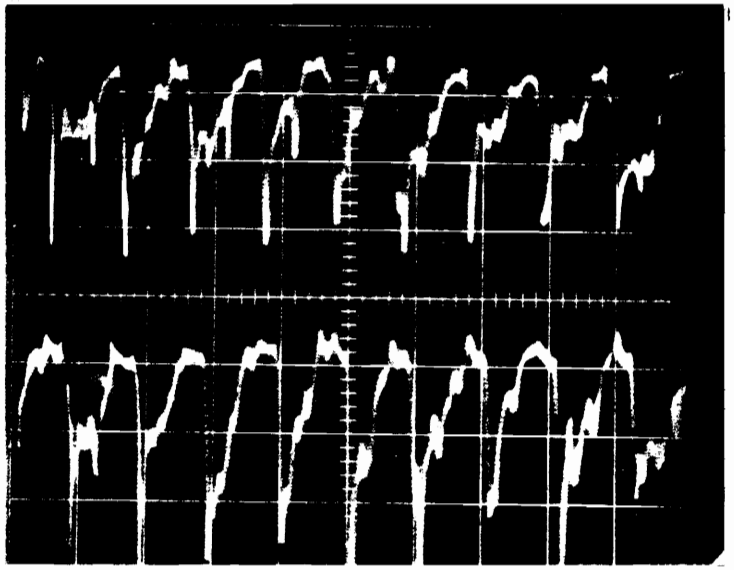

(c)

Probe 1 at 80 Per Cent Span
Probe 2 at Tip

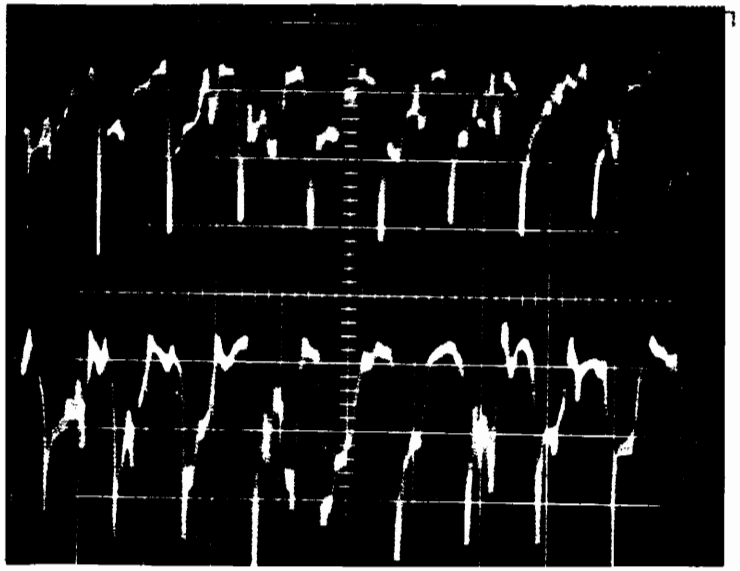

(d)

Probe 1 at 70 Per Cent Span
Probe 2 at Tip

Valve Position 7.25

Vertical Scale: 2.54 cm H_2O/Div. (1 in. H_2O/Div.)

Horizontal Scale: (c) 50 ms/Div.
(d) 50 ms/Div.

Figure 30. Typical Stall Cell Pressure Fluctuations With Undistorted Inlet

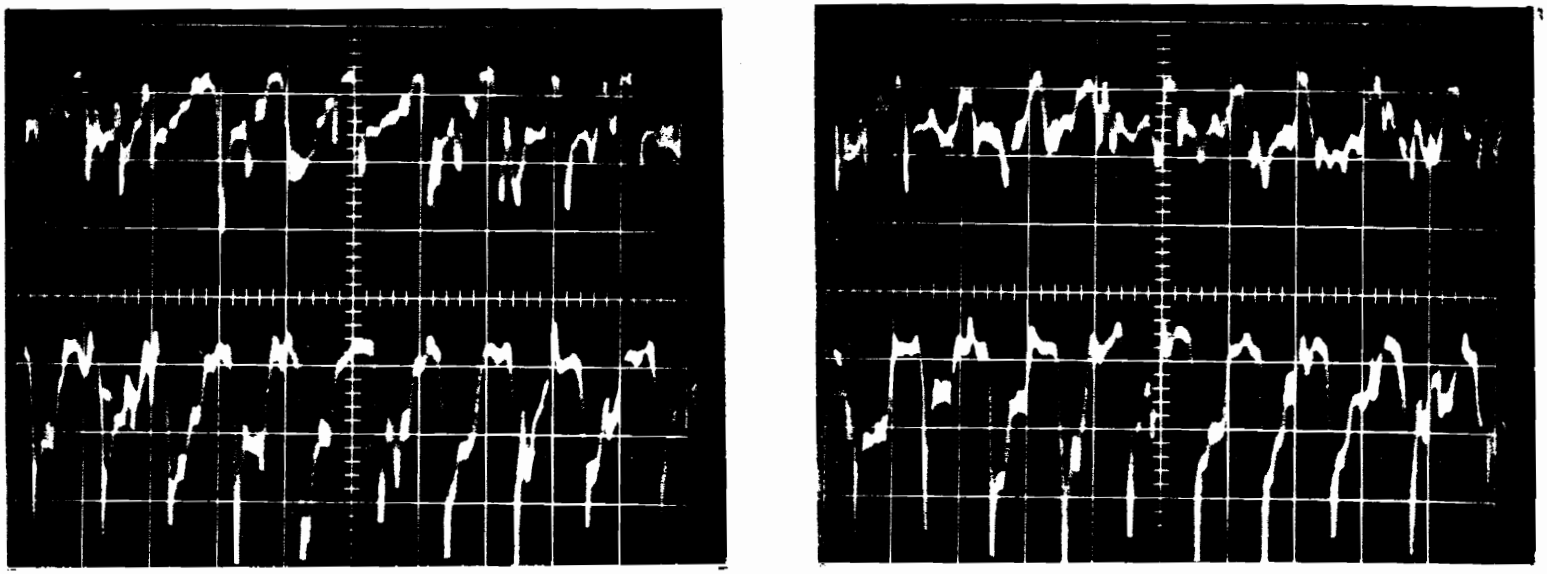

(e) (f)

Probe 1 at 60 Per Cent Span
Probe 2 at Tip

Valve Position 7.25

Probe 1 at 50 Per Cent Span
Probe 2 at Tip

Vertical Scale: 2.54 cm H_2O/Div. (1 in. H_2O/Div.)

Horizontal Scale: (e) 50 ms/Div.
(f) 50 ms/Div.

Figure 30. Typical Stall Cell Pressure Fluctuations With Undistorted Inlet

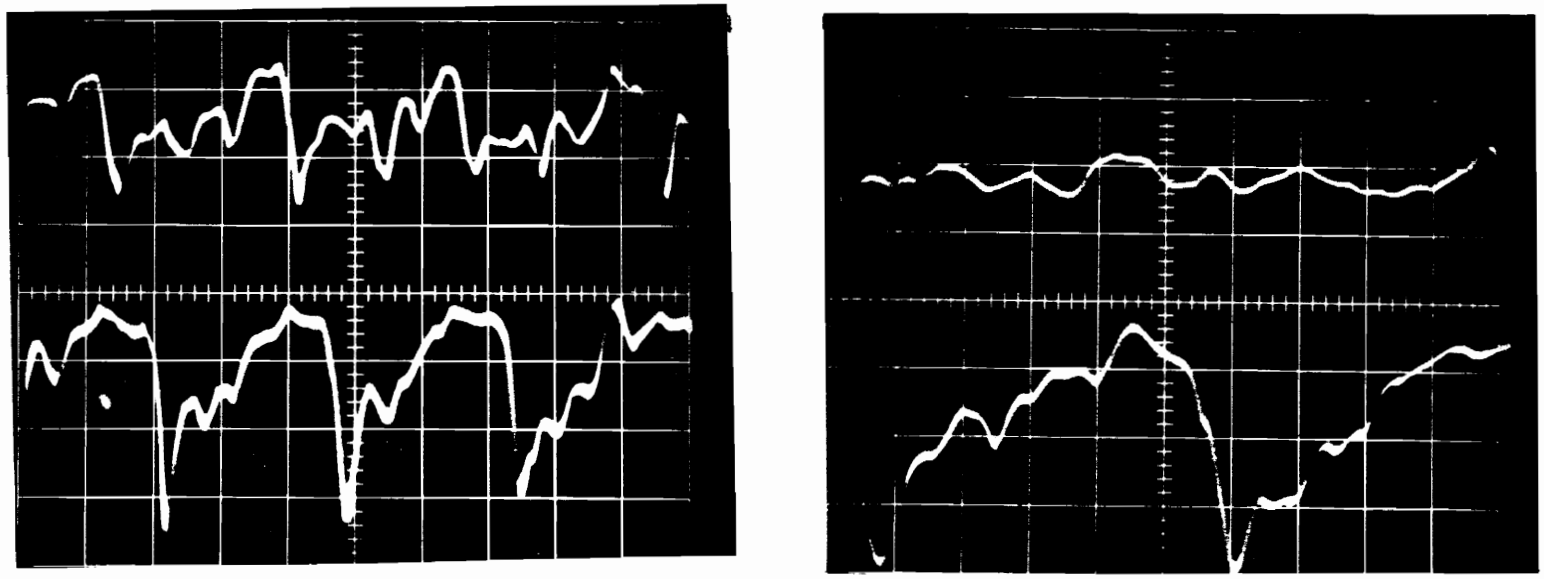

(a)

Probe 1 at 50 Per Cent Span
Probe 2 at Tip

Valve Position 7.25

(b)

Probe 1 at Hub
Probe 2 at Tip

Vertical Scale: 2.54 cm H_2O/Div. (1 in. H_2O/Div.)

Horizontal Scale: (a) 20 ms/Div.
(b) 10 ms/Div.

Figure 31. Typical Stall Cell Pressure Fluctuations With Undistorted Inlet

The photograph of Fig. 31 (b) depicts the difference in flow phenomena encountered at the rotor blade hub and tip during stable rotating stall.

To obtain representative stall cell data for the nine different distortion patterns tested, measurements were observed and recorded for the screen positions shown in Fig. 32. These screen positions were pre-selected such that rotating stall cell behavior was investigated at several points in and out of the distorted flow region. With the stall cell direction of rotation as shown in Fig. 32, the pressure signal of probe 1 was used to "track" the stall cell as it emerged from behind the distortion screen (position 1), revolved around the circumference (positions 2 and 3 for the 45 and 90-degree extents and position 2 for the 180-degree extent), and entered the distorted flow region at screen position 4 (position 3 for the 180-degree extent). In view of this relationship, the following discussion of rotating stall cell behavior for distorted inflow is based on the measurements provided by probe 1.

Figure 33 presents the rotating stall cell measurements recorded for screen positions 1, 2, 3, and 4 with the 180-degree extent of distortion level 3. It was determined from these measurements that the magnitudes of the pressure fluctuations in the stall cells were attenuated in the distorted flow region. Comparison of Figs. 33 (a) and (b) indicated that the stall cell was also attenuated as it approached the distorted region. From Figs. 33 (c) and (d), it was observed that as the stall cell passed through the center of the

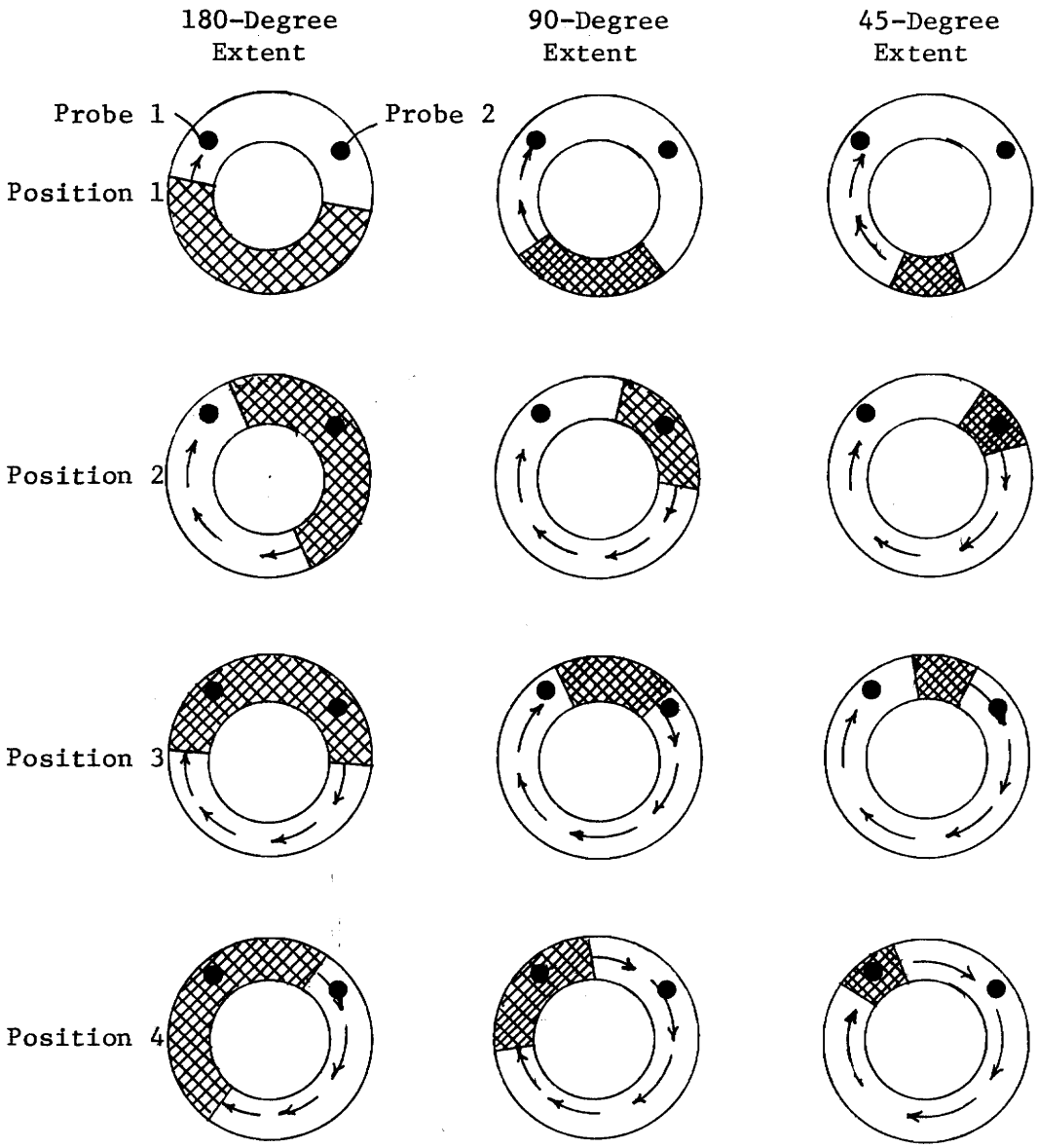

Figure 32. Distortion Screen Positions Tested; Shown Facing Downstream (Arrows Indicate Direction of Stall Cell Rotation)

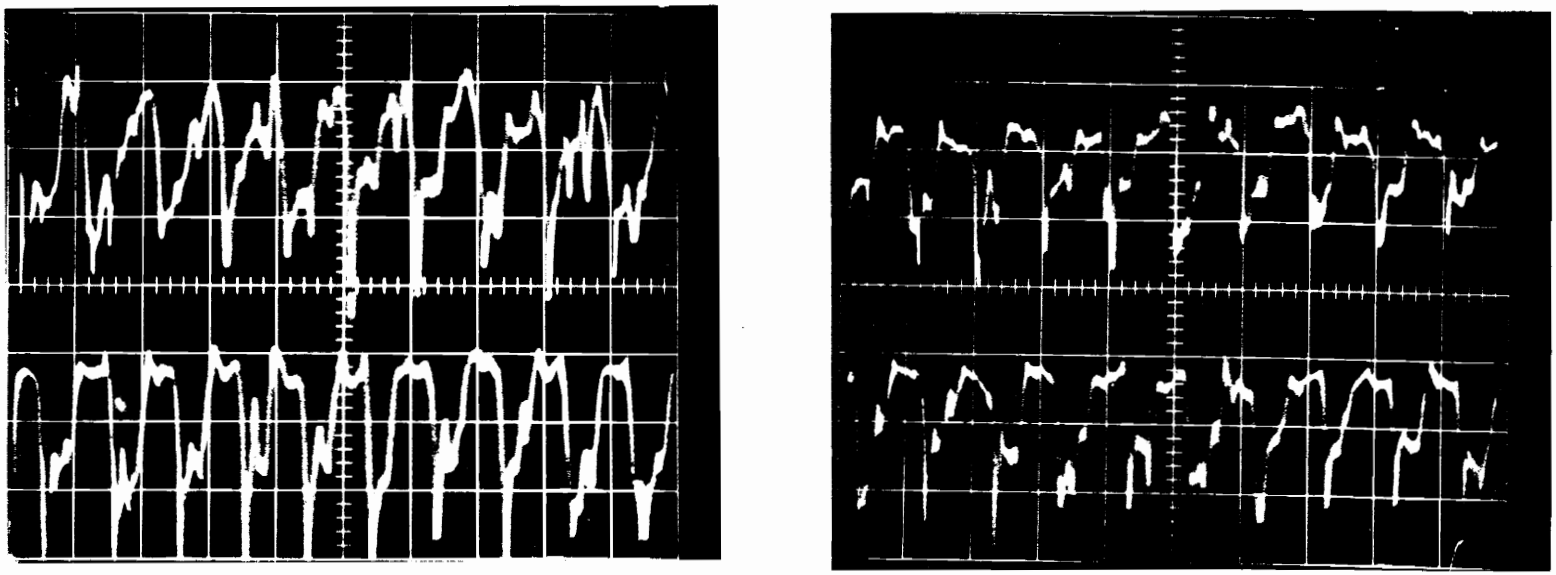

(a) (b)

Screen Position 1
Probe 1 at Tip
Probe 2 at Tip

Valve Position 6.6

Screen Position 2
Probe 1 at Tip
Probe 2 at Tip

Vertical Scale: 2.54 cm H_2O/Div. (1 in. H_2O/Div.)

Horizontal Scale: (a) 50 ms/Div.
(b) 50 ms/Div.

Figure 33. Typical Stall Cell Pressure Fluctuations With 180-Degree Extent of Distortion Level 3

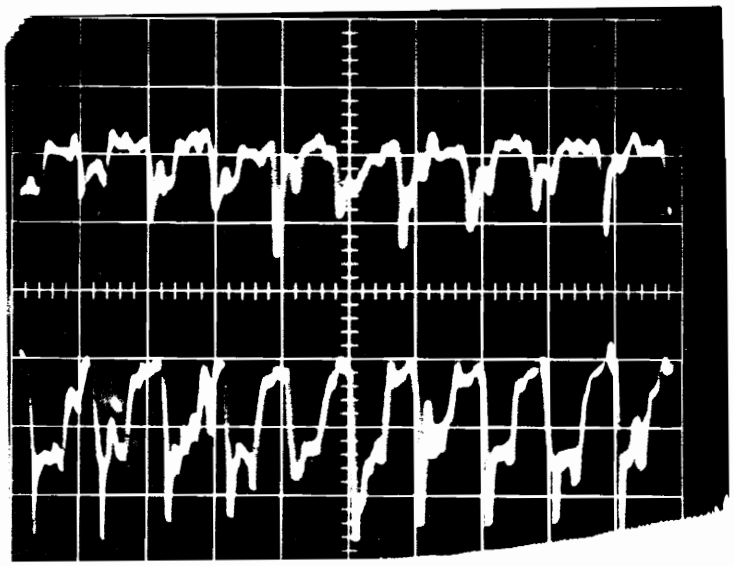

(c)

Screen Position 3
Probe 1 at Tip
Probe 2 at Tip

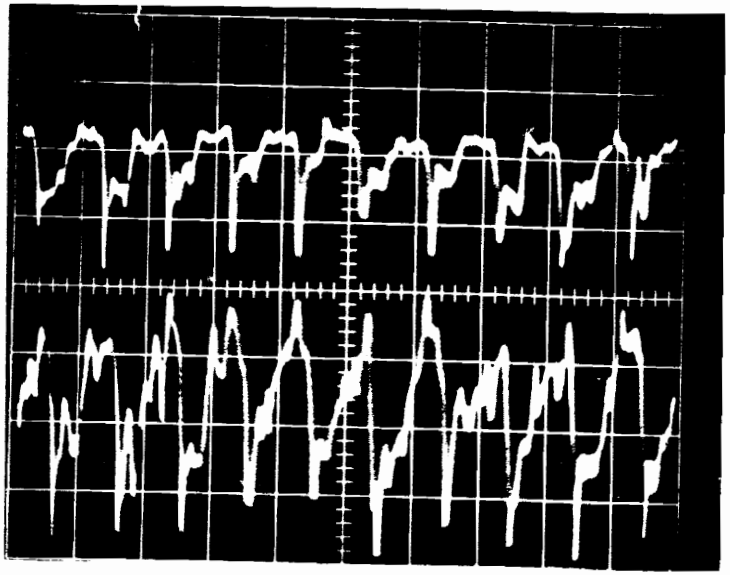

(d)

Screen Position 4
Probe 1 at Tip
Probe 2 at Tip

Valve Position 6.6

Vertical Scale: 2.54 cm H_2O/Div. (1 in. H_2O/Div.)

Horizontal Scale: (c) 50 ms/Div.
(d) 50 ms/Div.

Figure 33. Typical Stall Cell Pressure Fluctuations With 180-Degree Extent of Distortion Level 3

distorted flow region (d), it had increased in magnitude relative to its amplitude after just having entered the disturbed flow (c). The same results were obtained for similar data recorded for distortion level 1, shown in Fig. 34. Comparison of Figs. 33 and 34 indicated that the distortion level 1 screen did not attenuate the magnitude of the stall cell to the same degree as the distortion level 3 screen. The attenuation of the stall cell behind the distortion screens may be due to the lower axial velocity in the distorted flow region (see Figs. 13, 14, and 15). The air velocity essentially provided the "source" for the stall cell pressure fluctuations; therefore, lower velocities resulted in less severe relative pressure losses through the stall cell.

Similar tests conducted for the 90 and 45-degree extents of distortion levels 1, 2, and 3 revealed the same results. In each case, the magnitude of the stall cell was reduced behind the distortion screen, with level 3 providing the greatest degree of attenuation. The measurements recorded for the 90 and 45-degree distortion extents are shown in Appendix C. It should be noted that although data were measured and recorded for distortion level 2, it is not presented in this report because the results obtained were in agreement with those determined for levels 1 and 3. That is, the level 2 screen attenuated the stall cell more than the level 1 screen, but not as much as the level 3 screen.

For all nine distortion patterns, the radial extent of the stall cell was examined in the distorted flow region behind screen position

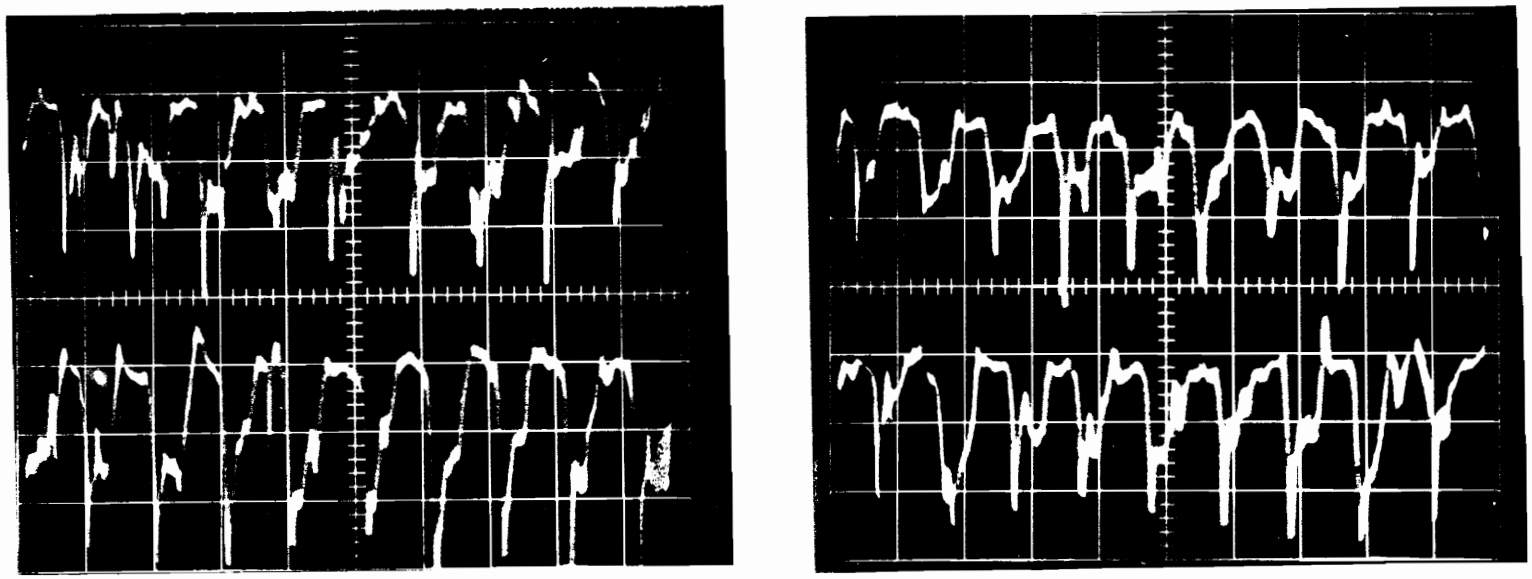

(a) (b)

Screen Position 1
Probe 1 at Tip
Probe 2 at Tip

Valve Position 7.0

Screen Position 2
Probe 1 at Tip
Probe 2 at Tip

Vertical Scale: 2.54 cm H_2O/Div. (1 in. H_2O/Div.)

Horizontal Scale: (a) 50 ms/Div.
(b) 50 ms/Div.

Figure 34. Typical Stall Cell Pressure Fluctuations With 180-Degree Extent of Distortion Level 1

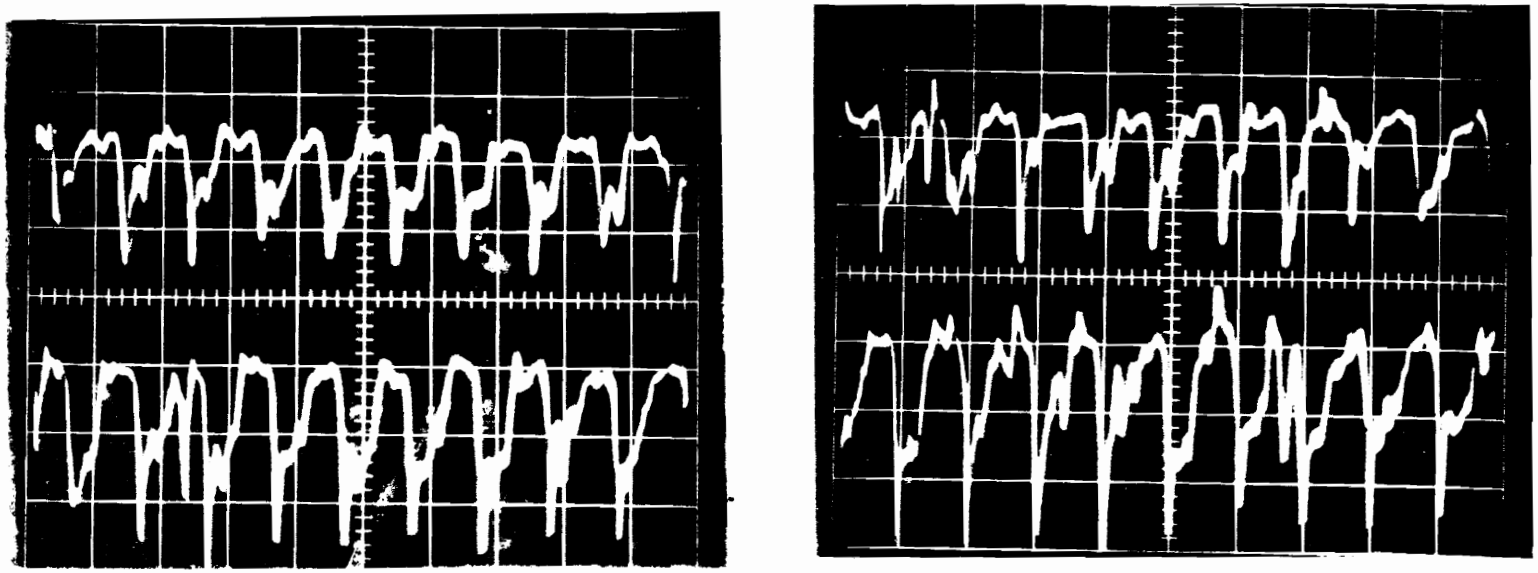

(c)

Screen Position 3
Probe 1 at Tip
Probe 2 at Tip

(d)

Screen Position 4
Probe 1 at Tip
Probe 2 at Tip

Valve Position 7.0

Vertical Scale: 2.54 cm H_2O/Div. (1 in. H_2O Div.)

Horizontal Scale: (c) 50 ms/Div
(d) 50 ms/Div.

Figure 34. Typical Stall Cell Pressure Fluctuations With 180-Degree Extent of Distortion Level 1

4. The results of this investigation for the 180 and 45-degree extents of distortion level 3 are shown in Fig. 35. Figures 35 (a) and (c) represent typical stall cell photographs obtained at 90 per cent span. The oscilloscope photographs in Figs. 35 (b) and (d) show the pressure distributions below the stall cell, at 30 per cent span. In the distorted flow region, it was observed that the stall cell encompassed the rotor blade tip region down to about 70 per cent span. Between 70 and 50 per cent span, the stable rotating stall pattern reduced to pressure fluctuations of a more random nature. Comparing Figs. 35 (a) and (c), it appeared that the 45-degree distortion extent attenuated the stall cell more severely than the 180-degree extent. However, this was due to the increase in stall cell amplitude noted previously for further penetration into the distorted flow region. The pressure signals in Figs. 35 (b) and (d) indicated a higher velocity at 30 per cent span for the 45-degree distortion extent than for the 180-degree screen. The circumferential extent of the stall cell behind the screens did not differ from the stall cell extent for undistorted flow. Perhaps, if the valve had been closed further to achieve a more severe stable rotating stall condition, differences in the stall cell extents would have been observed. Figure 36 presents the total pressure distribution at 30 per cent span during stall for undistorted inlet flow. As expected, this photograph indicated a higher velocity in this region for undistorted inlet flow than for the 180 and 45-degree extents of distortion level 3. Appendix D provides data similar to that of Fig. 35

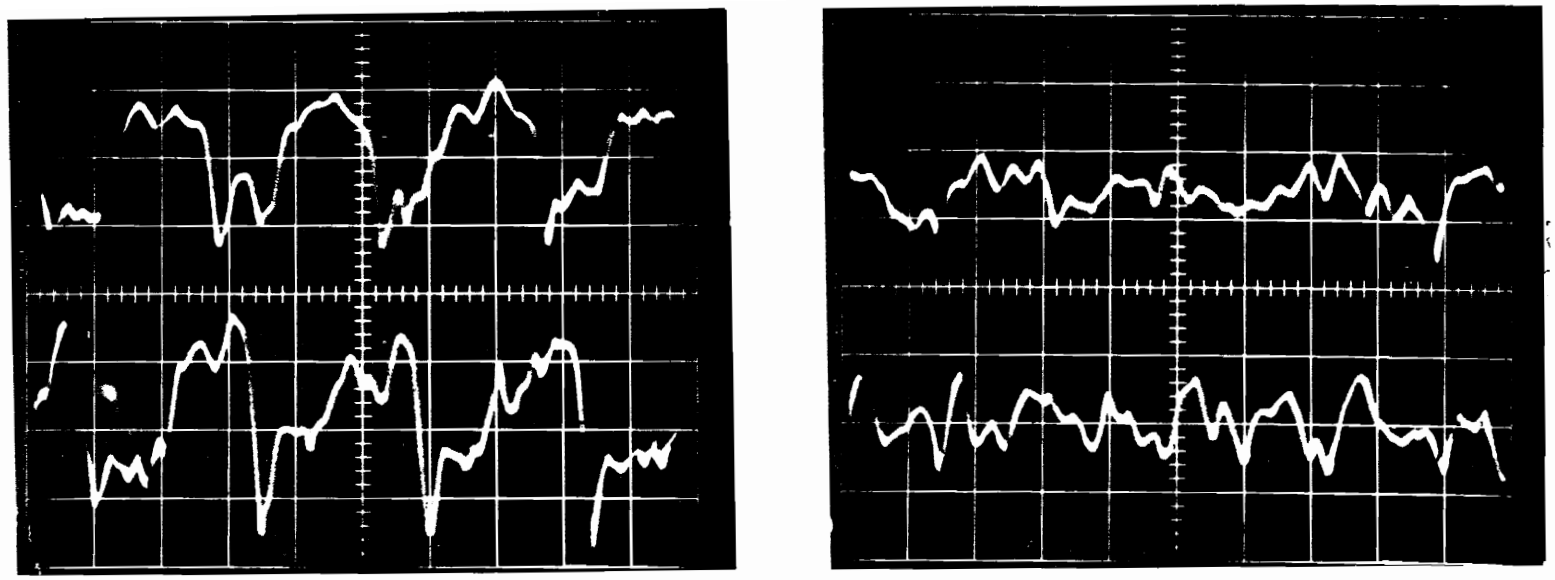

(a)

Screen Position 4
Probe 1 at 90 Per Cent Span
Probe 2 at 90 Per Cent Span

(b)

Screen Position 4
Probe 1 at 30 Per Cent Span
Probe 2 at 30 Per Cent Span

Valve Position 6.6

Vertical Scale: 2.54 cm H_2O/Div

Horizontal Scale: (a) 20 ms/Div.
(b) 20 ms/Div

Figure 35. Typical Stall Cell Pressure Fluctuations With 180-Degree Extent of Distortion Level 3

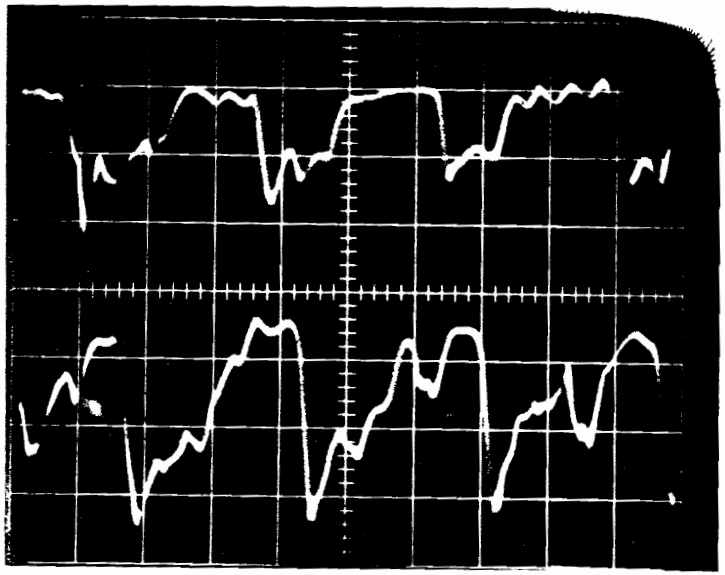

(c)

Screen Position 4
Probe 1 at 90 Per Cent Span
Probe 2 at 90 Per Cent Span

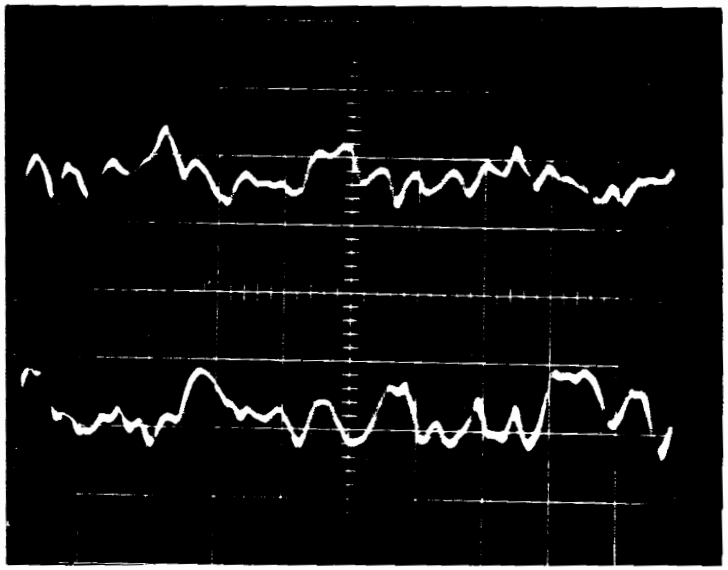

(d)

Screen Position 4
Probe 1 at 30 Per Cent Span
Probe 2 at 30 Per Cent Span

Valve Position 7.1

Vertical Scale: 2.54 cm H_2O/Div. (1 in. H_2O Div.)

Horizontal Scale: (c) 20 ms/Div.
(d) 20 ms/Div.

Figure 35. Typical Stall Cell Pressure Fluctuations With 45-Degree Extent of Distortion Level 3

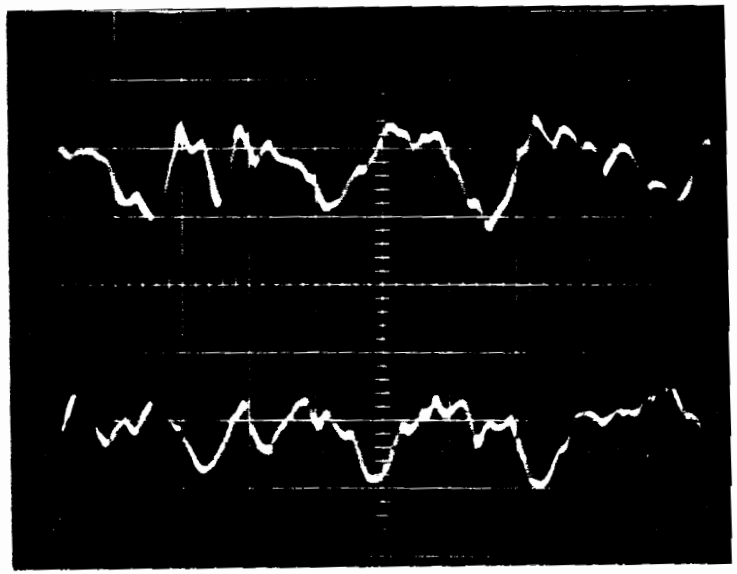

Valve Position 7.25

Probes 1 and 2 at 30 Per Cent Span

Vertical Scale: 2.54 cm H_2O/Div. (1 in. H_2O/Div.)

Horizontal Scale: 20 ms/Div.

Figure 36. Pressure Distribution Below Rotating Stall Cell With Undistorted Inlet

for tests conducted on distortion level 1. The results obtained for the two distortion levels were the same, differing only in the severity of the stall cell attenuation.

On-Rotor Results

In this portion of the investigation, rotor blade average pressures were measured to investigate blade pressure phenomena at the inception of stall and at stable stall.

The Scanivalve was used to measure the average pressures at mid-span for a range of chord positions. The average chordwise blade pressures for undistorted flow and for the 45, 90, and 180-degree extents of distortion levels 2 and 3 are tabulated in Appendix E. Figure 37 shows a typical rotor blade pressure distribution obtained for maximum, undistorted flow. As reported by Dancy in [13], very little change was noticed for the average pressure side measurements as the flow rate was lowered. The suction side pressure distributions exhibited an observable response to a reduction in flow rate. Figures 38 through 41 illustrate the change in the suction side pressure profile for undistorted flow and the 45, 90, and 180-degree extents of distortion level 3 as the flow rate is reduced to achieve stall. In these figures, the curves obtained for valve position 0 are properly aligned with the pressure axis. The curves representing the pressure profiles for other valve positions have been "offset" as indicated in the figures so that they may be viewed individually.

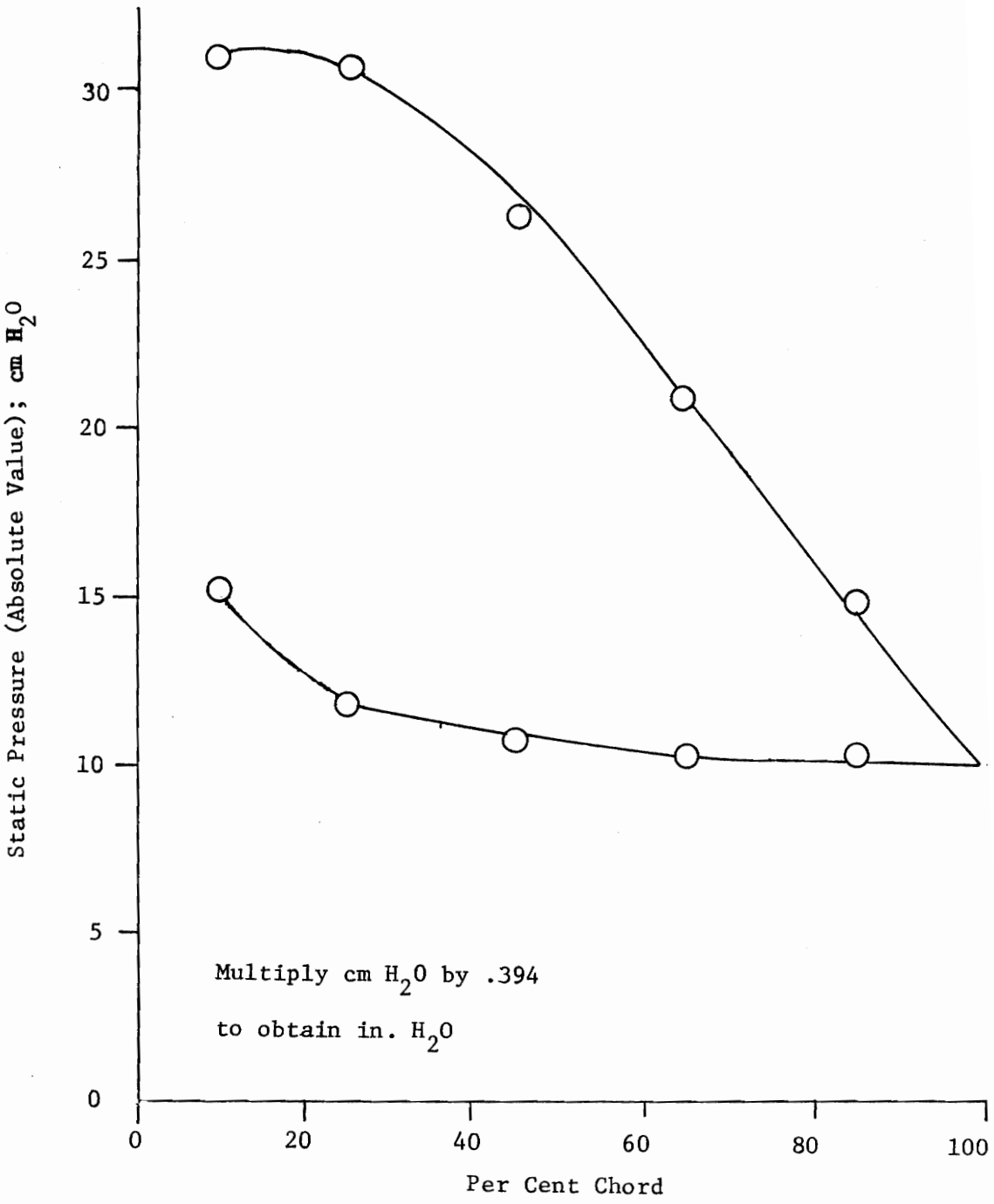

Figure 37. Typical Rotor Blade Pressure Distribution With Undistorted Inlet; Valve Position 0 (Max. Flow)

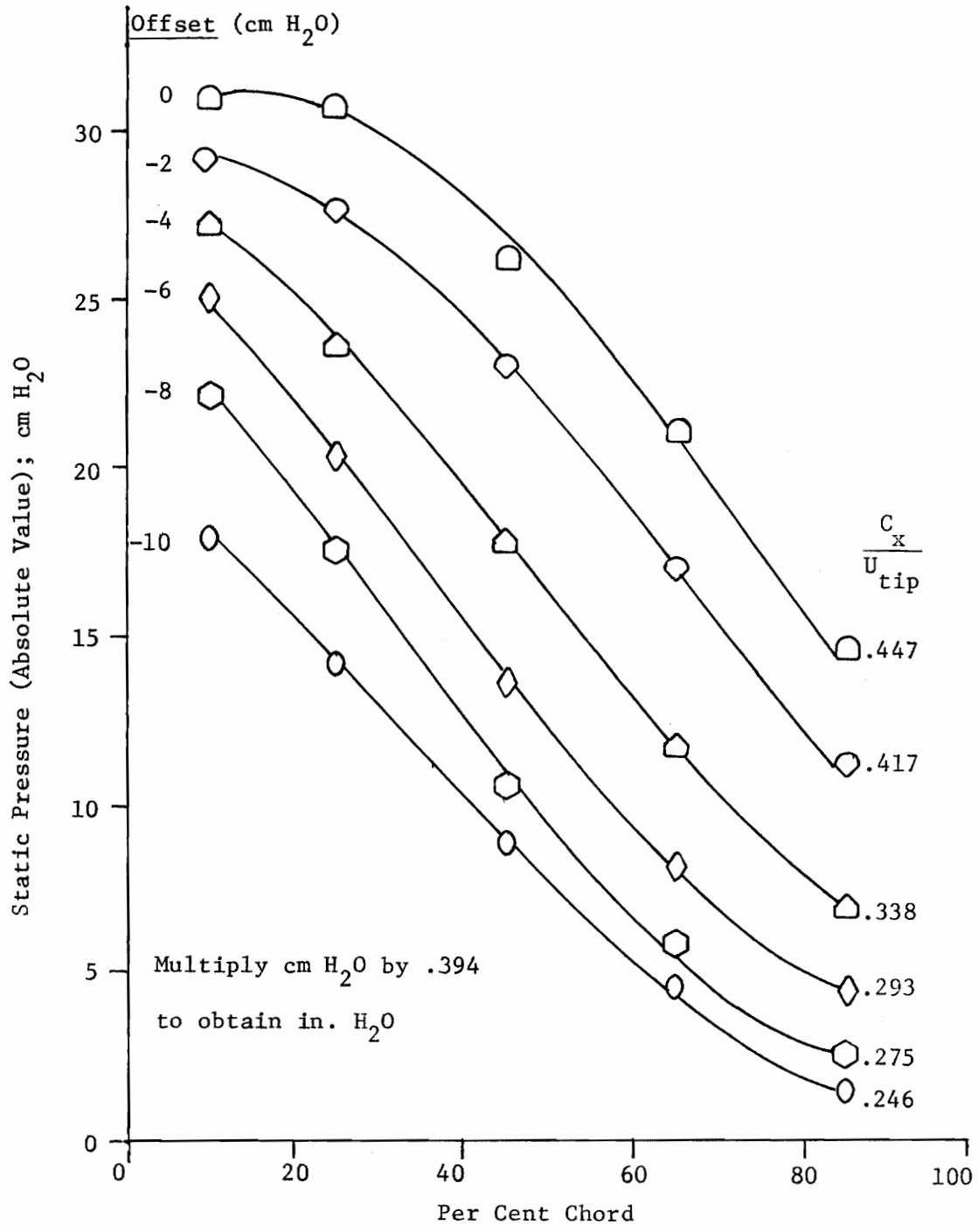

Figure 38. Blade Suction Side Pressure Profile at Several Flow Rates With Undistorted Inlet

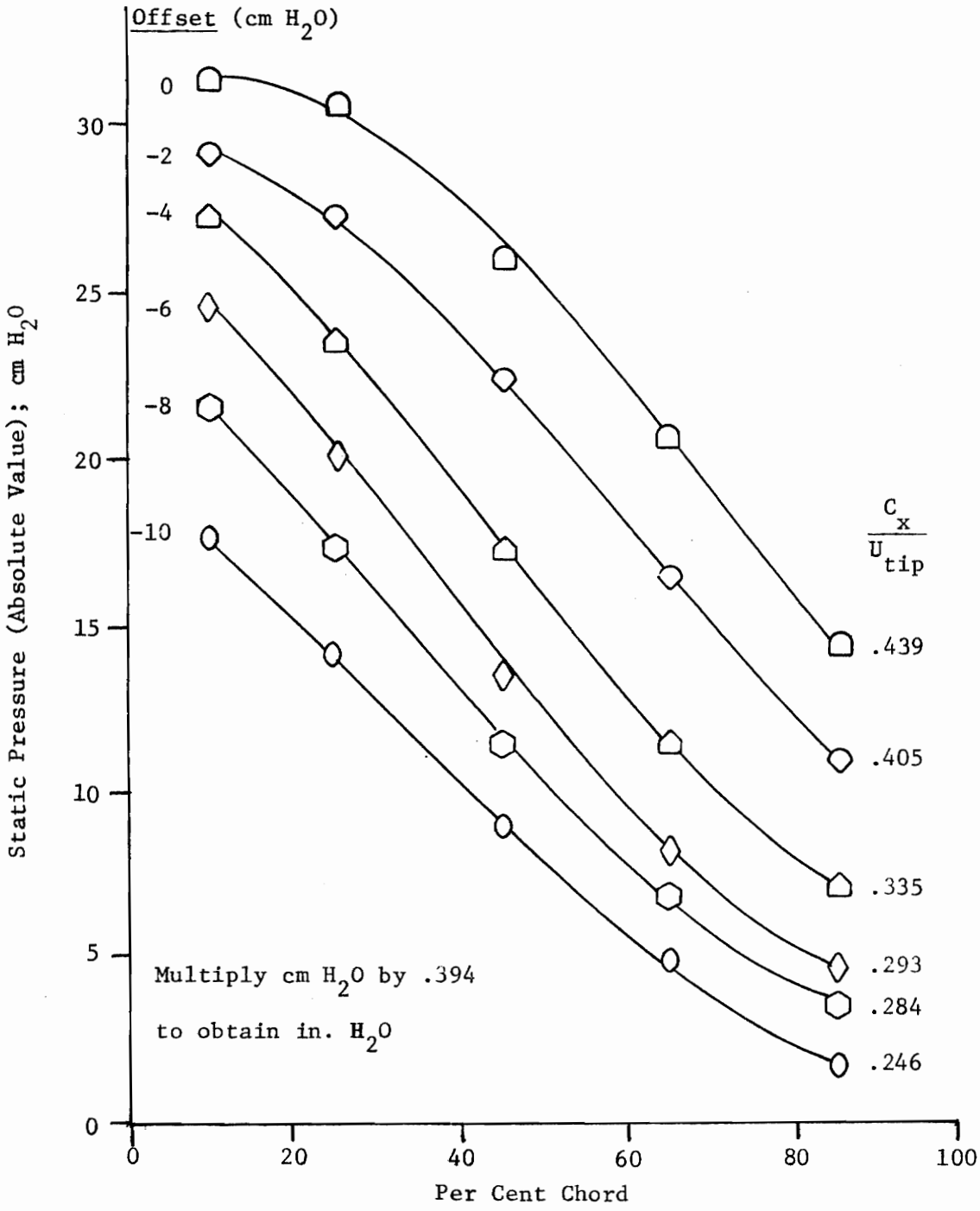

Figure 39. Blade Suction Side Pressure Profile at Several Flow Rates With 45-Degree Extent of Distortion Level 3

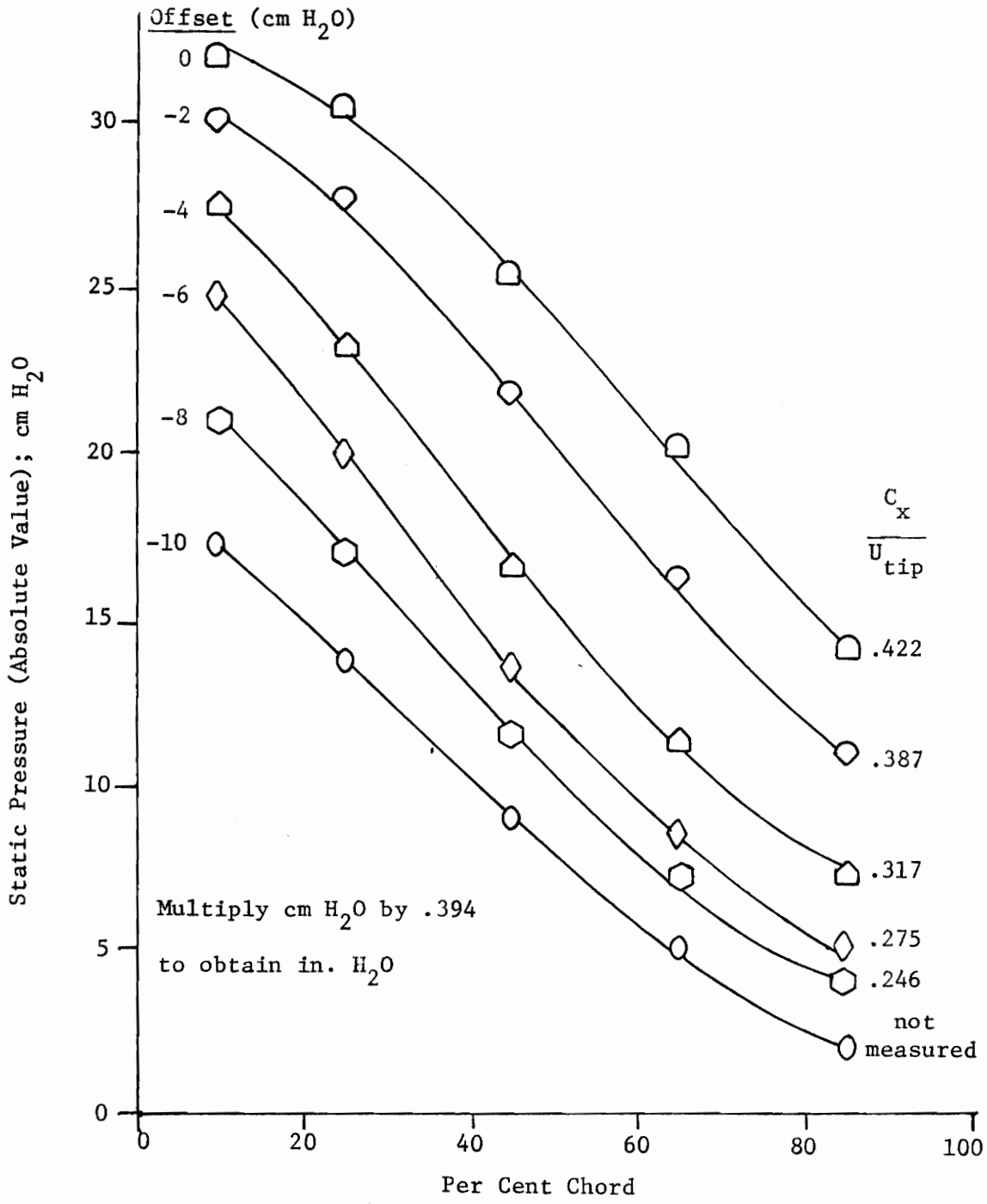

Figure 40. Blade Suction Side Pressure Profile at Several Flow Rates With 90-Degree Extent of Distortion Level 3

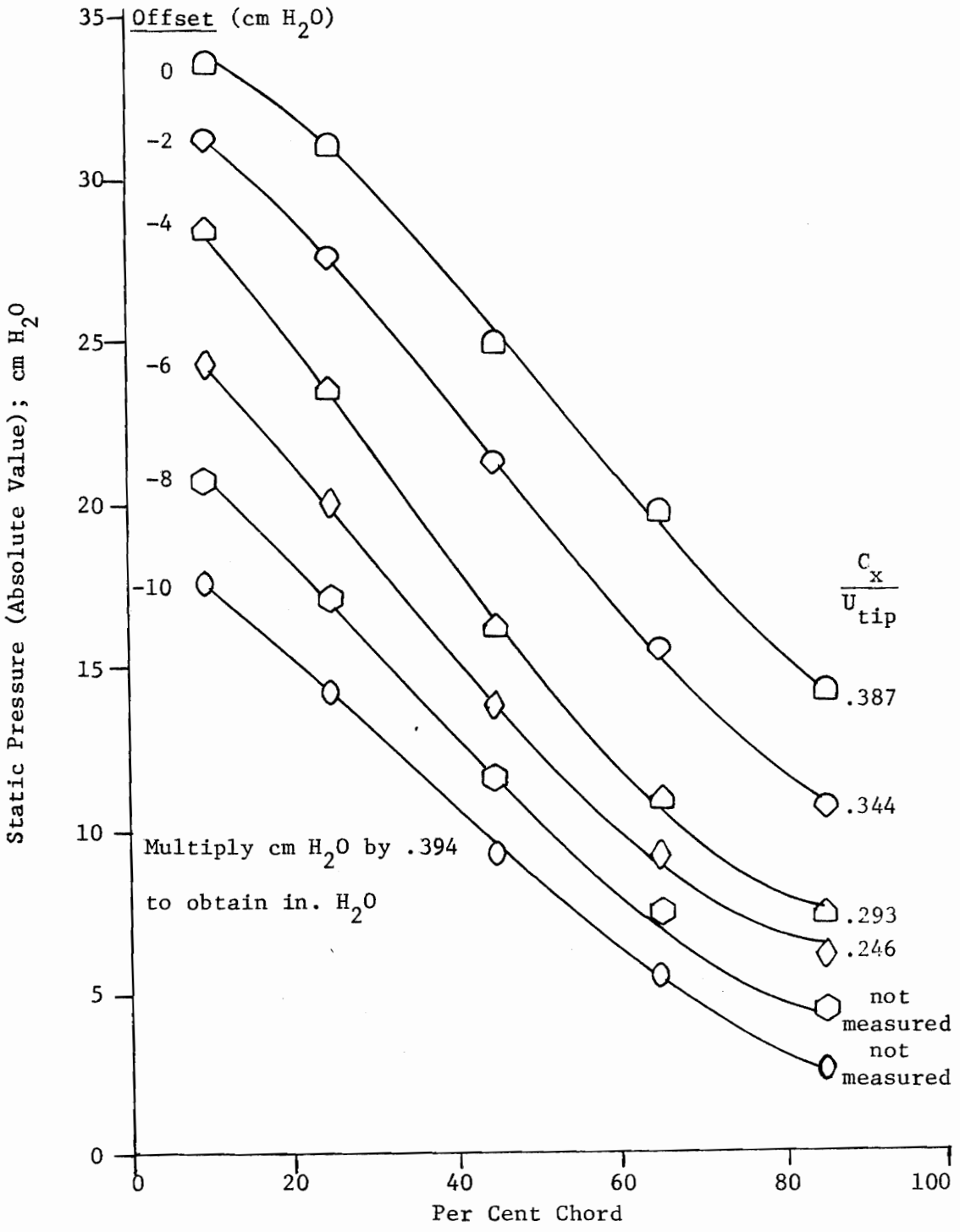

Figure 41. Blade Suction Side Pressure Profile at Several Flow Rates With 180-Degree Extent of Distortion Level 3

XI. DISCUSSION OF RESULTS

Stationary Pressure Measurements

The circumferential inlet static and total pressure profiles behind the 180-degree extents of distortion levels 2 and 3 are presented in Figs. 11 and 12, respectively. The pressure distributions in front of and behind the rotor are shown in these figures. At maximum flow, the total pressure loss behind distortion level 3 was as much as 17 per cent greater than that behind distortion level 2. Inspection of the pressure profiles behind the rotor indicated some attenuation of the distortion through the rotor. The circumferential exit static pressures were essentially uniform in both cases, supporting a major assumption of parallel compressor theory.

Figures 13, 14, and 15 present the circumferential inlet velocity profiles behind the nine distortion patterns tested. With respect to the direction of rotor motion, a sharp increase in axial velocity was observed as the distorted segment was approached. This was due to the low pressure area behind the screens. In the distorted flow region, the axial velocity was reduced until it leveled out at the departure end of the screen. Figures 16 through 19 indicated that the shape of the circumferential velocity profile remained about the same as the flow rate was decreased.

Behind the distortion screens, a significant increase in incidence angles resulted from the lower axial velocities. The circumferential incidence angle profiles for the 180-degree extents

of distortion levels 2 and 3 are shown in Fig. 20. Average incidence angle values for all inlet flow conditions are listed in Table 3.

To obtain the compressor performance characteristics for all inlet flow conditions, the orifice was calibrated to measure flow rate. Calibration of the orifice required the determination of "flow adjustment factors" to account for boundary layers near the inner and outer wall and wakes behind the inlet guide vanes. Radial velocity profiles at the compressor inlet such as shown in Fig. 22 were measured to find these adjustment factors. Table 4 lists the "flow adjustment factors" obtained for a range of valve positions. The orifice flow coefficient at stall was determined by measuring the flow rate behind the rotor from the radial velocity profile of Fig. 23. The final orifice calibration curve is shown in Fig. 24.

The performance characteristics for all ten inlet flow conditions are presented in Figs. 25, 26, and 27. The volumetric flow rates recorded for these characteristics are listed in Table 5. It was observed that for a given valve setting, the flow rate was reduced by the presence of the distortion screens. At valve position 0, the reduction in flow rate due to the 180-degree extent of distortion level 3 reached 13 per cent. However, at the onset of stall, the flow rates for all inlet conditions approached the same value. Inspection of Figs. 25, 26, and 27 revealed that distortion level 3 provided the greatest reduction in total pressure rise capability for all three distortion extents. A reduction in pressure rise at stall of 25 per cent was observed for the 180-degree extent of

distortion level 3. For the 45-degree extents of levels 2 and 3, the pressure rise at stall was essentially the same. It was concluded that although the distortion patterns reduced the total pressure rise at stall, the shape of the characteristic curves remained the same.

Stall Cell Analysis Measurements

Two high response dynamic pressure transducers were used to indicate the inception of stable rotating stall. The compressor was found to enter stall when the mass flow rate was reduced sufficiently. The inlet distortion screens decreased the flow rate through the compressor and induced stall at a more open valve setting than for undistorted flow. The valve positions at which stable rotating stall occured for the ten different inlet flow conditions are listed in Appendix B.

The determination of the critical angle of the compressor subjected to distortion levels 2 and 3 was made possible through the use of the dynamic pressure probes. The critical angle was defined as that circumferential extent of distortion at which the compressor entered stall for a relatively more open discharge valve setting than for undistorted flow. In this case, the compressor responded to a critical angle of 60 degrees when subjected to distortion levels 2 and 3. Dancy obtained the same critical angle value for the compressor subjected to distortion level 1. Thus, it appears that the critical angle phenomenon is a function of the compressor design and is independent of the distortion level.

The dynamic pressure transducers were used not only to indicate rotating stall, but, also to measure and record stall cell data. The stall cell measurements were recorded and interpreted from oscilloscope photographs. Measurements of the amplitudes of the stall cell pressure fluctuations and the circumferential and radial extents of coverage were of particular interest.

Figures 28 (a) and (b) represent typical stall cell photographs taken for undistorted inlet flow. It was determined from these measurements that the rotating stall cell revolved around the circumference in the direction of rotor motion at one-half the rotor speed. This result supported the observations of Dancy in the previous investigation [13]. Inspection of Figs. 28 (a) and (b) indicated that the circumferential extent of the stall cell ranged from 60 to 80 degrees at the tip. In this region, the relative pressure distributions of Figs. 28 (a) and (b) revealed a severe pressure drop from 7.62 cm (3 in.) to almost 0 cm of water pressure in the stall cell. Thus, the air velocity and hence, the flow rate through the stall cell was essentially negligible. From Fig. 30, it was concluded that the radial extent of the stall cell encompassed the rotor blade tip region down to about midspan. Figure 31 (a) indicated that the relative pressure drop through the stall cell at midspan was approximately 50 per cent of that at the tip. Therefore, during stall, the air flow rate at midspan maintained a finite value. The difference in relative pressure distributions at the rotor blade hub and tip during rotating stall is shown in Fig. 31 (b). There appeared to be no indication of

rotating stall in the hub region.

An analysis of the rotating stall behavior in the undistorted and distorted sections of a partially distorted inlet was conducted for the screen positions of Fig. 32. Figure 33 presents the rotating stall cell measurements recorded for screen positions 1, 2, 3, and 4 of the 180-degree extent of distortion level 3. From these measurements, it was determined that the amplitude of the stall cell was attenuated as it approached, and passed through the distorted flow region. Comparison of Figs. 33 (a) and (c) indicated that the magnitudes of the stall cell pressure fluctuations were reduced by as much as 66 per cent behind the distortion screen. From Figs. 33 (c) and (d), it was observed that the stall cell increased in amplitude as it proceeded through the distorted flow region. It was suggested that the attenuation of the stall cell behind the screen was due to the lower axial velocity in this region. The air velocity provided the "driving force" for the pressure fluctuations; hence, the reduction in axial velocity resulted in the stall cell attenuation. Similar stall cell measurements recorded for the 180-degree extent of distortion level 1 are shown in Fig. 34. The same results were obtained as for distortion level 3. However, comparison of Figs. 33 and 34 indicated that distortion level 1 did not attenuate the stall cell to the same degree as distortion level 3. This was due to the higher velocity behind the screen of distortion level 1.

Appendix C presents the rotating stall cell measurements recorded for the 90 and 45-degree extents of distortion for levels 1 and 3.

Results similar to those discussed above were obtained for these two lesser extents of distortion. In each case, the stall cell was attenuated behind the distortion screen, with level 3 accounting for the most severe attenuation.

It was observed from Figs. 35 (a) and (c) that the circumferential extent of the stall cell behind the distortion screens did not differ substantially from that for undistorted flow (60 to 80 degrees). The radial extent of the stall cell behind the distortion screens encompassed the rotor blade tip region down to about 70 per cent span. Between 70 and 50 per cent span, the stable rotating stall pattern reduced to random pressure fluctuations. Typical relative pressure distributions in the distorted flow region at 30 per cent span are shown in Figs. 35 (b) and (d). These pressure profiles indicated predominantly steady flow in this area, for it is below the radial extent of rotating stall. For comparison, Fig. 36 presents the pressure distribution at the same span position for undistorted flow.

On-Rotor Pressure Measurements

The average chordwise pressure profiles for distorted and undistorted flow are tabulated in Appendix E for several valve positions. For all inlet conditions, it was found that rotor blade pressure side measurements differed only slightly at high volumetric flow rates and approached constant values as the flow rate was reduced. However, the average suction side pressure profiles were found to change shape as the flow rate was reduced towards stall.

Figures 38 through 41 show the changes in the suction side pressure profiles with flow rate for several inlet conditions. It was apparent from these curves that as the flow rate was decreased, the pressure profiles changed from a concave-downward shape into a slightly concave-upward orientation. This change in shape was initially observed as an inflection point which appeared at 50 per cent chord. Further reduction of the flow rate produced a definite concave-upward profile beyond 50 per cent chord. This indicated that the blade surface boundary layer separated at some point and probably reattached close to the trailing edge. The transitions in shape occured at the same flow rates for both the undistorted inlet and the 45-degree extent of level 3. The change in shape occured at higher flow rates for the 90 and 180-degree distortion extents. It appeared that increasing the circumferential extent of distortion above some "critical" value induced blade stall at higher volumetric flow rates. At the valve position corresponding to stall for each inlet flow condition, the inflection point appeared closer to the blade leading edge. This earlier boundary layer separation indicated that the blade had stalled. The results presented and discussed above agreed with those obtained by Dancy [13].

XII. CONCLUSIONS

It was determined from this investigation that circumferential inlet total pressure distortion altered the overall performance of the compressor. The total pressure rise achieved at stall was reduced for distorted inlet flow. The compressor entered stable rotating stall when the mass flow rate was lowered sufficiently. For undistorted flow, the rotating stall cell encompassed the rotor blade tip region down to midspan. Total pressure loss through the stall cell reached 7.62 cm (3 in.) of water pressure. For distorted inlet flow, the character of the rotating stall appeared the same for the screens used. However, in the distorted flow region, the magnitude of the stall cell was attenuated due to the lower velocity behind the distortion screen. For extents of distortion greater than some "critical" value, the compressor appeared to enter stall at higher volumetric flow rates. The critical angle was determined to be 60 degrees for the compressor subjected to distortion levels 2 and 3. This value is the same as that determined for a less severe distortion level. Fow the low speed compressor used, it appears that the critical angle phenomena is a function of compressor design and is independent of the distortion level.

XIII. RECOMMENDATIONS

The results of this investigation suggest the following topics for further study:

1) Investigation of the effects of inlet distortion on the inception of surge.
2) Analysis of stall cell formation and behavior for flow rates ranging from the maximum value to that at "shut-off" with the compressor subjected to a single circumferential extent of the most severe distortion level used in the present study. The Mechanical Engineering Department of VPI&SU recently completed a similar investigation for undistorted compressor operation.
3) Conduction of a multi-parameter investigation where the effects of inlet distortion may be related to rotor speed, blade stagger angles, number of stages, radial and circumferential extent of distortion, distortion level, axial location of distortion screens, and other variables.
4) Implementation of a computer interface system to permit rapid reduction of pressure measurements. The development of such a system by the Department of Mechanical Engineering at VPI&SU has reached the final design stages.

XIV. BIBLIOGRAPHY

Cited References

1. Pearson, H., McKenzie, A., "Wakes in Axial Compressors," Journal of Royal Aeronautical Society, Vol. 63, July, 1959.

2. Braithwaite, W., Graber, E., Mehalic, C., "The Effect of Inlet Temperature and Pressure Distortion on Turbojet Performance," AIAA Paper No. 73-1316, 1973.

3. Calogeras, J., Mehalic, C., Burstadt, P., "Experimental Investigation of the Effect of Screen-Induced Total Pressure Distortion on Turbojet Stall Margin," NASA TMX-2239, 1971.

4. Reid, C., "The Response of Axial-Flow Compressors to Intake Flow Distortion," ASME Paper No. 69-GT-29, 1969.

5. Calogeras, J., Johnsen, R., Burstadt, P., "Effect of Screen-Induced Total Pressure Distortion on Axial Flow Compressor Stability," NASA TMX-3017, 1974.

6. Roberts, F., Plourde, G., Smakula, F., "Insights Into Axial Compressor Response to Distortion," AIAA Paper No. 68-565, 1968.

7. Graber, E., Braithwaite, W., "Summary of Recent Investigations of Inlet Flow Distortion Effects on Engine Stability," AIAA Paper No. 74-236, 1974.

8. Plourde, G., Stenning, A., "Attenuation of Circumferential Inlet Distortion in Multistage Axial Compressors," Journal of Aircraft, Vol. 5, May-June, 1968.

9. Mikolajczak, A., Pfeffer, A., "Methods to Increase Engine Stability and Tolerance to Distortion," in Distortion Induced Engine-Instability, Agard Lecture Series No. 72, 1974.

10. Ehrich, F., "Circumferential Inlet Distortions in Axial Flow Turbomachinery," Journal of the Aeronautical Sciences, Vol. 24, June, 1957.

11. Hartmann, M., Sanger, N., "The Effect of Circumferential Distortion on Fan Performance at Two Levels of Blade Loading," in Compressor Response to Distorted Inflow, Agard Conference Proceedings No. 177, 1975.

12. Peacock, R., Overli, J., "Dynamic Internal Flows in Compressors with Pressure Maldistributed Inlet Conditions," in Compressor

BIBLIOGRAPHY (Continued)

Response to Distorted Inflow, Agard Conference Proceedings No. 177, 1975.

13. Dancy, B., "Performance and Stalling Behavior of an Axial Flow Compressor with Circumferential Inlet Flow Distortion," M.S. Thesis, Virginia Polytechnic Institute and State University, 1976.

14. Schultz, P., "Pressure Distribution on a Rotating Axial-Flow Compressor Blade," M.S. Thesis, Virginia Polytechnic Institute and State University, 1976.

15. Mokelke, H., "Prediction Techniques," in Distortion Induced Engine-Instability, Agard Lecture Series No. 72, 1974.

16. Holman, J. P., Experimental Methods for Engineers, 1971, p. 191.

Uncited References

1. Hercock, R., Williams, D., "Aerodynamic Response," in Distortion Induced Engine-Instability, Agard Lecture Series No. 72, 1974.

2. Korn, J., "The Effect of Inlet Distortion on the Performance and Stability of the Low-Speed Spool of a Turbofan Engine," AIAA Paper No. 74-234, 1974.

3. Mazzawy, R., "Multiple Segment Parallel Compressor Model for Circumferential Flow Distortion," in Compressor Response to Distorted Inflow, Agard Conference Proceedings No. 177, 1975.

4. Milner, E., Wenzel, L., "Performance of a J85-13 Compressor with Clean and Distorted Inlet Flow," NASA TMX-3304, 1975.

5. Povolny, J., Burcham, F., Calogeras, J., Meyer, C., Rudey, R., "Effects of Engine Inlet Disturbances on Engine Stall Performance," NASA SP-259, 1970.

XV. APPENDICES

Appendix A

Table A. Loss in Stall Margin Data

Distortion Level	2			3		
Extent	45°	90°	180°	45°	90°	180°
P_{max} (cm H_2O)	-.28	-.20	-.28	-.30	-.28	-.18
P_{screen} (cm H_2O)	-2.03	-2.16	-2.29	-2.46	-2.51	-2.90
P_2 (cm H_2O)	-4.90	-4.78	-4.27	-4.85	-4.65	-3.96
ΔPSM_N (Per Cent)	22.1	21.2	15.3	25.8	23.4	19.8

Appendix B.

Table B. Valve Position at Stable Rotating Stall For Inlet Flow Conditions Tested

Distortion Pattern	Valve Position
Undistorted Inlet	7.25
Distortion Level 1; Extent 45°	7.2
90°	7.1
180°	7.0
Distortion Level 2; Extent 45°	7.1
90°	7.0
180°	6.75
Distortion Level 3; Extent 45°	7.1
90°	6.9
180°	6.6

Appendix C. Typical Stall Cell Photographs - Distortion Levels 1, 3; Extents 90, 45-Degrees

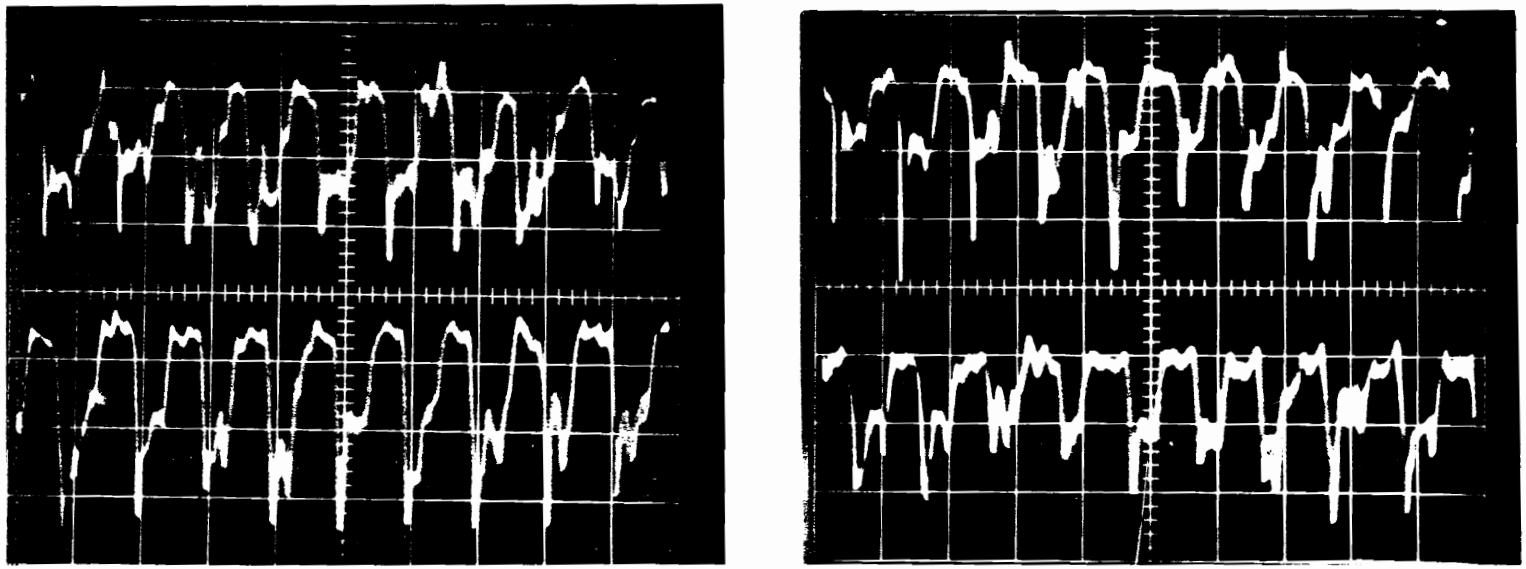

(a)

Screen Position 1
Probe 1 at Tip
Probe 2 at Tip

(b)

Screen Position 2
Probe 1 at Tip
Probe 2 at Tip

Valve Position 6.9

Vertical Scale: 2.54 cm H_2O/Div. (1 in. H_2O/Div.)

Horizontal Scale: (a) 50 ms/Div.
(b) 50 ms/Div.

Figure C-1. Typical Stall Cell Pressure Fluctuations With 90-Degree Extent of Distortion Level 3

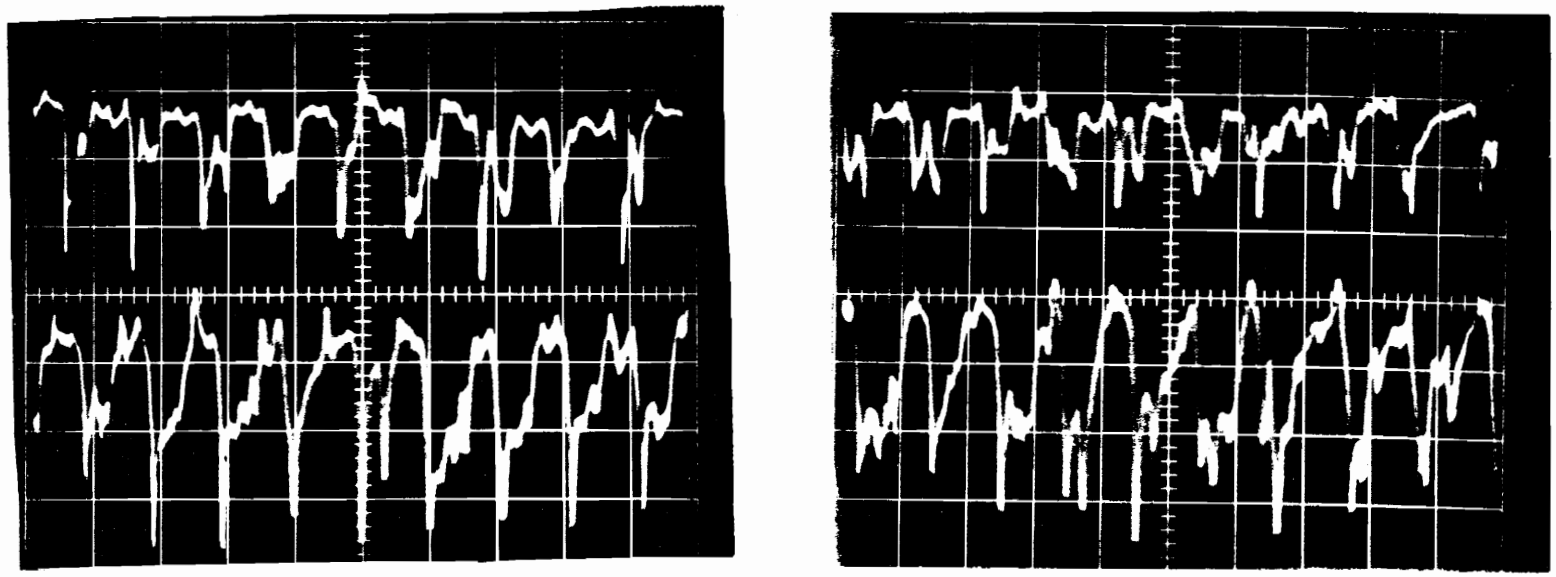

(c)

Screen Position 3
Probe 1 at Tip
Probe 2 at Tip

(d)

Screen Position 4
Probe 1 at Tip
Probe 2 at Tip

Valve Position 6.9

Vertical Scale: 2.54 cm H_2O/Div. (1 in. H_2O/Div.)

Horizontal Scale: (c) 50 ms/Div.
(d) 50 ms/Div.

Figure C-1. Typical Stall Cell Pressure Fluctuations With 90-Degree Extent of Distortion Level 3

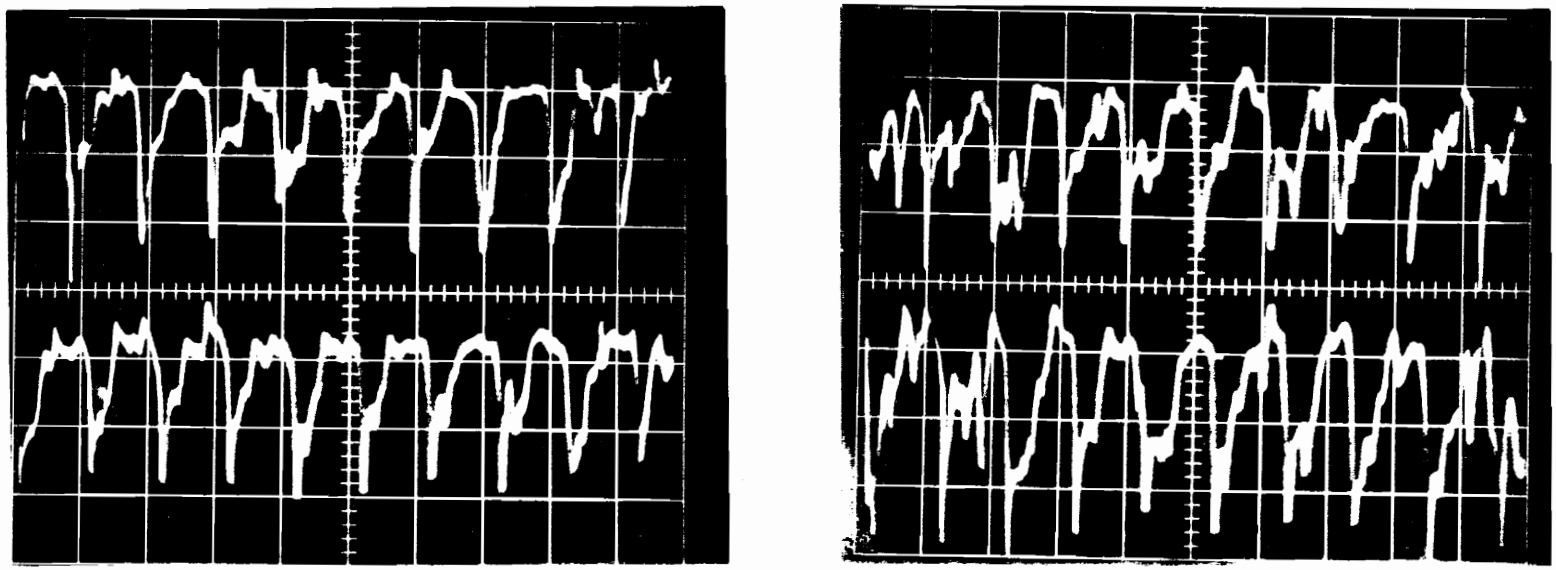

(a)

Screen Position 1
Probe 1 at Tip
Probe 2 at Tip

(b)

Screen Position 2
Probe 1 at Tip
Probe 2 at Tip

Valve Position 7.1

Vertical Scale: 2.54 cm H_2O/Div. (1 in. H_2O/Div.)

Horizontal Scale: (a) 50 ms/Div.
(b) 50 ms/Div.

Figure C-2. Typical Stall Cell Pressure Fluctuations With 90-Degree Extent of Distortion Level 1

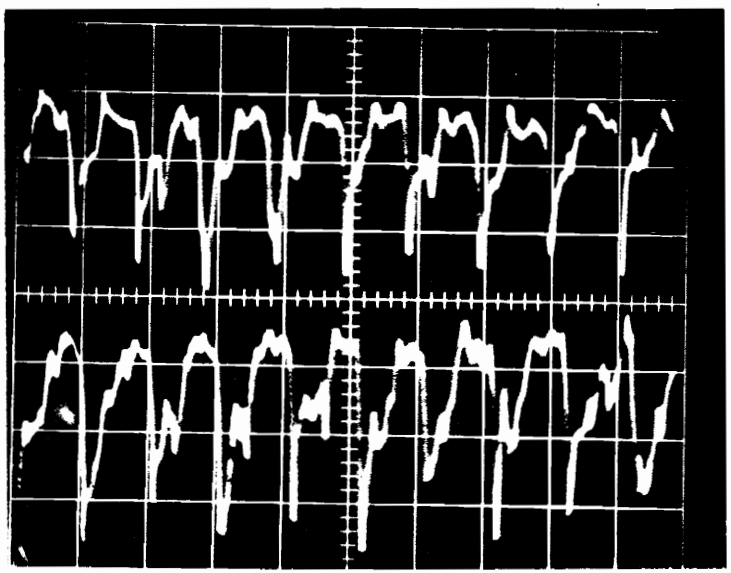

(c)

Screen Position 3
Probe 1 at Tip
Probe 2 at Tip

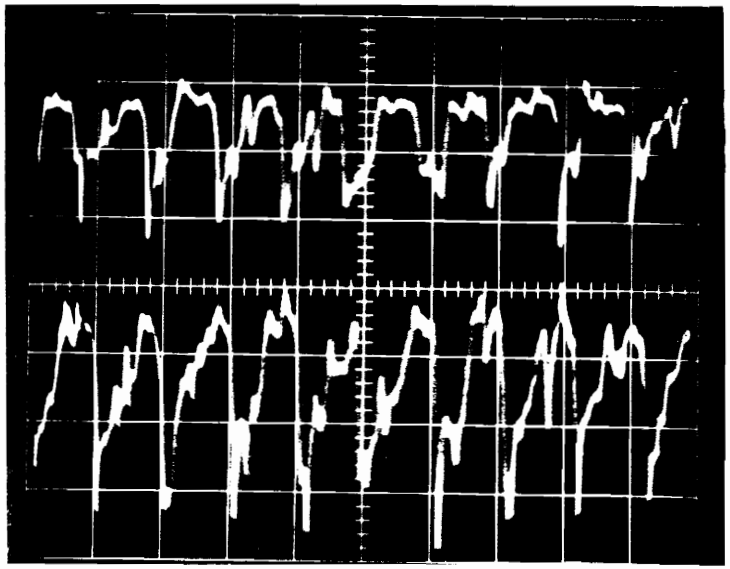

(d)

Screen Position 4
Probe 1 at Tip
Probe 2 at Tip

Valve Position 7.1

Vertical Scale: 2.54 cm H_2O/Div. (1 in. H_2O/Div.)

Horizontal Scale: (c) 50 ms/Div
(d) 50 ms/Div.

Figure C-2. Typical Stall Cell Pressure Fluctuations With 90-Degree Extent of Distortion Level 1

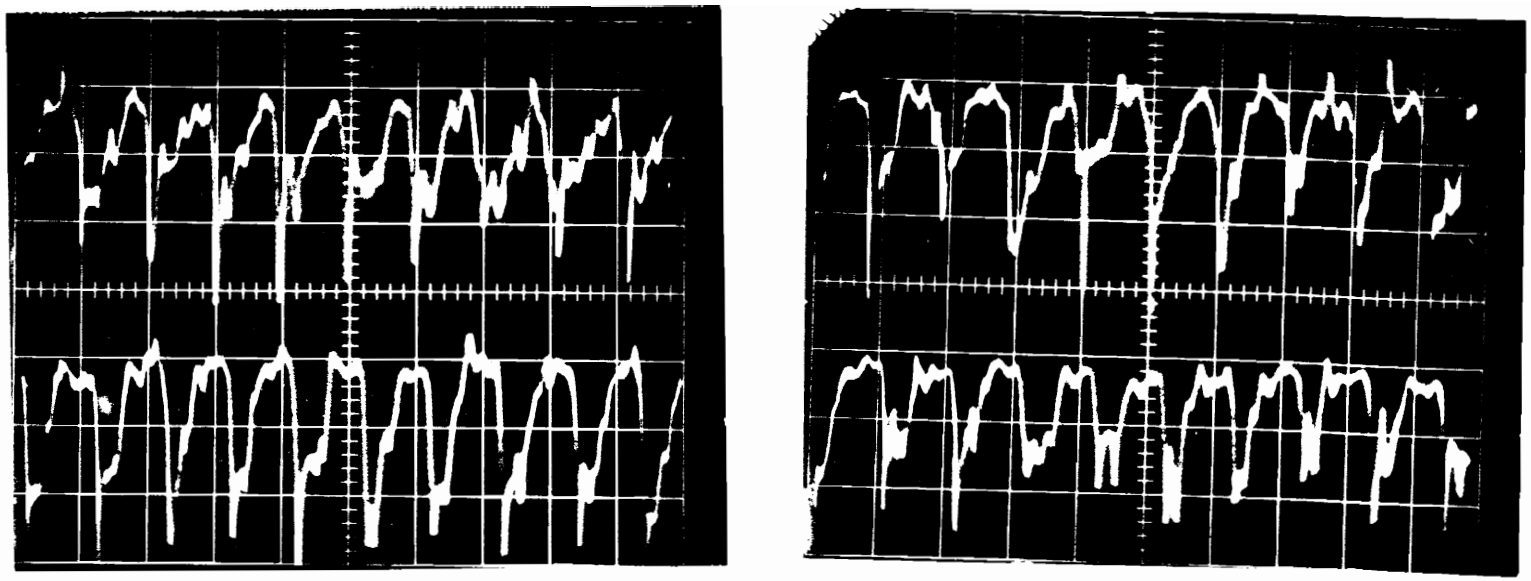

(a) (b)

Screen Position 1
Probe 1 at Tip
Probe 2 at Tip

Valve Position 7.1

Screen Position 2
Probe 1 at Tip
Probe 2 at Tip

Vertical Scale: 2.54 cm H_2O/Div. (1 in. H_2O/Div.)

Horizontal Scale: (a) 50 ms/Div.
(b) 50 ms/Div

Figure C-3. Typical Stall Cell Pressure Fluctuations With 45-Degree Extent of Distortion Level 3

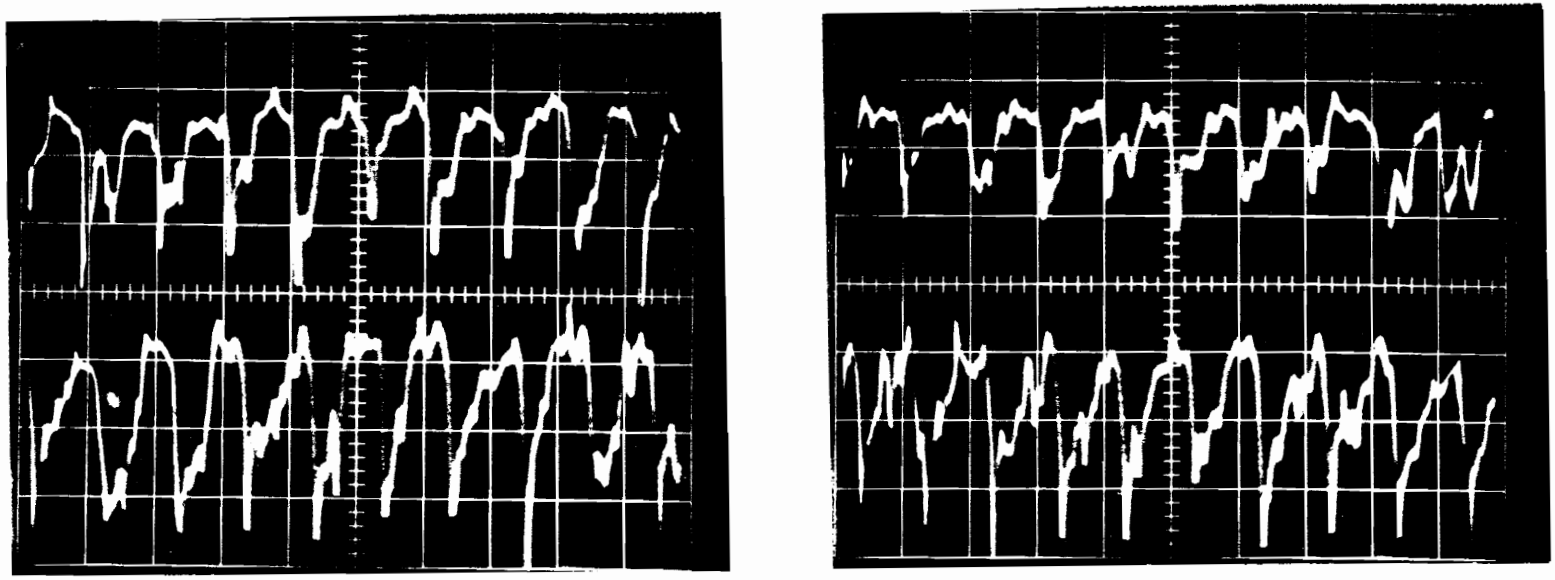

(c)

Screen Position 3
Probe 1 at Tip
Probe 2 at Tip

(d)

Screen Position 4
Probe 1 at Tip
Probe 2 at Tip

Valve Position 7.1

Vertical Scale: 2.54 cm H_2O/Div. (1 in. H_2O/Div.)

Horizontal Scale: (c) 50 ms/Div.
(d) 50 ms/Div.

Figure C-3. Typical Stall Cell Pressure Fluctuations With 45-Degree Extent of Distortion Level 3

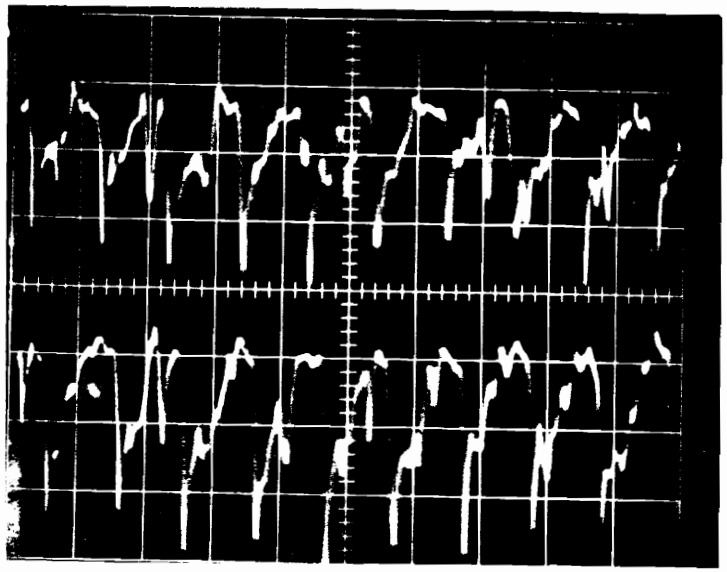

(a)

Screen Position 1
Probe 1 at Tip
Probe 2 at Tip

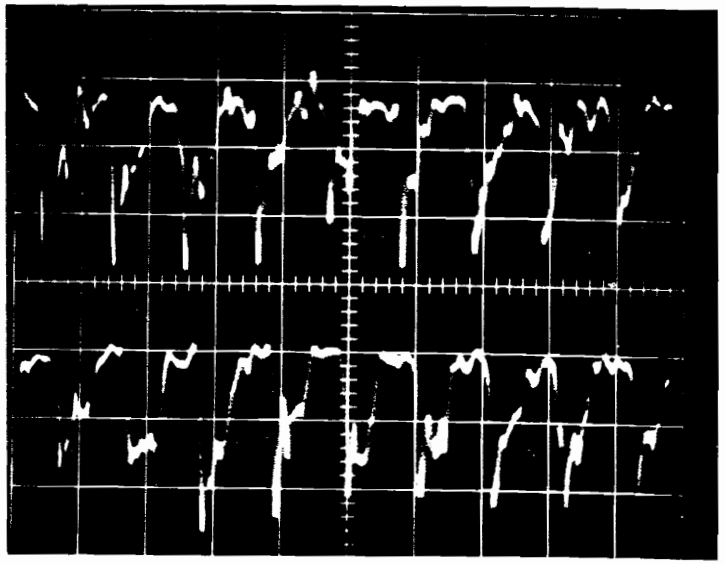

(b)

Screen Position 2
Probe 1 at Tip
Probe 2 at Tip

Valve Position 7.2

Vertical Scale: 2.54 cm H_2O/Div. (1 in. H_2O/Div.)

Horizontal Scale: (a) 50 ms/Div.
(b) 50 ms/Div.

Figure C-4. Typical Stall Cell Pressure Fluctuations With 45-Degree Extent of Distortion Level 1

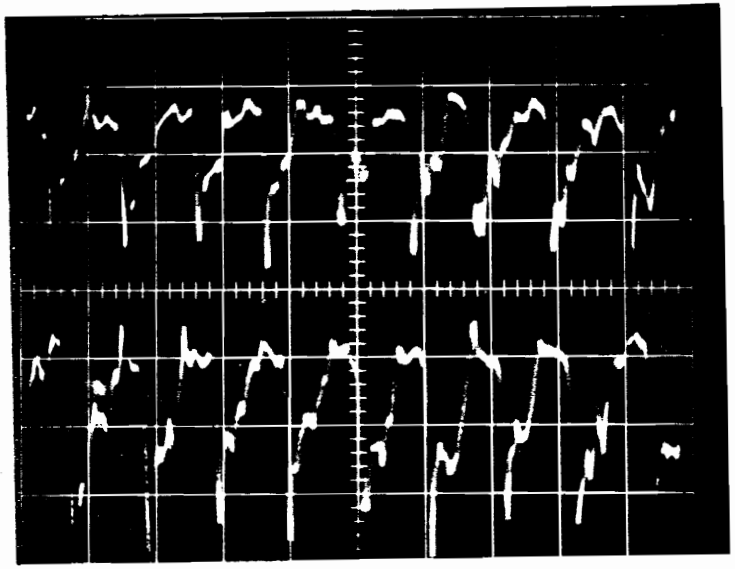

(c)

Screen Position 3
Probe 1 at Tip
Probe 2 at Tip

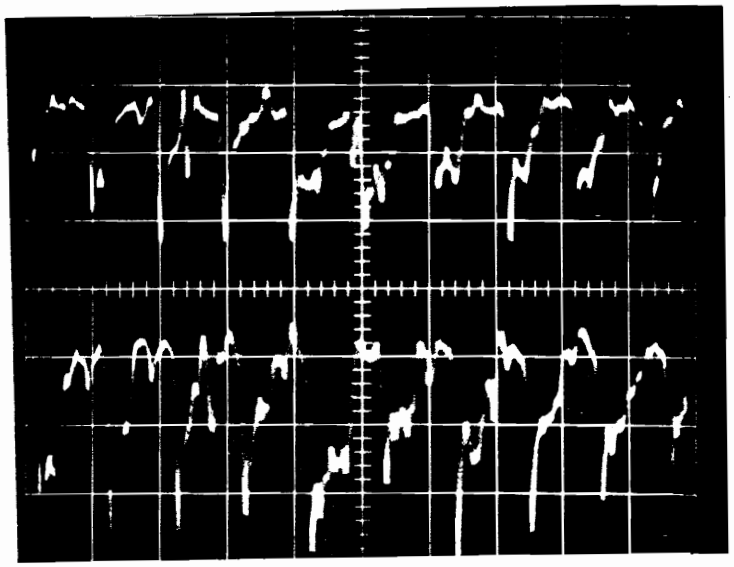

(d)

Screen Position 4
Probe 1 at Tip
Probe 2 at Tip

Valve Position 7.2

Vertical Scale: 2.54 cm H_2O/Div. (1 in. H_2O/Div.)

Horizontal Scale: (c) 50 ms/Div.
(d) 50 ms/Div.

Figure C-4. Typical Stall Cell Pressure Fluctuations With 45-Degree Extent of Distortion Level 1

Appendix D. Typical Stall Cell Photographs - Distortion Level 1; Extents 180, 45-Degrees

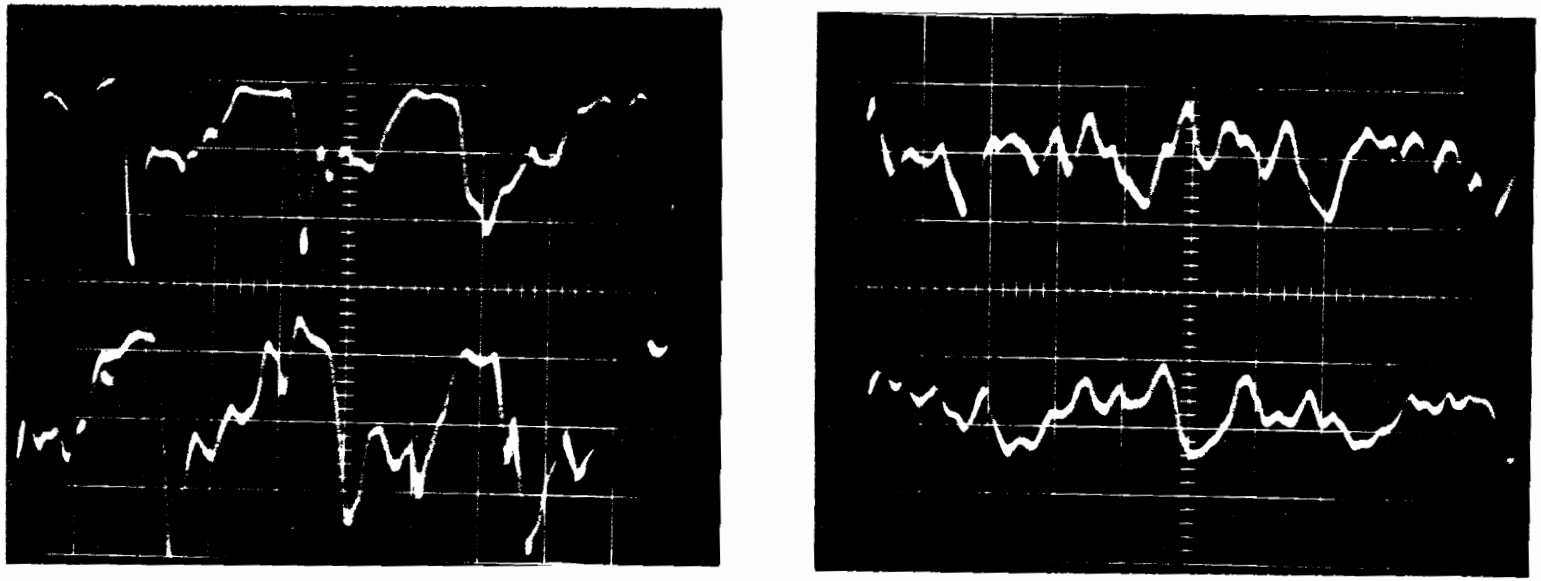

(a)

Screen Position 4
Probe 1 at Tip
Probe 2 at Tip

(b)

Screen Position 4
Probe 1 at Tip
Probe 2 at Tip

Valve Position 7.0

Vertical Scale: 2.54 cm H_2O/Div. (1 in. H_2O/Div.)

Horizontal Scale: (a) 20 ms/Div.
(b) 20 ms/Div.

Figure D-1. Typical Stall Cell Pressure Fluctuations With 180-Degree Extent of Distortion Level 1

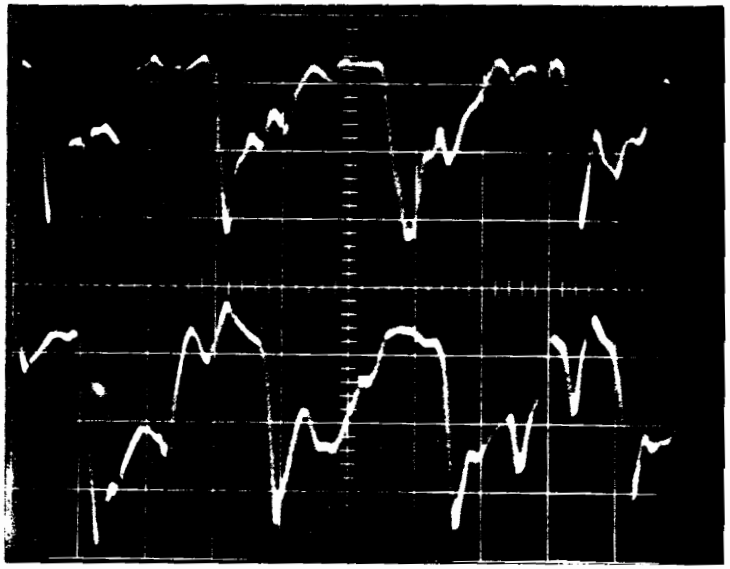

(c)

Screen Position 4
Probe 1 at Tip
Probe 2 at Tip

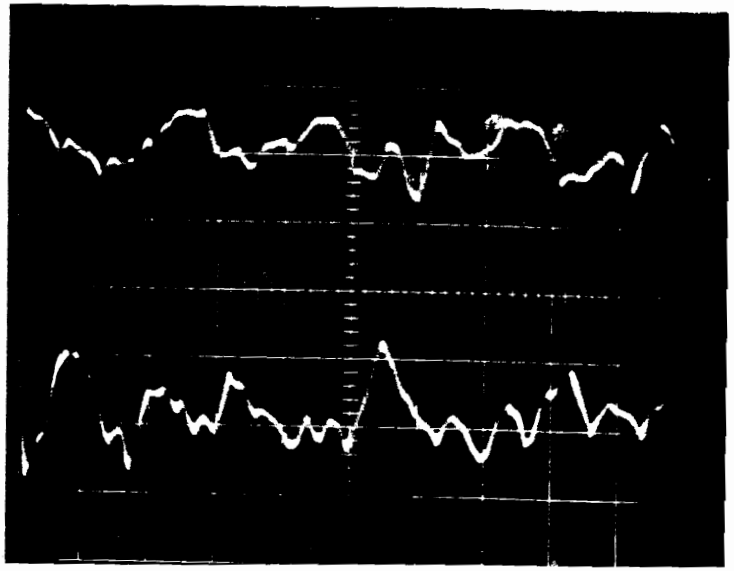

(d)

Screen Position 4
Probe 1 at Tip
Probe 2 at Tip

Valve Position 7.2

Vertical Scale: 2.54 cm H_2O/Div. (1 in. H_2O/Div.)

Horizontal Scale: (c) 20 ms/Div.
(d) 20 ms/Div.

Figure D-1. Typical Stall Cell Pressure Fluctuations With 45-Degree Extent of Distortion Level 1

Appendix E. On-Rotor Pressure Measurements

Table E-1. Midspan Average Blade Pressures - Undistorted Inlet (cm H_2O)

	Per Cent	Valve Position					
	Chord	0	3	5.5	6.5	7	7.5
Suction Side	10	-30.9	-31.2	-31.1	-30.8	-30.1	-27.8
	25	-30.6	-29.6	-27.4	-26.1	-25.6	-24.1
	45	-26.2	-24.9	-21.7	-19.5	-18.6	-18.8
	65	-21.0	-18.8	-15.6	-14.1	-13.9	-14.6
	85	-14.7	-13.0	-10.8	-10.4	-10.6	-11.5
Pressure Side	10	-15.2	-13.2	- 9.1	- 7.8	- 7.8	- 9.3
	25	-11.7	- 9.9	- 8.0	- 7.6	- 7.7	- 8.6
	45	-10.7	- 9.2	- 7.7	- 7.5	- 7.6	- 8.1
	65	-10.3	- 8.9	- 7.6	- 7.5	- 7.6	- 8.0
	85	-10.3	- 9.0	- 7.8	- 7.8	- 7.9	- 8.3

Table E-2. Midspan Average Blade Pressures - Distortion Level 3; 45-Degree Extent (cm H_2O)

	Per Cent	Valve Position					
	Chord	0	3	5.5	6.5	7	7.5
Suction Side	10	-31.3	-31.1	-31.2	-30.6	-29.4	-27.6
	25	-30.6	-29.3	-27.3	-26.0	-25.2	-24.0
	45	-25.8	-24.2	-21.1	-19.4	-19.4	-18.9
	65	-20.6	-18.3	-15.3	-14.2	-14.8	-14.9
	85	-14.3	-12.8	-11.0	-10.7	-11.5	-11.7
Pressure Side	10	-15.0	-13.6	- 9.6	- 8.3	- 9.2	- 9.8
	25	-11.3	- 9.7	- 8.1	- 7.6	- 8.5	- 8.7
	45	-10.5	- 9.1	- 7.8	- 7.5	- 8.1	- 8.2
	65	-10.1	- 8.9	- 7.8	- 7.5	- 8.1	- 8.1
	85	-10.2	- 9.0	- 8.1	- 7.8	- 8.5	- 8.4

Table E-3. Midspan Average Blade Pressures - Distortion Level 3; 90-Degree Extent

	Per Cent	Valve Position					
	Chord	0	3	5.5	6.5	7	7.5
Suction Side	10	-31.8	-32.0	-31.4	-30.7	-28.9	-27.2
	25	-30.4	-29.5	-27.1	-26.0	-25.0	-23.7
	45	-25.2	-23.7	-20.6	-19.5	-19.4	-18.9
	65	-20.1	-18.1	-15.1	-14.4	-15.1	-14.9
	85	-14.1	-12.8	-11.2	-11.0	-11.9	-11.9
Pressure Side	10	-15.1	-14.0	-10.4	- 8.8	-10.1	-10.2
	25	-11.3	- 9.8	- 8.2	- 7.8	- 8.9	- 8.9
	45	-10.5	- 9.4	- 8.0	- 7.7	- 8.5	- 8.4
	65	-10.4	- 9.2	- 8.0	- 7.6	- 8.4	- 8.3
	85	-10.4	- 9.3	- 8.3	- 8.1	- 8.7	- 8.6

Table E-4. Midspan Average Blade Pressures - Distortion Level 3; 180-Degree Extent (cm H_2O)

	Per Cent	Valve Position					
	Chord	0	3	5.5	6.5	7	7.5
Suction Side	10	-33.5	-33.1	-32.3	-30.2	-28.7	-27.6
	25	-30.9	-29.5	-27.4	-25.9	-25.0	-24.2
	45	-24.8	-23.0	-20.1	-19.7	-19.5	-19.2
	65	-19.6	-17.4	-14.8	-15.2	-15.4	-15.4
	85	-14.1	-12.5	-11.3	-12.0	-12.3	-12.5
Pressure Side	10	-15.5	-13.7	-10.4	- 9.7	-10.7	-10.7
	25	-11.2	- 9.6	- 8.2	- 8.8	- 9.2	- 9.3
	45	-10.7	- 9.3	- 8.1	- 8.4	- 8.8	- 8.8
	65	-10.5	- 9.3	- 8.1	- 8.6	- 8.7	- 8.7
	85	-10.7	- 9.4	- 8.5	- 8.6	- 9.0	- 9.0

Table E-5. Midspan Average Blade Pressures - Distortion Level 2; 45-Degree Extent (cm H_2O)

	Per Cent	Valve Position					
	Chord	0	3	5.5	6.5	7	7.5
Suction Side	10	-31.2	-31.1	-31.0	-30.6	-29.3	-28.0
	25	-30.5	-29.3	-27.1	-25.9	-25.1	-24.5
	45	-25.9	-24.4	-21.1	-19.2	-19.0	-19.1
	65	-20.1	-18.4	-15.3	-14.0	-14.6	-15.0
	85	-14.0	-12.9	-10.8	-10.5	-11.3	-11.8
Pressure Side	10	-14.7	-13.5	- 9.2	- 7.9	- 9.0	- 9.6
	25	-11.2	- 9.8	- 8.0	- 7.6	- 8.4	- 8.8
	45	-10.4	- 9.2	- 7.8	- 7.4	- 8.1	- 8.3
	65	-10.1	- 9.0	- 7.8	- 7.4	- 8.1	- 8.2
	85	-10.1	- 9.1	- 8.0	- 7.8	- 8.4	- 8.5

Table E-6. Midspan Average Blade Pressure - Distortion Level 2; 90-Degree Extent (cm H_2O)

	Per Cent Chord	Valve Position					
		0	3	5.5	6.5	7	7.5
Suction Side	10	-32.0	-32.2	-31.8	-31.1	-28.8	-27.9
	25	-30.8	-29.8	-27.6	-26.3	-25.0	-23.9
	45	-25.6	-24.2	-21.0	-19.5	-19.4	-19.1
	65	-20.5	-18.5	-15.3	-14.3	-15.0	-15.1
	85	-14.4	-13.0	-11.2	-10.9	-10.9	-12.0
Pressure Side	10	-15.0	-13.9	-10.0	- 8.4	- 9.9	-10.1
	25	-11.6	-10.0	- 8.2	- 7.8	- 8.8	- 8.9
	45	-10.7	- 9.4	- 8.1	- 7.7	- 8.4	- 8.5
	65	-10.4	- 9.2	- 8.1	- 7.6	- 8.4	- 8.4
	85	-10.5	- 9.4	- 8.4	- 8.0	- 8.7	- 8.7

Table E-7. Midspan Average Blade Pressures - Distortion Level 2; 180-Degree Extent (cm H_2O)

	Per Cent Chord	Valve Position					
		0	3	5.5	6.5	7	7.5
Suction Side	10	-33.9	-33.1	-32.5	-31.1	-29.1	-27.9
	25	-31.6	-29.8	-27.7	-26.4	-25.3	-24.4
	45	-25.7	-23.4	-20.5	-19.3	-19.6	-18.9
	65	-19.9	-17.9	-15.1	-14.3	-15.3	-15.2
	85	-14.3	-12.7	-11.3	-11.2	-12.3	-12.2
Pressure Side	10	-15.6	-14.1	-10.6	- 9.0	-10.5	-10.7
	25	-11.5	- 9.8	- 8.3	- 8.5	- 9.1	- 9.4
	45	-10.9	- 9.4	- 8.2	- 8.0	- 8.6	- 8.9
	65	-10.7	- 9.3	- 8.2	- 7.9	- 8.6	- 8.7
	85	-10.8	- 9.6	- 8.6	- 8.4	- 9.0	- 9.1

XVI. VITA

The author, William Hartland Gauden, was born September 8, 1954 in Charleroi, Pennsylvania.

In the fall of 1972, he entered Virginia Polytechnic Institute and State University, where he majored in Mechanical Engineering. As an undergraduate, he was a member of the American Society of Mechanical Engineers; Pi Tau Sigma, Tau Beta Pi, and Phi Eta Sigma honorary fraternities, and Theta Chi fraternity. He was awarded the Bachelor of Science Degree in Mechanical Engineering in June, 1976.

In September, 1976, he returned to VPI&SU to pursue the Master of Science Degree in Mechanical Engineering.

William Hartland Gauden

William Hartland Gauden

PERFORMANCE AND STALLING BEHAVIOR OF AN AXIAL-FLOW COMPRESSOR SUBJECTED TO THREE CIRCUMFERENTIAL INLET DISTORTION LEVELS

by

William H. Gauden

(ABSTRACT)

The performance and stalling behavior of an axial-flow compressor subjected to several different inlet distortion patterns was investigated. The effect of inlet distortion on overall compressor performance was determined through the measurement of compressor characteristics for each inlet flow condition. Dynamic pressure transducers were employed to investigate rotating stall cell behavior during the inception of stall. Rotor blade response to distorted inflow was measured in the form of average blade pressure profiles by using a scanning valve.

Results indicated a substantial reduction in total pressure rise capability for distorted operation. A 25 per cent loss in stall pressure rise was observed for the most severe distortion level. The stall cell was found to rotate in the direction of rotor motion, but at one-half the rotor speed. The cell encompassed the rotor blade tip region down to approximately midspan. During the onset of stall, the circumferential extent of the cell was observed to vary from 60 to 80 degrees. At the rotor blade tip the stall cell relative pressure fluctuations indicated zero flow through the cell. The amplitude of

the stall cell was attenuated in the distorted flow region due to the lower air velocity behind the distortion screens. Rotor blade suction side pressure measurements indicated that increasing the circumferential extent of distortion above some "critical" value induced blade stall at higher flow rates. For the low speed compressor used, it appears that the critical angle phenomena is a function of compressor design and is independent of distortion level.